3-31-2015

Polymer Brushes: Surface Initiated and Bottlebrush Self-Assembly

Andre P. Martinez
University of Connecticut - Storrs, andre.martinez@uconn.edu

Polymer Brushes: Surface-Initiated and Bottlebrush Self-Assembly

Andre P. Martinez, Ph.D.

University of Connecticut, 2015

Abstract: The term "polymer brush" may refer to chains closely bound to one another on a surface or chains bound to a central polymer backbone forming an architecture that has been described as a bottlebrush. Polymer brushes exhibit unique properties arising from the repulsive excluded volume interactions between adjacent polymer chains. These interactions can cause polymers chains that would normally exist as random coils to take on a highly extended conformation depending on the density of grafted chains. Surface bound polymer brushes have been used for a myriad of applications including colloidal stability, biocompatibility, and low-friction surfaces among others. Bottlebrushes are being studied for applications similar to those of linear block copolymers due to their ability to self-assemble. However, their chain conformation and self-assembly is dictated by architecture in a way that linear block copolymer assembly is not. We have investigated both surface bound brushes, grown by controlled radical surface-initiated polymerization, and bottlebrushes grown by anionic polymerization. We find that the distribution of polymers grown by surface-initiated polymerization contains a low molecular weight fraction that we argue is a result of terminations occurring early during polymerization. We have performed preliminary investigations into techniques for the reduction of brush polydispersity and have also used surface-initiated polymerization to enhance the dispersibility of nanofillers for composite materials. Our studies of amphiphilic bottlebrushes describe self-assembly trends and indicate a structural difference in the coronas of micelles formed by dense versus sparsely grafted bottlebrushe

Polymer Brushes: Surface-Initiated and Bottlebrush Self-Assembly

Andre P. Martinez

B.A. Williams College, 2009

A Dissertation

Submitted in Partial Fulfillment of the

Requirements for the Degree of

Doctor of Philosophy

at the

University of Connecticut

2015

APPROVAL PAGE

Doctor of Philosophy Dissertation

Polymer Brushes: Surface-Initiated and Bottlebrush Self-Assembly

Presented by Andre P. Martinez, B.A.

Major Advisor:

Prof.
Douglas H. Adamson

Associate Advisor:

Prof.
Thomas A.P. Seery

Associate Advisor:

Prof.
Andrey V. Dobrynin

Associate Advisor:

Prof.
Alexandru D. Asandei

Associate Advisor:

Dr.
Edward Neth

University of Connecticut 2015

Acknowledgements – I would like to thank all of the friends I have made over my years at UConn. You guys have made the last several years an incredible experience. I especially want to thank everyone in the UConn Ultimate community for taking me in and for the great times we've had both on and off the field. I also have to thank my family for being supportive and encouraging.

Thank you to my research group and other students of from chemistry program and the polymer program for your help and for being great people to work alongside. Specific thanks go out to group members, Zhenhua Cui for being a collaborator and Chetan Hire for being a mentor when I was new to the group. Both Yan Xia and Katie Moon have also been greatly helpful and I have spent many hours in their labs, often with their assistance. I am also indebted to the Institute of Material Science laboratory technicians who trained me in so many instrumental techniques. I would not have been at UConn if not for my undergraduate advisor, Professor Christopher Goh at Williams College. Thank you, Professor Goh, for introducing me to the study of polymers and encouraging me to pursue an advanced degree.

I want to thank my advisory committee, made up of Professors Asandei, Dobrynin, Neth, and Seery, all of whom have individually helped and contributed towards my development as a researcher. Most important has been my major advisor, Professor Douglas Adamson. Thank you for allowing me to join your group and for continually teaching me, in the lab and in individual and group meetings. Thank you for being interested, supportive and patient. I wish only the best for you and everyone else mentioned.

Table of Contents

List of Figures

List of Tables

List of Equations

Chapter 1 – Introduction to Polymer Brushes

1.1 Introduction: The term "polymer brush" may refer to one of two materials. The first is surface-grafted polymer. Polymer may be grown from a given surface or free polymer chains may be physically or chemically attached to a surface. Second, polymer brush refers to a branched chain structure such that the polymer is composed of a central chain to which multiple additional chains are grafted. Such polymers have been referred to as "bottlebrush" due to the architectural resemblance chains grafted to the backbone bare to the bristles of a brush. Below we separately discuss these two forms of polymer brushes.

1.2 Surface Grafted Brushes: Surface grafted polymers, or polymer brushes, are being developed for a range of applications that include non-biofouling[1,2], cell adhesion[3,4], low friction surfaces[5,6], organic electronics[7,8], tunable colloidal systems[9,10], and stimuli-responsive materials.[11,12] As shown in **figure 1** below, H Sakata et al. investigated tribological properties of poly(methyl methacrylate) brushes on silicon wafers and saw that brushes had a lower friction coefficient and better ware resistance than corresponding spin-coated PMMA films.[5] Huck and Friend et al. used polyacrylate brushes grown from ITO to generate ordered composites with semiconducting cadmium selenide semiconducting nanoparticles.[7] **Figure 2** below illustrates the optoelectronic device they constructed, which gave internal quantum efficiencies as high as 50%.

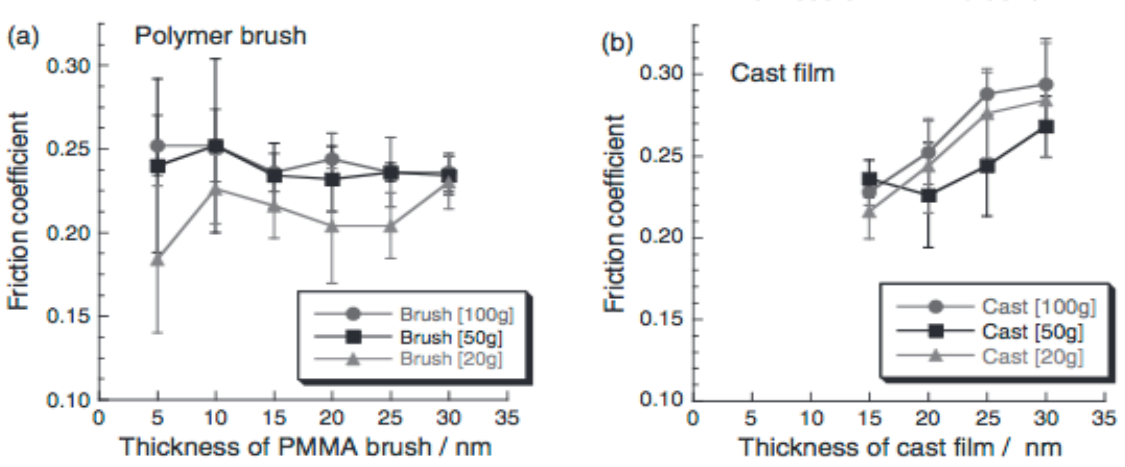

Figure 1: Friction coefficients of polymer brushes versus spin coated films. Reduced friction coefficients were seen for silicon surfaces with PMMA brushes compared with PMMA cast films of the same mass.[5]

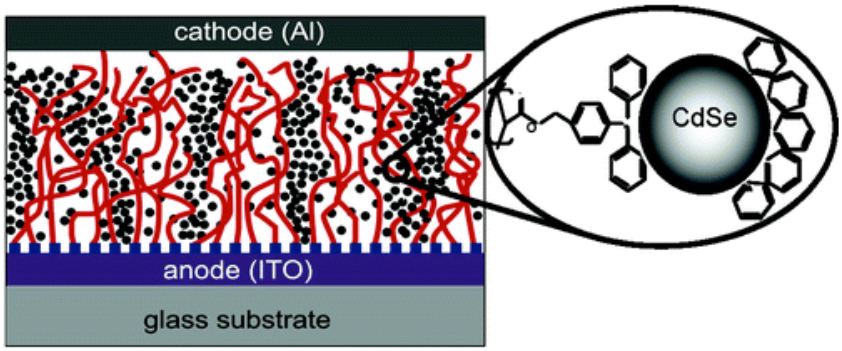

Figure 2: Optoelectronic device using polymer brush/CdSe nanoparticle composite as active layer.[7]

Surface grafted polymer brushes may be formed by two general methods. First is the grafting-to method wherein premade polymers are attached to a surface. Second, the grafting-from method, wherein initiation sites are formed on a surface, allowing polymer to be grown by addition of monomer. Making polymer chains beforehand using the grafting-to approach allows for greater control of molecular weight (MW) and polydispersity (PDI). It also allows one to employ any desired chemistries in the synthesis of the polymer without consideration of challenges associated with growing from a surface so long as the chains

contain a chemical group that will allow attachment to the surface. Premade chains may be immobilized on a surface covalently or through physisorption.[13] This method cannot be used to form densely grafted or thick brushes. Attached chains maintain a random coil conformation. The volume taken up by these coils blocks other chains from attaching to the surface within a certain proximity. This is commonly referred to as the "mushroom" conformation. Grafting-from benefits from the ability to form dense polymer brushes. The very short chains that are present towards the start of grafting do not block surrounding sites from initiation or monomer addition. As these chains grow, steric repulsion causes them to extend outward causing brushes to become thicker. The use of controlled polymerization techniques for grafting-from can afford similar control over MW, PDI, composition, and architecture to that afforded in solution polymerization by controlled techniques.[12] Methods for forming polymer brushes are depicted in **figure 3**.

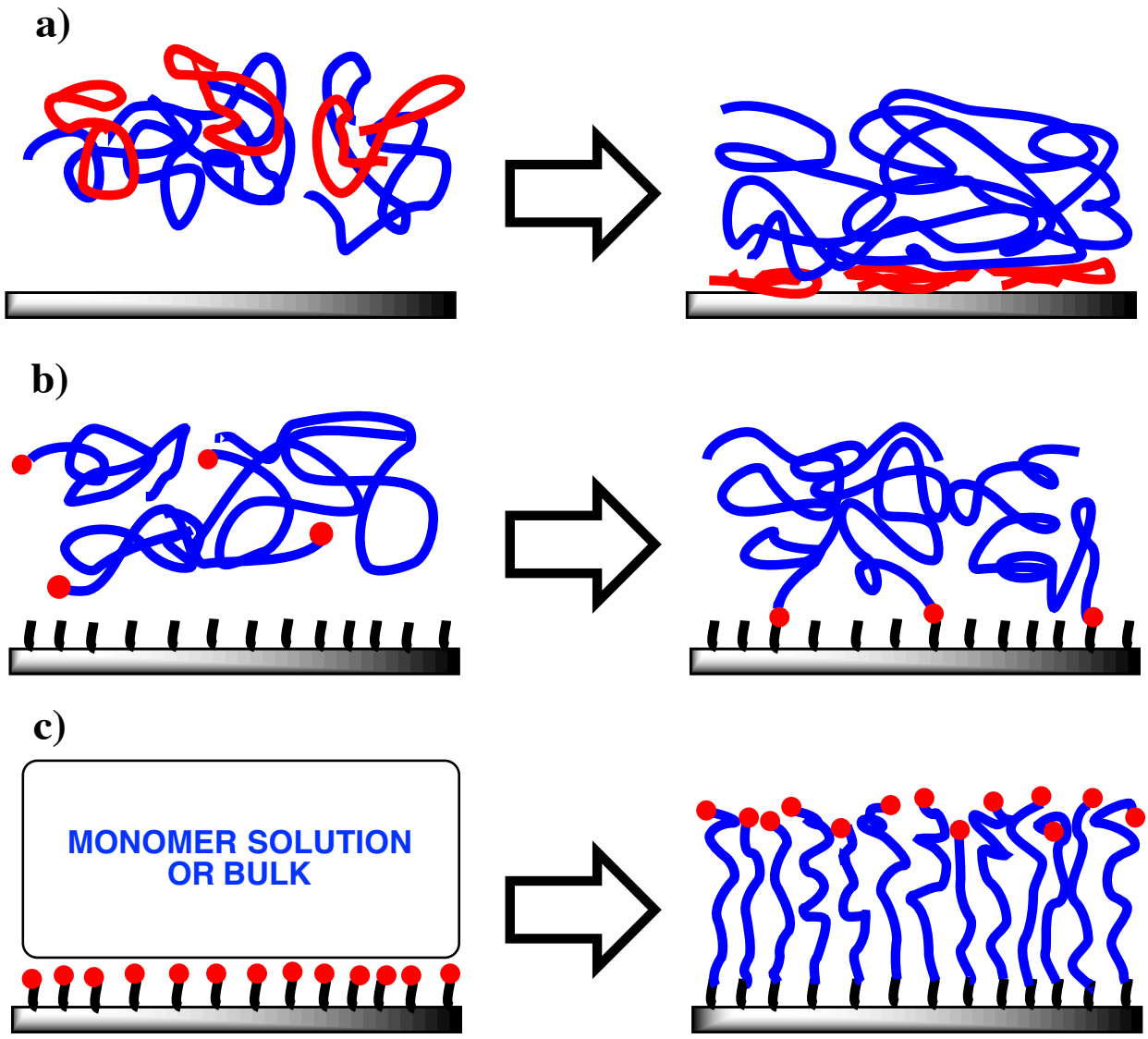

Figure 3: Representation of brushes formed by a) physisorption, b) grafting-to, and c) grafting-from.

Characterization of brushes made by grafting-from is difficult because of the small amount of polymer generated. Brushes are typically less than 100nm in thickness. A brush composed of a polymer having a bulk density of 1.0g/cm^2 and height of 100nm would have a mass of 0.010mg/cm^2. While few groups have detached polymer for analysis[14–16], interpretation of MW by indirect methods is more common. A "sacrificial initiator" technique is typically used in determining MW and PDI of the polymer grown. The

sacrificial initiator technique has also been reported to contribute to controlling the polymerization.[12] Initiator is added to the solution with the surface to be grafted-from and polymer is grown concurrently from the surface and in solution. Solution grown polymer is much more plentiful and can be easily analyzed following precipitation. Analysis of solution grown polymer is used as representative of the characteristics of the surface grown polymer. Marutani first reported the SI technique in growing PMMA from magnetite nanoparticles. **Figure 4** shows Marutani's technique. Comparing polymer grown in solution with polymer cleaved from the nanoparticles, he found MW and PDI were very similar with MW higher and PDI lower for solution grown polymer. Similarities diverged with percent conversion but not drastically.[17] Using MWs determined by the SI technique as well as measuring brush height allows for the calculation of grafting density using **equation 1**,

$$\sigma = (h\, p\, N_A) / M_n$$

Equation 1: Grafting density.

where σ is grafting density, h is brush height, ρ is bulk density of brush composition, and N_A is Avagadro's number.[18]

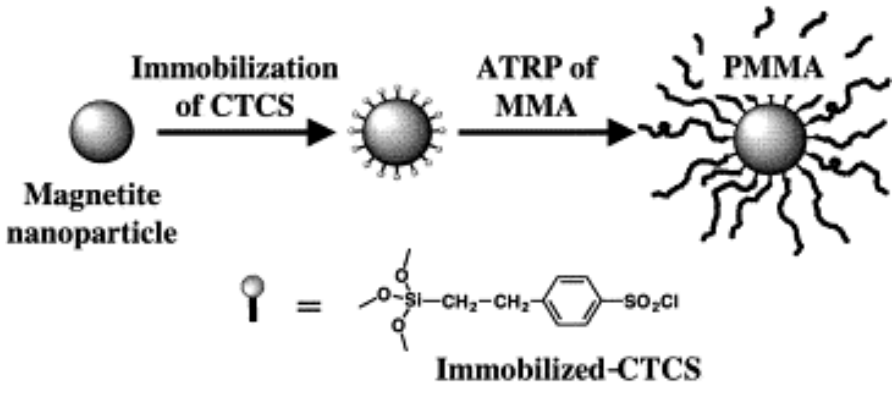

Figure 4: Marutani's ATRP of MMA onto functionalized magnetite particles. Sacrificial initiator technique was employed.[17]

1.3 Techniques for Brush Growth - ATRP: We have grown all our surface grafted polymer brushes using atom transfer radical polymerization (ATRP). ATRP is a widely used technique that allows for a high degree of control over polymer MW and low PDI's (<2). ATRP works via halogen exchange wherein a bromine or chlorine atom is transferred between the growing end of a polymer chain and a catalyst. While various catalyst systems have been developed, copper based catalysts are the most studied and commonly employed. The catalyst is solubilized by an organic ligand that typically contains tertiary or aromatic amines, which bind to the copper. The catalyst cycles between two oxidation states during the polymerization. Cu^{I} is an activator in that it can remove a halogen atom thus exposing a radical chain end allowing polymerization to occur. In this process Cu^{I} becomes the deactivator, Cu^{II}, which can then donate a halogen atom to a radical end thus rendering it dormant; suspending its polymerization. Controling the equilibrium between oxidation states of the catalyst controls the rate of polymerization. ATRP begins when an initiator, typically an organic halide, loses a halogen atom to Cu^{I}, exposing a carbon radical that attacks monomer thus beginning a polymer chain. As the polymerization proceeds, a certain ratio of active to dormant chains is formed, mirrored by a ratio of Cu^{I} to Cu^{II} species. These ratios, rates of activation and deactivation, choice of solvent and ligand, temperature, concentrations of monomer, catalyst, and initiator, among other factors, determine the rate of polymerization and degree of control. A lower concentration of active chains will confer a slower rate of polymerization but higher degree of control. If two active chain ends come into close enough proximity they will terminate by combination. ATRP greatly reduces termination events by reducing the number of chains that are simultaneously active. Polymerization of a wide variety of vinyl monomers is possible by ATRP including

functional monomers allowing for the formation of polyelectrolyte, hyperbranched, crosslinked, and biocompatible brushes among other possibilities.[19–23]

ATRP has been used as a technique for growing high-density polymer brushes on various substrates. As mentioned above, polymer brushes formed by grafting-to techniques result in low-density brushes due to the "mushroom" conformation grafted chains adopt, thereby blocking the surrounding surface from grafting of additional polymer chains. Traditional free radical polymerization can form high-density brushes but these brushes do not reach high MW and are polydisperse because of termination reactions. Controlled radical techniques such as ATRP allow for the production of brushes having both high density and MW. To reach high MW and brush thicknesses it is generally necessary to use both Cu^{I} and Cu^{II} in the polymerization. Kim et al. determined, due to the small amount of initiator in a brush growth system as compared to solution polymerization, a sufficient concentration of deactivator will not build up naturally to effectively control termination so it is necessary to add Cu^{II} as the start of the polymerization.[24] Their kinetic results are shown below in **figure 5**.

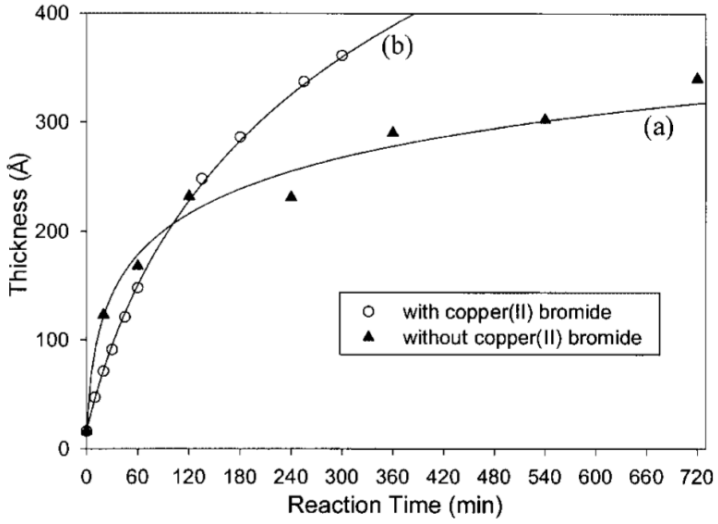

Figure 5: Brush thickness with reaction time using only Cu^{I} or 1/0.3 CuI/Cu^{II} molar ratio. Kim et al. polymerized methyl methacrylate from a gold surface using tris[2-(dimethylamino)ethyl]amine as a ligand in a THF/Me_3CN solvent mixture at room temperature. Initiator density was 0.25/nm^2.[24]

Brushes are considered in the high-density regime at roughly 0.10 chains/nm^2 or greater. Reports of grafting densities as high as 0.8 chains/nm^2 are uncommon[25] although we know of at least one report of grafting approximately 2 chains/nm^2 from magnetite nanoparticles.[26] The abnormal grafting density in this report was achieved using small particles (~10nm) as the grafting surface. The high curvature allows effective grafting density to decrease quickly with distance from the core.

Dense packing of brushes imparts favorable qualities for various applications. Due to inter-chain repulsion, chains in high-density brushes adopt a stretched conformation. This stretching scales with chain density and causes chain ends to be located at the surface of the brush.[25,27,28] Some resulting properties include resistance to compression and increased glass transition temperatures versus cast films.[29] Resistance to compression can translate to improved colloidal stability. Stabilization of silicon[30–32], gold[33], and magnetite[34] nanoparticles has been achieved through the growth of dense brushes via ATRP. Surface absorption and size exclusion properties are grafting density dependent. Increasing density

effectively creates smaller pores that allow for only particles of a certain size to penetrate the brush.[35] These properties are of particular importance in biological applications where surface adsorption of proteins must be avoided to prevent an immune response. The biocompatible polymer, poly(ethylene oxide) (PEO) has been used extensively in this regard,[35] sometimes through the use of oligo(ethylene glycol) methacrylate type monomers, which can be polymerized by ATRP.[19]

1.4 Block Copolymers and Bottlebrushes: Block copolymers (BCPs) have the ability to form ordered self-assembled structures based on the characteristics of their different blocks. While self-assembly of BCPs in the bulk is of tremendous importance and has allowed lithography techniques that have revolutionized electronics,[36] we focus on solution self-assembly here. BCP self-assembly in solution has been studied extensively for myriad of morphologies that can be formed[37,38] and their applications. BCP self-assembly is being utilized in medicine as drug-delivery vessels and probes for bioimaging,[39–44] and in catalysis as nanoreactors[45], among other applications.

Synthesis of BCPs including bottlebrushes can be achieved using various controlled techniques. However, the three general strategies employed in synthesizing specifically bottlebrush polymers are grafting-to, grafting-from, and grafting-through. Both the grafting-to and grafting-from strategies are analogous to strategies for surface brushes. A polymer backbone is synthesized then modified either by the grafting-to technique, wherein preformed grafts are covalently attached to the backbone, or the grafting-from technique wherein grafts are grown from initiation sites along the backbone. The “click” reaction has become popular in the grafting-to technique while various forms of controlled

polymerization are used to achieve grafting-from.[46,47] A third strategy is grafting-through wherein the monomers used may have oligomeric pendant groups or be macromonomers. In this way a bottlebrush may be synthesized in a single step if monomer synthesis is not required. Functionalized norbornenes or cyclobutenyl monomers for ring opening metathesis polymerization (ROMP)[48,49] and poly(ethylene glycol) methacrylate[50–52] for addition polymerizations have been employed in the grafting-through technique.

Self-assembly of BCPs including bottlebrushes in solution occurs as a result of interactions of the blocks with the solvent and each other, and the structure of the polymer itself as certain supramolecular morphologies are more favorable than others given certain relative block lengths. The hydrophobic effect is the major driving force for self-assembly in aqueous solutions and describes why it is possible for the self-assembly of amphiphilic molecules such as BCPs to be a spontaneous process although assembly decreases entropy. When the hydrophobic portion of an amphiphilic molecule is exposed to the aqueous solution, water molecules are ordered surrounding it. Upon assembly, the interfacial area between hydrophobic portions of the molecules and the solution is minimized and far fewer water molecules are ordered surrounding the hydrophobic portions. In this way the decrease in entropy associated with assembly of the amphiphilic molecules is more than offset by the increase in entropy associated with water molecules so the overall entropy of the system increases.[53]

Predicting and accounting for assembled structures becomes more complex with the increase of variables such as number of solvents, number and variation of blocks, and architecture of the polymers. Certain polymer blocks may also be especially sensitive to changes in temperature, pH, salt content or other stimuli.[11,54,55] Despite complexities, it is

possible to make approximations as to the behavior of BCP self-assembly based on packing parameter and reduction of free energy. Packing parameter (p) for BCPs is analogous to that for surfactants. Structure is predicted based on the volume (v), interfacial area (a), and length (l) of the solvophobic block using **equation 2**. For a packing parameter < ⅓,

$$p = v / a\, l$$

Equation 2: Packing parameter.

spherical micelles are predicted. Increasing to p = ⅓ – ½ tends to form cylindrical micelles, p = ½ – 1 forms vesicles and bilayers, $p \sim 1$ forms bicontinuous bilayers and increasing p further brings about inverted structures.[56] **Figure 6** illustrates amphiphilic polymers of different packing parameter. Free energy arguments used predict that the structures most likely to be formed are those giving the lowest free energy for **equation 3**, where G(core)

$$G(\text{micelle}) = G(\text{core}) + G(\text{interface}) + G(\text{corona})$$

Equation 3: Micelle free energy.

is the elastic free energy of the core, G(interface) is free energy of the core blocks at the interface with the solvent, and G(corona) is free energy arising from repulsive interactions between corona forming blocks.[57]

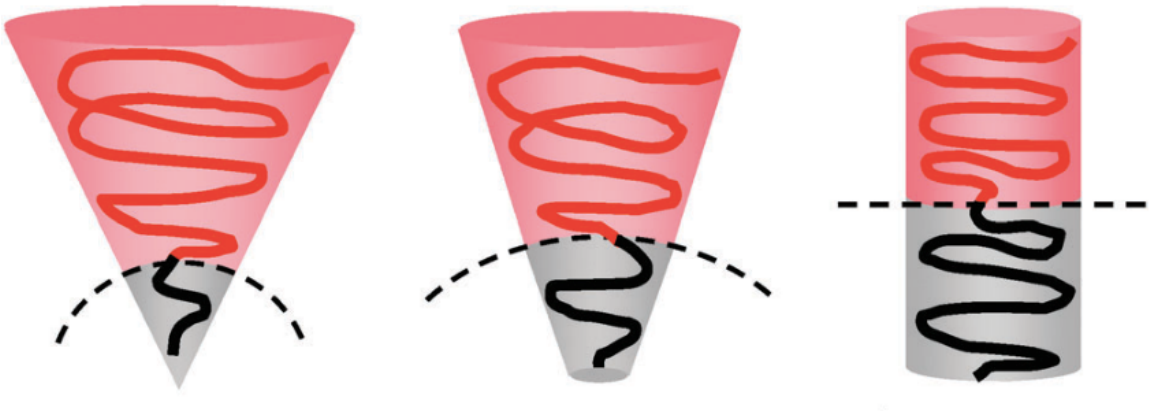

Figure 6: Packing parameter of block copolymers. Volume of solvophobic block increases left to right, increasing packing parameter. At low packing parameter, structures with highly curved interfaces such as spherical micelles are favored. At intermediate packing parameter and interfacial curvature, cylindrical micelles are common. At high packing parameter, structures such as lamellae and vesicles with low interfacial curvature are favored.

Bottlebrush polymers are a class of BCP and have been studied for many of the same applications but have certain unique characteristics based on their structure. Bottlebrushes are composed of many chains grafted along one central chain. Excluded volume interactions between grafts cause the central chain to exist in a highly stretched conformation. In this way, depending on grafting density, it is possible to design nanostructures or microstructures based directly upon the contour length of the central chain. Using core-shell or BCP architectures, depicted in **figure 7**, allow for self-assembly similar to linear BCPs in addition to stable single molecule structures such as nanocylinders.[58–60]

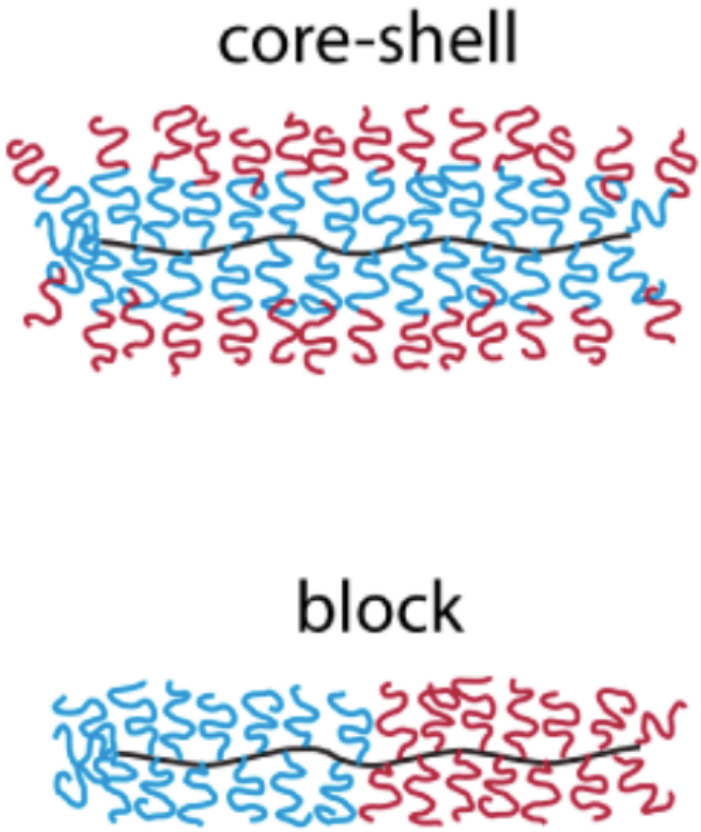

Figure 7: Core-shell and block bottlebrush structures.

1.5 Techniques for BCPs – Principals of Anionic Polymerization: The formation of well-defined BCPs including bottlebrushes requires the use of ionic, controlled radical, or metathesis polymerization. We have chosen to use anionic polymerization to form our bottlebrush copolymers. Anionic polymerization is a "living" technique capable of forming well-defined polymers of various architectures, including BCPs, with a high degree of control over MW and PDI. Polymerizations are commonly initiated by negatively charged nucleophiles such as alkyl lithiums. Electron transfer is another initiation mechanism by which an alkali metal transfers an electron to a neutral molecule, which may then transfer that electron to a monomer. Propagation occurs by nucleophillic attack from chain end to

monomer. A positive counterion pairs with the anionic chain end. This counterion may be tightly bound or well solvated depending on the solvating power of the reaction media. Solvation of the counterion controls the rate of propagation. Generally, solvents used are hydrocarbons or ethers. Such solvents have no acidic protons and because of their low dielectric constants, do not solvate the counterion to an extent that allows the chain end to behave as a free anion. No internal mechanisms of termination are inherent to anionic polymerization. Unlike in radical polymerization, chain ends cannot coterminate by coupling. Termination occurs by transfer of a positively charged atom or fragment that has been intentionally added to the reaction media or is present as an impurity. MW can be directly controlled by the ratio of monomer to initiator and increases linearly with monomer conversion. Synthesis of BCPs can be achieved through sequential monomer addition when the carbanion of the second monomer is of comparible or greater stability than the initial monomer. BCPs can also be formed using multifunctional initiators or functional terminating agents that allow reinitiation.[61,62]

PART 1 – Surface Grafted Polymer Brushes

Chapter 2 – Brush Growth from Nylon Membranes

2.1 Introduction: We have grown PMMA brushes by ATRP from porous nylon membranes. We cleaved the brush from the membrane and, using GPC, saw significant differences in MW and PDI versus solution-grown polymer. The MW distribution was consistently seen to be bimodal for the brush. While the chains that grow to high MW may effectively hide the population of low MW oligomers from surface analysis techniques, they composed a significant fraction of the distribution as observed by GPC. This oligomeric fraction may result from a combination of chains experiencing stunted growth due to low monomer diffusion to the base of the brush and early terminations occurring when the chains are very densely packed. Several groups have hypothesized termination as playing a role in brush thickness.[24,28] Huang et. al. grew 2-hydroxyethyl methacrylate (HEMA) from gold surfaces by ATRP. They reported loose packing of grafted chains indicating only 10% of surface bound initiator led to high MW polymer. Remaining initiator was hypothesized to have never reacted with monomer or to have been lost via termination reactions.[63] Our results corroborate and elaborate upon these findings, indicating that termination of many chains early during the surface-initiated polymerization is common. This can cause brush density to be much lower than if each initiation site grew high MW polymer. We are aware of only one other study that has reported bimodal MW distributions during surface initiated ATRP and the authors did not devote any discussion to this result.[16]

We also investigated the effect of adding sacrificial initiator to the solution. The sacrificial initiator technique for measuring MW and PDI of brush polymers remains contentious. Substrate geometry has been shown to affect the MW of grafted polymer.

Genzer et al. studied PMMA grown by ATRP from porous silicon (pore size ~50nm), anodically etched aluminum oxide (pore size~200nm) and in solution.[64] They found that MW was lowest for the porous silicon grown polymer and highest in solution. These findings were attributed to the progressive confinement of polymer chains, from solution to being tethered in an increasingly concave environment. Our nylon membranes are roughly flat or convex on the scale of graft spacing (see **appendix 1**). Computational studies of brush growth both with[65] and without[27] sacrificial initiator indicate brush density decreases with distance from the surface due to the stunted growth of shorter chains arising from a monomer concentration gradient as well as from termination. Increasing initiator density in these simulations exacerbates this phenomenon.

2.2 Membrane functionalization: Nylon membranes were hydroxymethylated in an acidic solution of formaldehyde. The resulting hydroxyl groups were reacted with 2-bromoisbutyryl bromide (BrIbB) to generate surface bound ATRP initiators. **Figure 8** depicts membrane functionalization. The functionalization was followed by Fourier transform infrared spectroscopy (FTIR) and x-ray photoelectron spectroscopy (XPS) shown in **figures 9** and **10** respectively. Both techniques verified the presence of the desired chemical groups. We chose XPS as a complementary technique because using FTIR, the carbonyl peak associated with the ATRP initiator overlapped partially with the nylon carbonyl peak and was relatively small.

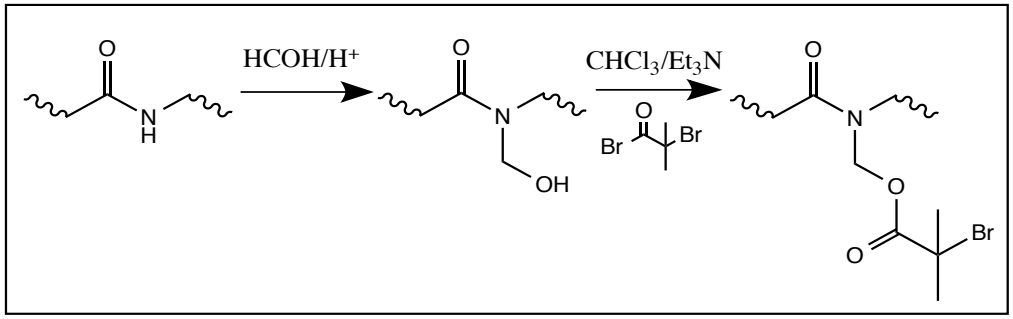

Figure 8: Reaction scheme for functionalization of nylon membrane.

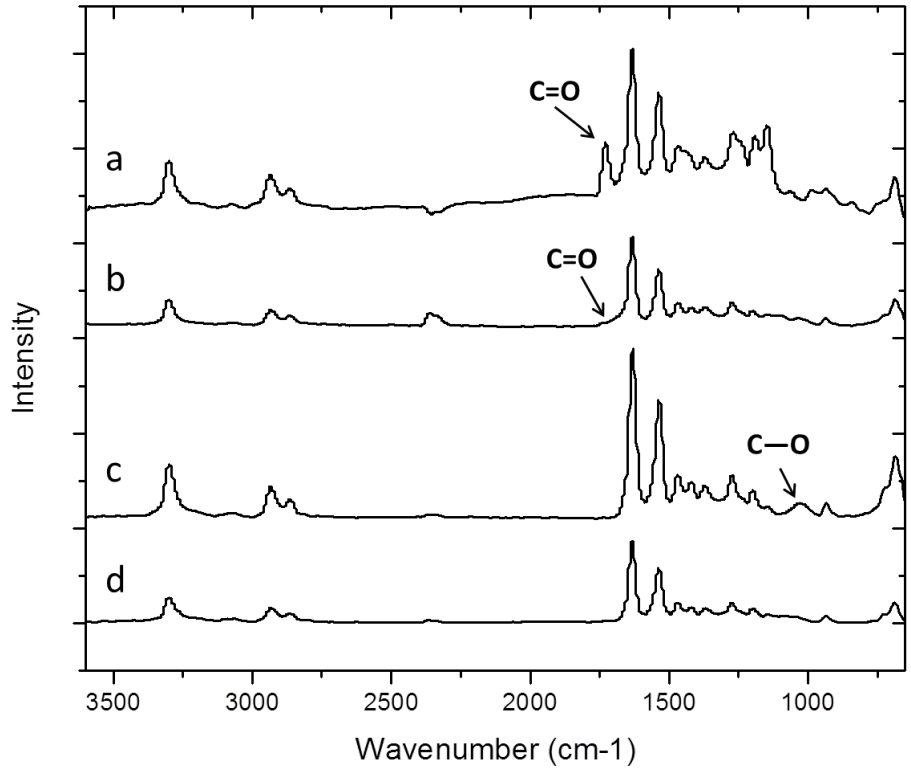

Figure 9: ATR-FTIR of nylon membrane in various stages of functionalization. a) PMMA grafted membrane showing carbonyl stretch at approximately 1700cm^{-1}. b) BrIbB functionalized membrane showing a shoulder on the nylon amide peak corresponding to carbonyl stretching. c) Hydroxymethylated membrane showing a carbon-oxygen single bond stretch at approximately 1030cm^{-1}. d) Unfunctionalized nylon membrane.

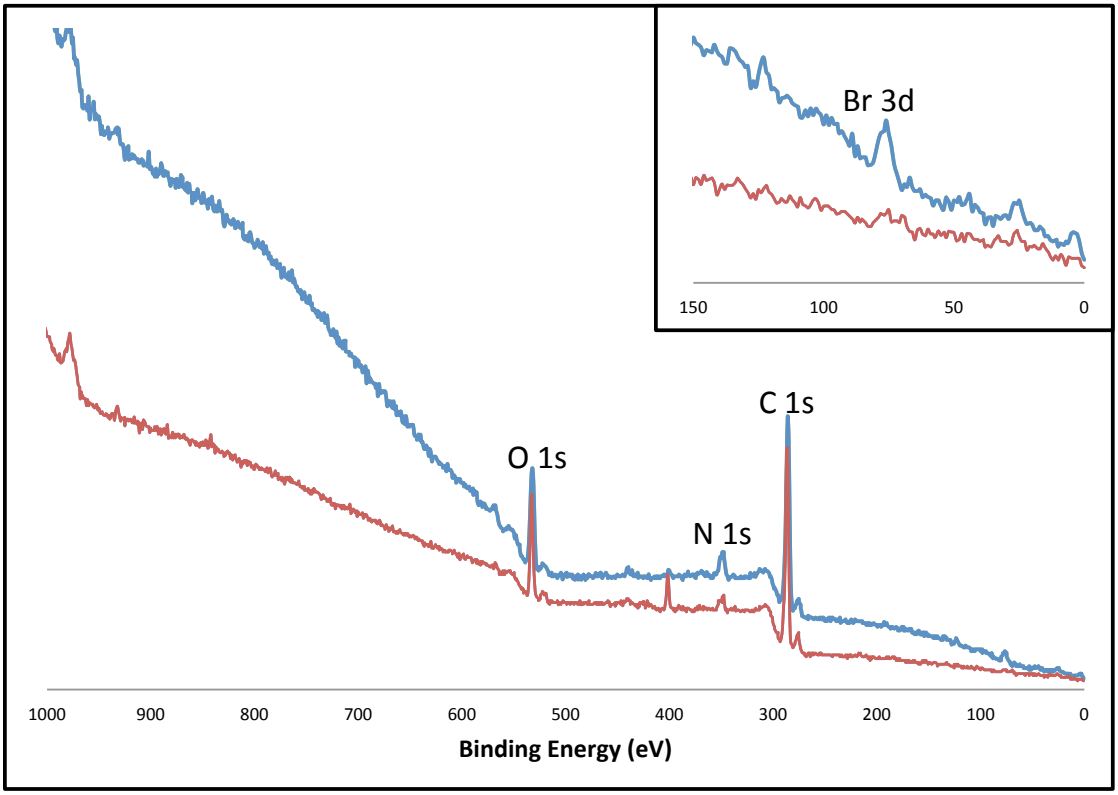

Figure 10: XPS spectrum of unfunctionalized (red) and initiator functionalized (blue) membranes. Inset, the region from 150eV to 0eV has been expanded. Electrons from the oxygen, nitrogen and carbon 1s shell were detected in both samples. Electrons from the bromine 3d shell were detected only in the initiator functionalized sample.

2.3 Polymerization from Nylon Membranes: All surface initiated polymerizations were performed by ATRP using methyl methacrylate (MMA) in acetone with CuBr, $CuBr_2$, and N,N,N′,N′,N″-pentamethyldiethylenetriamine (PMEDTA). Unless otherwise specified, our reaction media was as listed in the table below. Polymerizations were performed at room temperature in 50%vol. acetone.

Table 1: MMA polymerization reaction ratios.

	MMA	**CuBr**	**$CuBr_2$**	**PMDETA**
Molar Ratio	100	1.0	0.10	1.1

The relative density of polymer brushes was controlled by initiator density. We reacted hydroxymethylated membranes with 2-bromoisobutyryl bromide (BrIbB) and isobutyryl bromide (IbB). The two reagents were mixed in certain molar ratios before being added to the reaction mixure. Structures of the two molecules are seen in **figure 11**. Reaction with BrIbB imparts an ATRP initiator while IbB serves as a blocker that lacks the bromine necessary to initiate ATRP. We refer to the different initiator densities by the molar percentage of BrIbB in the BrIbB/IbB mixture that was used when functionalizing the membranes.

To get an idea of the relative reactivity of BrIbB and IbB, we performed the initiator functionalization reaction on hydroxymethylated cryogenically ground nylon in an NMR tube using equimolar amounts of the two reagents and $CDCl_3$ as our solvent. When reagents reacted with the nylon they were essentially removed from contributing to an NMR signal because the nylon floated at the top of the tube. We compared the relative integrations of peaks associated with either BrIbB or IbB in solution with and without added hydroxymethylated cryogenically ground nylon to determine how much of each reagent was being consumed by the reaction. Starting with a 50/50 molar mixture of the two, approximately 25% more BrIbB was consumed than IbB when hydroxymethylated cryogenically ground nylon was present versus when it was not. The NMR spectra are seen in **figure 12**. The greater reactivity of BrIbB compared with IbB indicates that our initiator densities are somewhat greater than we have listed.

Figure 11: Structures of a) 2-bromoisobutyryl bromide (BrIbB) and b) isobutyryl bromide (IbB).

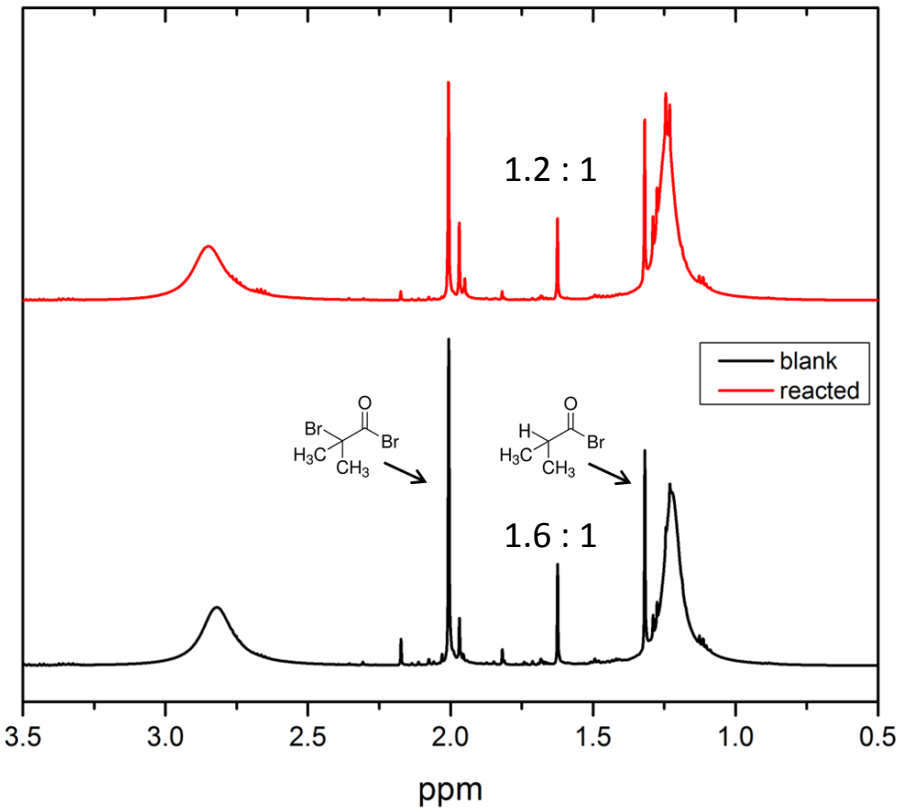

Figure 12: H¹-NMR of solutions of BrIbB, IbB, and triethylamine in deuterated chloroform. The reacted (red) sample contained cryogenically ground nylon that was not dissolved but reacted with the acid bromides. Changes in the BrIbB/IbB methyl peak area ratios indicate BrIbB is more reactive.

After a given reaction time, polymerizations were stopped with degassed methanol. Next, the solution was decanted into methanol to precipitate the polymer. The membranes were rinsed thoroughly with acetone, THF, and water to remove physically adsorbed free polymer and copper salts. Polymer was removed from the membranes using $NaOH_{(aq)}$ to cleave the ester bond anchoring the chains. Aside from cleaving chains for GPC analysis, the presence of polymer was confirmed by FTIR (**figure 15**), SEM (**figure 21**), and the increased hydrophobicity (**figure 13**) of the membranes. We also observed an expansion of the membranes in all dimensions as a result of grafting PMMA. When only IbB was used for membrane functionalization, no polymer was formed in solution or on the membranes.

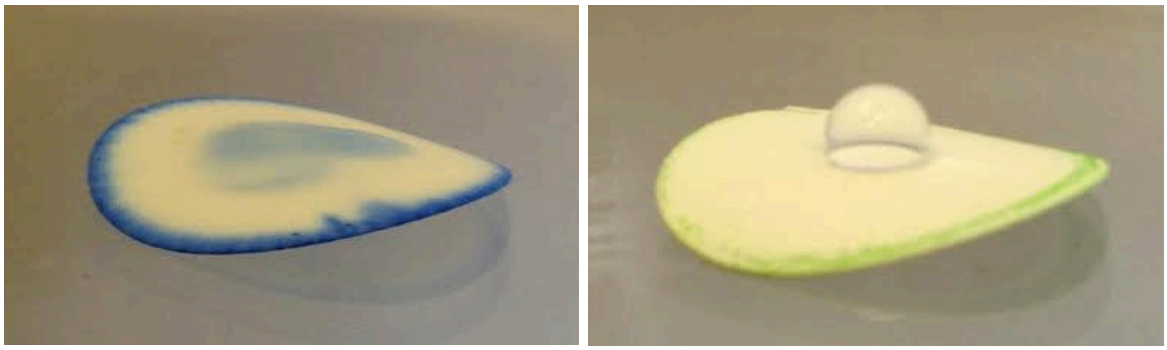

Figure 13: Demonstration of hydrophobicity of nylon membranes after PMMA grafting. A drop of water was applied to the surface of the membranes after ATRP for 5 minutes (left) and one hour (right). The drop applied to the membrane on the left was fully absorbed within seconds. Membranes pictured had not been rinsed to remove copper salts.

Although it was unclear why polymer formed in solution in the absence of sacrificial initiator, we hypothesize that either chains detached from the surface during polymerization or that a certain amount of initiator was physically absorbed to the membrane rather than covalently bonded. Although we thoroughly rinsed prior to polymerization it is likely that, due to the highly porous nature of our substrates, we may not have removed all unbound initiator.

Table 2: PMMA grafted nylon membrane results. SI is the molar ratio of sacrificial initiator relative to CuBr. The oligomeric peak fraction is GPC peak area of the oligomeric peak over total area of all peaks.

Sample	Initiator Density	SI	Time (hr)	MW_{soln} (kg/mol)	$MW_{surface}$ (kg/mol)	PDI_{soln}	$PDI_{surface}$	Oligomeric Peak Fraction
A1	100%	0.34	19	37.1	36.2	1.03	1.07	0.290
B1	25%	0.17	23	67.3	46.8	1.08	1.05	0.278
B2	100%	0.17	23	44.2	40.3	1.09	1.1	0.244
B3	50%	0	23	75.5	60.5	1.07	1.14	0.244
B4	100%	0	23	76.6	53.2	1.07	1.21	0.267
C1	30%	0	111	1070	321	2.46	3.15	0.073
C2	50%	0	111	862	314	2.55	3.38	0.048
C3	75%	0	111	960	337	2.39	2.73	0.350
C4	100%	0	111	948	229	2.33	3.29	0.272
D1	100%	0	2	n/a	17.6	n/a	1.18	0.752
D2	100%	0	4	n/a	27.5	n/a	1.08	0.559
D3	100%	0	8	n/a	20.3	n/a	1.15	0.273

2.4 Characterization of Brushes: In all of our polymerizations we have seen the GPC traces of surface-grown polymer chains to show both a high MW fraction similar to solution-grown polymer, and a low MW fraction corresponding to an oligomeric degree of polymerization (DP $\leq$ 20). Although we would predict this fraction should scale with initiator density whether originating from termination or stunted growth, we have seen an inconsistent relationship between initiator density (as determined by BIbB/IbB ratio in functionalization) and the relative ratio of the oligomeric MW peak area to total peak area in the GPC analysis. Lower initiator densities would be expected to delay either shielding or termination by coupling, thus allowing for higher MW to be achieved. In certain cases we observed the oligomeric fraction to be bimodal with its two peaks differing in MW by a factor of roughly two (see **figure 14** below). This possibly indicates that chains terminate by coupling. However, aside from the observation of the double MW peak, we did not observe the position of oligomeric peaks in the GPC to change significantly with either initiator density or time.

As seen in **figure 16** below, the position of the oligomeric peak was unchanged when we allowed the polymerization to proceed for 2, 4, or 8 hours. We would expect that even if growth was stunted due to shielding by larger chains, MW should show at least slight change over time if the chains are not terminated. Massing nylon membranes after polymerization shows a mass increase in a decaying fashion over time as seen in **figure 17**. We see this observation as comparable to similar trends in brush height, which others have attributed to termination.[24]

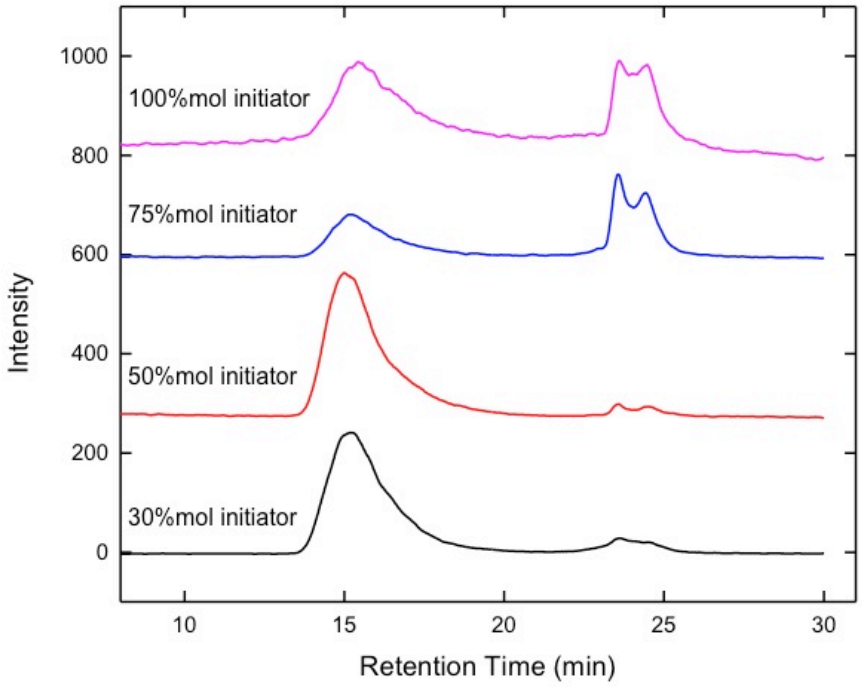

Figure 14: GPC spectra of polymer cleaved from nylon membranes made with varying molar ratios of BrIbB to IbB. Polymerizations ran 111 hours.

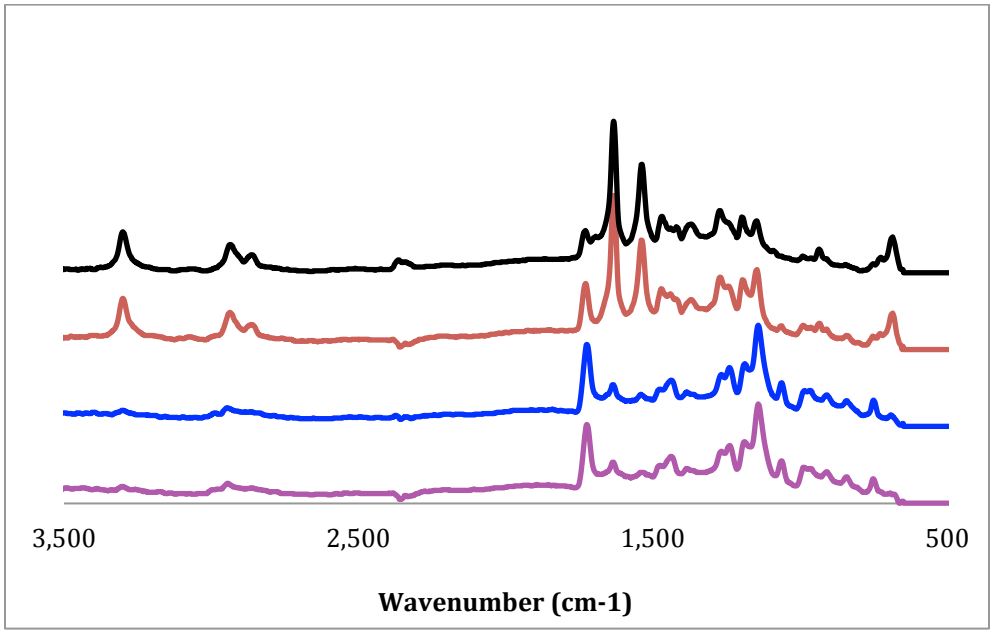

Figure 15: ATR-FTIR of nylon membranes after PMMA grafting 111 hours. The 30% (black), 50% (red), 75% (blue), and 100% (purple) initiator samples increase in amount of polymer grafted, which can be followed by increasing intensity of PMMA peaks and decreasing intensity of nylon peaks.

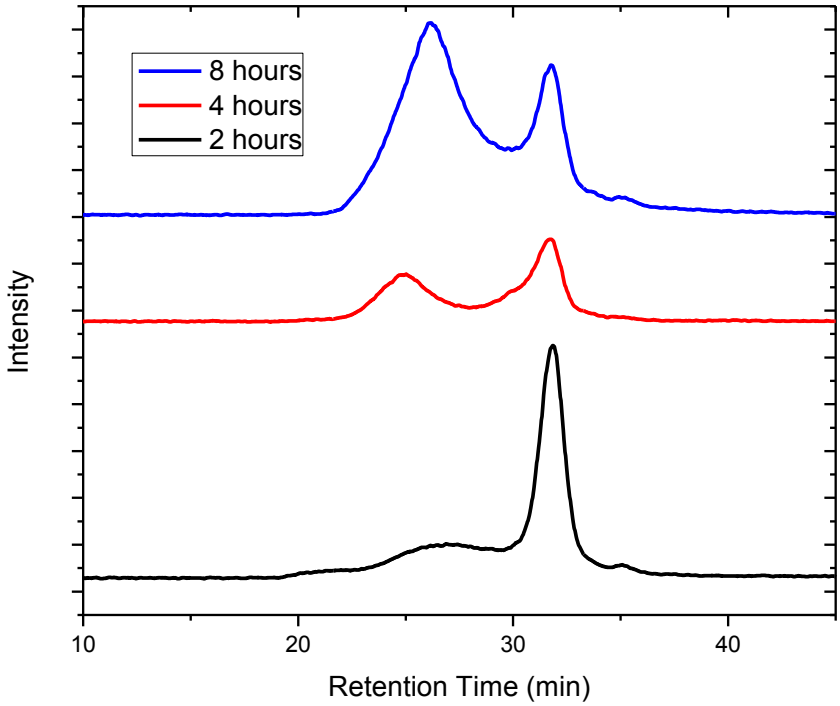

Figure 16: GPC of PMMA cleaved from filters after 2, 4, and 8 hours corresponding to samples D1, D2, and D3 respectively. The fraction total polymer made up by oligomeric chains decreases with reaction time

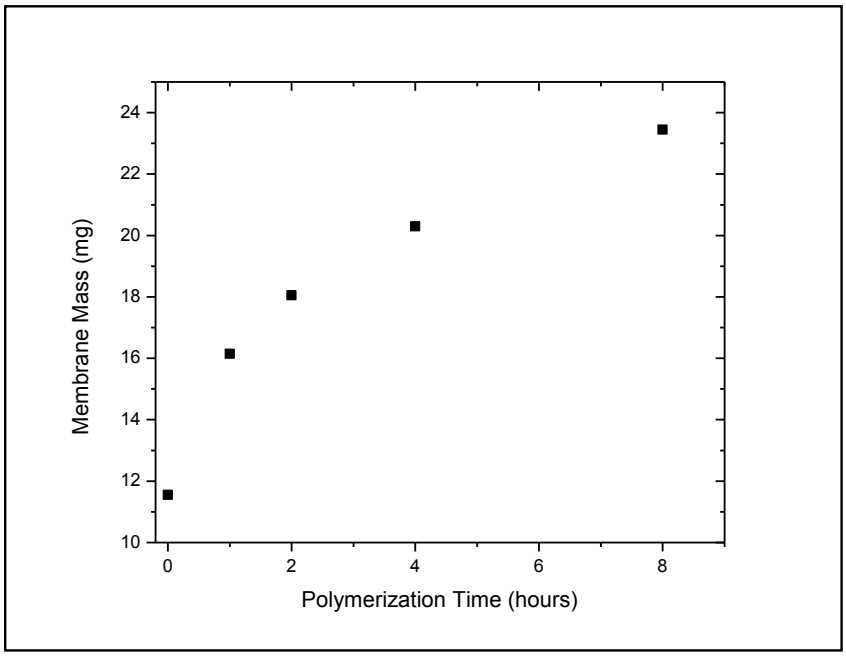

Figure 17: Mass of membranes with polymerization time after rinsing and drying. Times 2-8 hours correspond to samples D1-3. The sample at one hour was done in the same series as samples D1-3 however we could not remove enough polymer to perform GPC.

We investigated the possibility that the oligomeric GPC fraction was produced as a result of the process of cleaving chains from the membrane surface. This fraction could conceivably be from degradation of the polymer, hydrolysis of the polymer to poly(methacrylic acid), or could simply be a component of the nylon filter contaminating the sample. **Figure 18** shows the NMR spectra of polymer cleaved from the surface and polymer grown from sacrificial initiator in the same reaction. The two spectra are essentially identical indicating no contamination of the sample by nylon or other soluble impurities. We also do not observe any peaks that indicate PMMA is hydrolyzed to poly(methacrylic acid).

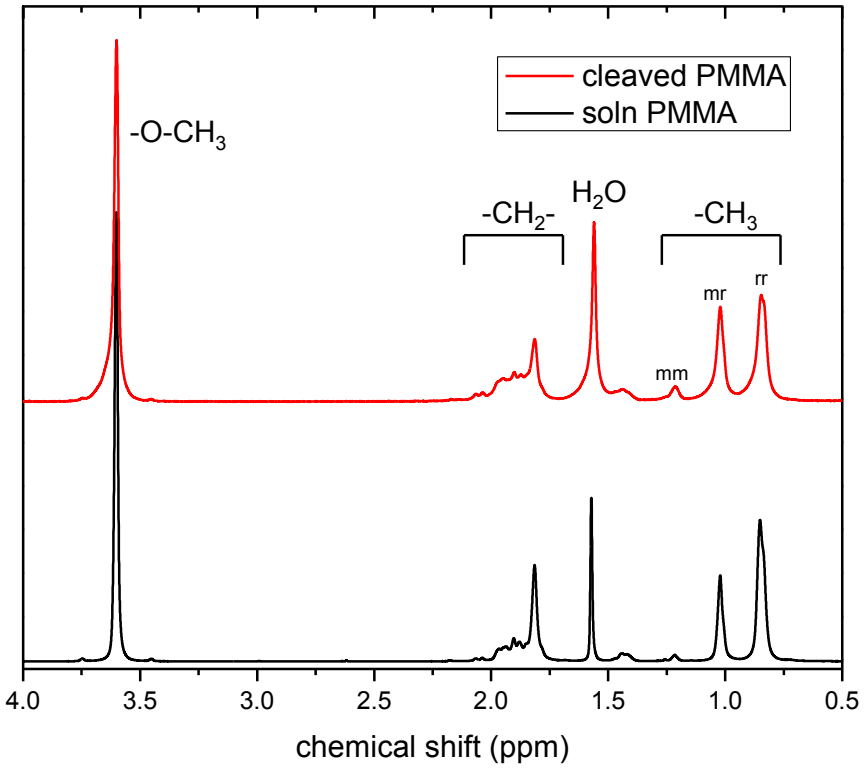

Figure 18: H1-NMR spectra of solution polymerized (black) and surface polymerized and cleaved (red) PMMA. Setting methoxy protons to an integration of 3.00 in each spectrum, the integrations for CH_2 and CH_3 protons are, respectively, 1.70 and 2.88 for cleaved PMMA and 1.76 and 2.99 for solution PMMA.

A control reaction in which commercially available 35kg/mol PMMA was treated with the same conditions used to cleave the surface bound polymer was used to show these conditions did not cause the degradation of the polymer, generating a low MW fraction. GPC in **figure 19** indicates no degradation of polymer. In order to make sure the polymer was appropriately exposed to the treatment we first dissolved the polymer in acetone then precipitated into the 0.5M $NaOH_{(aq)}$ solution before heating overnight.

Work by Sumita et al. on the hydrolytic degredation of poly(L-lactide)/PMMA blends show that even with twice the hydroxide concentration utilized in our cleaving step only poly(L-lactide) was degraded.[66]

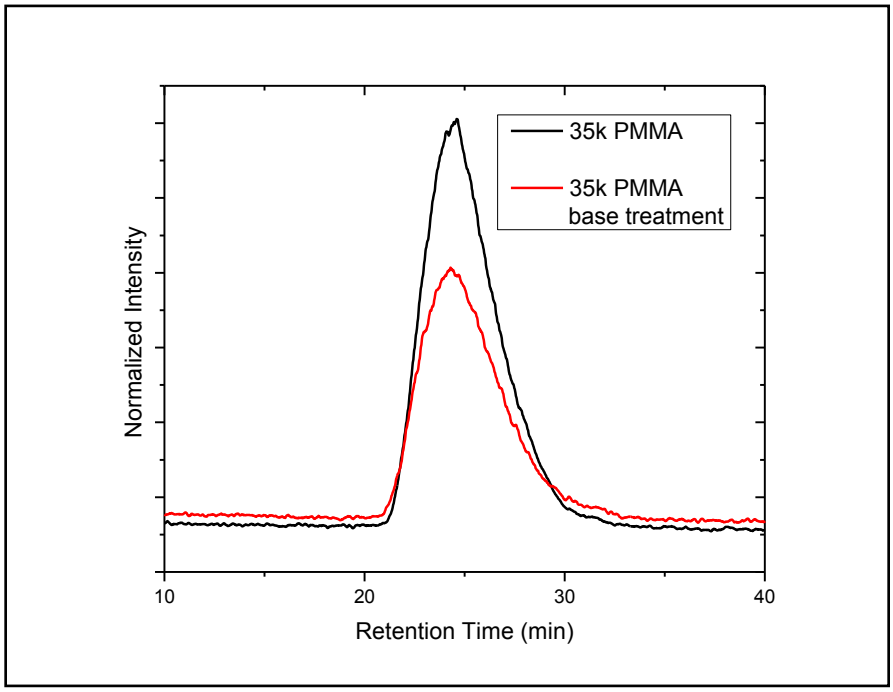

Figure 19: GPC of commercially available 35k PMMA before and after treatment with basic conditions used to cleave brushes. Intensiy offset for ease of viewing.

We also observed the membranes to expand over time uniformly in all dimensions during polymerization. SEM images show individual fibers in the membrane becoming

thicker and more spread apart from one another after polymerization and as initiator density was increased as shown in **figure 21**. After polymerization, membranes swell in good solvents for PMMA and contract in bad solvents as well as when dry. An approximately 30% increase in length was observed for a rectangular strip cut from a PMMA grafted membrane when soaked in THF after having been dry as shown in **figure 20**. Dense brushes can expand by more than 100% compared with their dry height once solvated[25] however, our brush expands within the framework of the membrane. Much of the expansion is therefore into empty porous space rather than contributing to pushing individual fibers of the membrane apart. **Figure 22** shows samples C1-C4 from **table 2** after PMMA grafting.

Figure 20: PMMA grafted membrane expansion in THF. A strip of PMMA-grafted nylon membrane dry (left) and in THF (right). The length increases by approximately 30%.

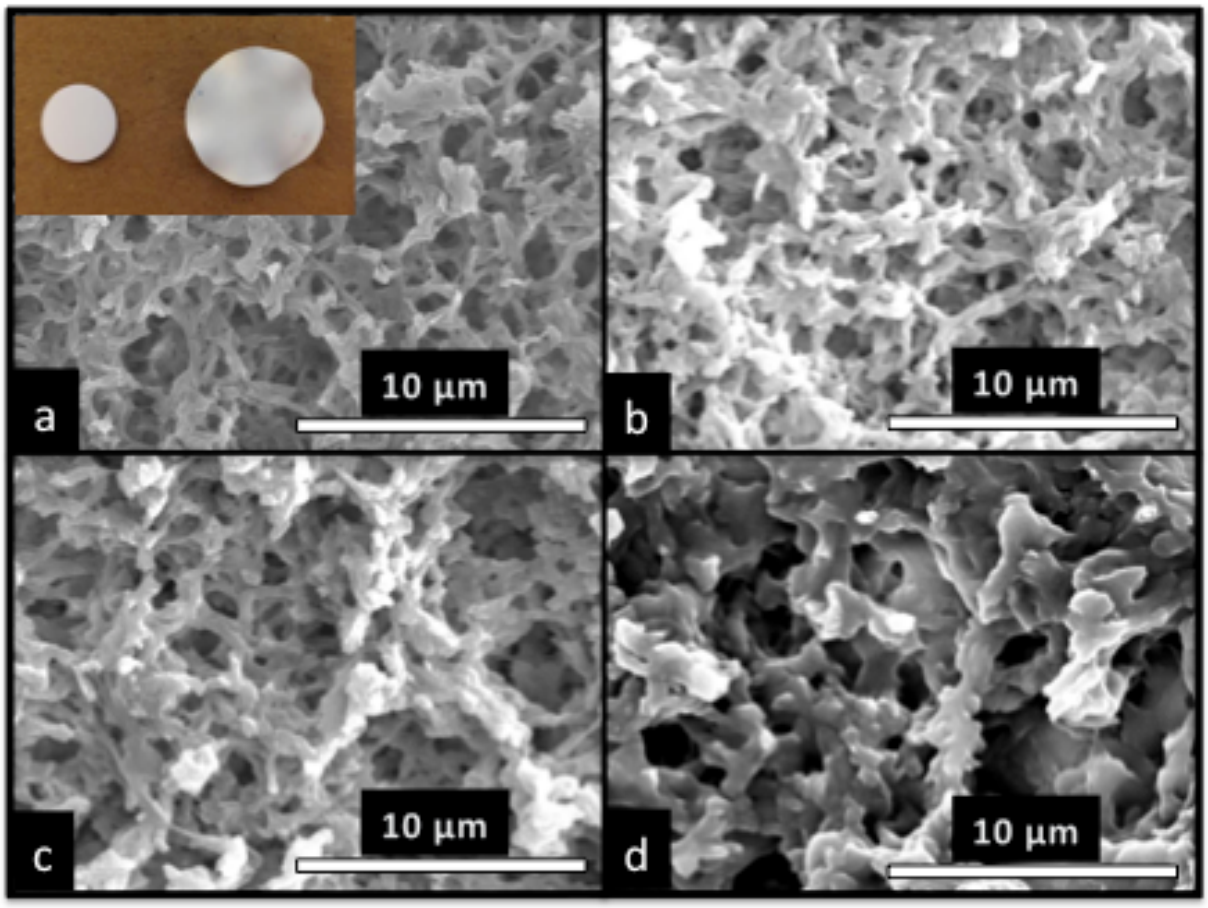

Figure 21: SEM images samples C1-C4 after PMMA grafting. a) unfunctionalized, b) 30%initiator, c) 50%initiator, d)100%initiator. Inset, a PMMA grafted membrane aside an ungrafted membrane. Ungrafted membranes are 13mm in diameter.

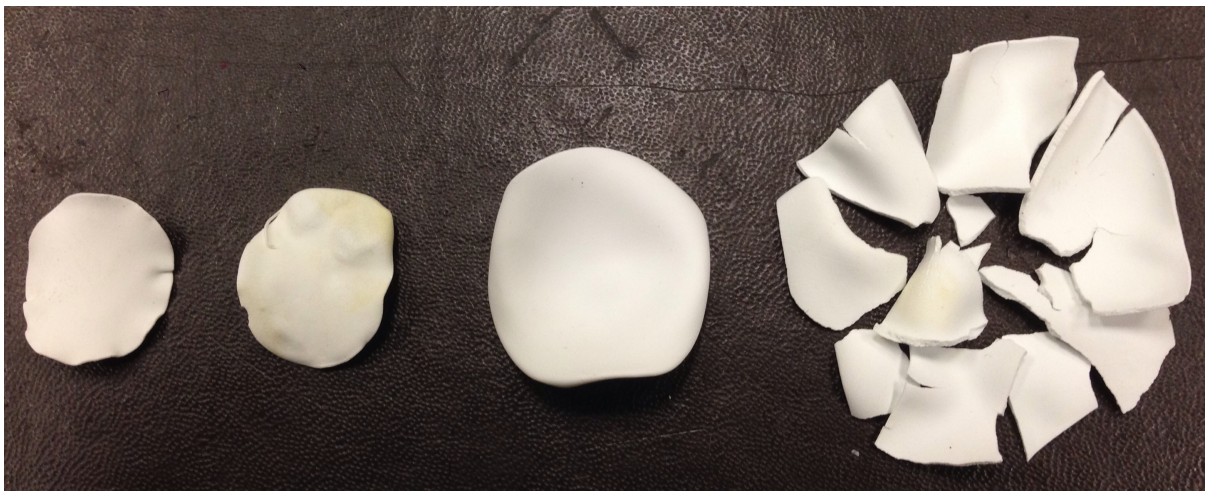

Figure 22: Samples C1-C4 from Table 2 after PMMA grafting. From left to right 30%initiator, 50%initiator, 75%initiator, 100%initiator.

2.5 Discussion: We believe that the oligomeric peak is a result of termination early during the polymerization. We see the dense packing of radical chain ends as facilitating termination in the brush as compared with solution grown polymer. Monomer exclusion may contribute to the oligomeric fraction although we do not have direct evidence of its effect. Cochran et al. reported the only other observation of a bimodal MW distribution for a brush grown by ATRP to our knowledge.[16] They do not discuss the result. However, the bimodal distribution was only observed for the highest initiator and grafting density studied, which was ~1 chain/nm^2, the highest reported value we are aware of for grafting from a flat surface. The fact that their lower MW for the bimodal sample was 39.9kDa rather than the oligomeric MWs we observed may be a result of their specific system, which had very high rates of polymerization.

We did not focus on calculating our grafting densities because the architecture of our substrate makes accurate measurements difficult. Cross-sectional SEM showed no contrast between nylon and PMMA. AFM would not be applicable because membrane fibers were uniformly coated. X-ray reflectivity would give poor signal due to the similar densities of PMMA and nylon as well as the rough nature of the membrane. Finally, ellipsometry would also be difficult due to membrane roughness as well as give poor signal due to similar refractive indices of nylon and PMMA. However, we did use the image analysis software, ImageJ, and **equation 1** to determine average fiber diameter in our membrane before and after grafting in one instance allowing the calculation of grafting density using 1.13g/cm^3 as the bulk density of PMMA.[67] The result, summarized in **Table 3**, is a grafting density that is very high for surface-initiated ATRP. We believe that at early stages of the polymerization,

grafting density is even greater to such an unsustainable degree that a fraction of the chains stop polymerizing due to a termination and monomer exclusion.

Table 3: Calculation of PMMA grafting density of sample C4 based upon average fiber diameter before and after polymerization.

Sample	Average fiber diameter (nm)	Average brush height (nm)	Grafting density (chains/nm^2)
Unmodified Membrane	411±132	N/A	N/A
C4	978±171	284	0.842

We find that the fraction of total polymer made up by oligomeric chains decreases with reaction time as seen in **figure16** showing samples D1-3. **Figure 17**, also corresponding to samples D1-3 shows that during the polymerization, membrane mass increases quickly over the first hour then slows such that mass increases nearly linearly with time. We believe the fast mass increase early in the polymerization is due to many densely packed chains growing and that the slower rate of mass takes over once many oligiomeric chains stop growing. These results support our hypothesis that there is a major termination event or confinement of short chains early during the polymerization.

The presence of a low MW fraction is not the only effect surface attachment has on the polymers that make up the brush. It is consistently observed that surface grown polymer is of lower MW and higher PDI than polymer grown concurrently in solution. **Figure 23** illustrates a typical comparison of solution grown and grafted polymer GPC traces. This finding agrees with previous computational and experimental reports by Genzer[64,65], Milchev[27], and Kim.[24] Additional BrIbB was used as sacrificial initiator for certain polymerizations. Polymer was formed in solution regardless of whether additional BrIbB was used however the MWs and PDIs of surface and solution grown polymer were more

similar when BrIbB was added. We also find that the use of sacrificial initiator does not appear effect the appearance of an oligomeric fraction.

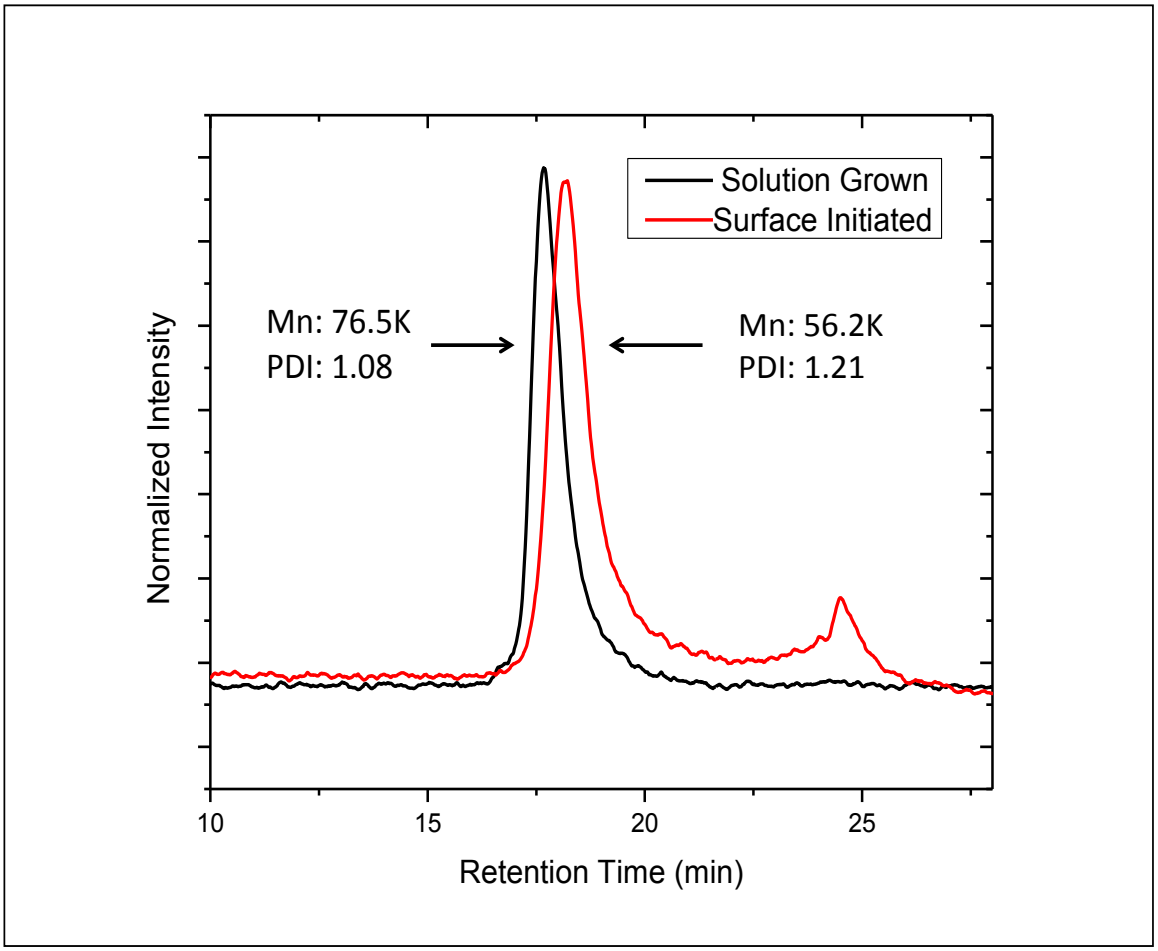

Figure 23: GPC spectra of solution grown (black) and surface initiated (red) PMMA. Sample B4 from table 2.

2.6 Conclusion: Our work is an example of how analysis of solution-grown polymer does not give an accurate representation of surface-grown polymer. We have observed, as have others, that polymer grown from a surface by controlled radical techniques will yield a lower MW and higher PDI than polymer concurrently grown in solution. While this disparity is less stark when using sacrificial initiator, we see the largest inconsistency between solution and surface grown polymer as being the oligomeric fraction that develops

only in the brush. We attribute the oligomeric fraction largely to termination. Termination of short chains may accelerated by impeded monomer diffusion into the brush causing short chains to be in an environment of depleted monomer. We also see the high local concentration of active chain ends in surface initiated polymerization (especially early during polymerization) as a source of bimolecular terminations.

2.7 Experimental:

Materials: 2-bromoisobutyryl bromide (BrIbB, Acros, 98%), isobutyryl bromide (IbB, TCI, >95%)**,** copper (I) bromide (Strem Chemicals, 98%), copper (II) bromide (Fisher, reagent grade), N,N,N',N",N"-pentamethyldiethylenetriamine (PMDETA, Aldrich, 99+%), methanol (Aldrich, 99.8%), tetrahydrofuran (THF, Fisher, histological grade), NaOH (Fisher, pellets), formaldehyde (Fisher, 37%wt., Certified ACS), phosphoric acid (Acros, 85%wt.) and 35k PMMA (Scientific Polymer Products Incorporated) were used as purchased without further purification. Acetone (Fisher, histological grade) was dried with $CaSO_4$ then distilled and stored over 3Å molecular sieves. Methyl methacrylate (Aldrich, 99%) was rinsed three times with 5%wt. $NaOH_{(aq)}$ to remove monomethyl ether hydroquinone, three times with distilled water to remove NaOH, then dried with $CaCl_2$, distilled under reduced pressure, and stored over CaH_2 at -32^{o}C. Triethylamine (Acros, 99%) and chloroform (Fisher, histological grade) were dried with $CaSO_4$, distilled under reduced pressure, then stored over CaH_2.

Membrane Functionalization: 13mm diameter Whatman 0.2μm nylon membrane filters were functionalized for ATRP by techniques previously employed[68]. Membranes were rinsed with acetone and dried with air. Membranes were placed in 10ml 37%wt.

formaldehyde and 0.4ml 85%wt. phosphoric acid was added. Membranes were stirred in this solution for approximately two hours at 60-70°C then rinsed with distilled water followed by acetone and dried under vacuum. Next, membranes were placed in a vial with 10ml chloroform and 0.8ml triethylamine and chilled on an ice bath while solutions of BrIbB and IbB were made at various molar ratios from 0-100% BrIbB. 0.2ml of acid bromide solution was added to the vial in each case and white smoke was formed. If acid bromide was not added in an air-free environment, the flask was topped with argon or nitrogen before sealing and stirring on ice bath. The bath was allowed to come to room temperature and the membranes sat in the solution approximately two hours. Next, the membranes were rinsed with acetone and distilled water before drying under vacuum.

Polymerization: Polymerization was set up inside a nitrogen filled glovebox to avoid oxygen contamination. CuBr (0.48mmol, 0.067g), $CuBr_2$ (0.048mmol, 0.011g) and PMDETA (0.51mmol, 0.11ml) were dissolved in acetone (5.0ml) then MMA (48mmol, 5.0ml) and initiator functionalized membranes were added and allowed to stir for an allotted period of time. If sacrificial initiator was used it was added last via syringe at the start of the polymerization. Polymerization was terminated with degased methanol. Membranes were rinsed extensively with acetone. Sonication was employed to assist in the removal of physically adsorbed solution grown polymer.

Precipitation and Chain Cleavage: Solutions were decanted to methanol. The resulting precipitated polymer was redissolved in THF and precipitated into methanol to assist in the removal of copper salts. Polymer chains were cleaved from nylon membranes by stirring overnight in a 0.5M $NaOH_{(aq)}$ solution at approximately 60°C then the solutions were decanted into methanol.

FTIR: Fourier transform infrared spectroscopy (FTIR) was performed using a Magna-IR 560 spectrometer with an ATR accessory. Samples were prepared by drying in a vacuum oven and were used without further modification.

XPS: X-ray Photoelectron Spectroscopy (XPS) was performed using a Phi Multiprobe Model 25−120 instrument. Samples were adhered to a sample holder using carbon tape. The binding energies were used to determine the presence of carbon, oxygen, nitrogen, and bromine atoms.

GPC: Gel Permeation Chromatography (GPC) was preformed using a Waters 717 plus autosampler with THF as eluent, a Waters 1515 isocratic HPLC pump, a Jordi fash gel DVB column, and a Varian 380-LC ELSD detector. Samples were prepared by dissolving in THF then filtering through a 0.45micron syringe filter. Molecular weights were determined by comparison with a standard curve constructed with narrow PMMA standards.

Electron Microscopy: For scanning electron microscopy (SEM) analysis, nylon samples were adhered to a SEM stub using carbon tape. Samples were then coated with gold/palladium using a Polaron Instruments SEM coating unit E5100 for approximately 40s. Images were taken on a JEOL 6335F field emission FESEM instrument operating at 12 kV accelerating voltage and a 8-15mm working distance.

NMR: Nuclear magnetic resonance (NMR) was performed using a Bruker DMX500 high-resolution digital NMR spectrometer and analyzed with Bruker XWINNMR software. Samples were prepared in $CDCl_3$ with TMS standard.

Chapter 3 – Brush Growth from Boron Nitride Nanosheets

3.1 Introduction: Boron nitride, a chemical compound with the formula BN, has excellent thermal and chemical properties. Its hexagonal form (hBN) has a structure analogous to graphite including having a stacked morphology and is used commercially as a cosmetic additive or lubricant in high temperature applications.[69] Additionally, like graphite, hBN shows high thermal conductivity and mechanical strength. In contrast to graphite, hBN is more chemically inert, stable at high temperature in air, and is an electrical insulator.[70] Like graphite and other two-dimensional materials, to exploit the favourable properties of hBN in a composite material, it is advantageous to exfoliate its stacked structure and hinder the tendency towards aggregation and restacking.[71–74] Cui et al. among others have developed methods for the exfoliation and functionalization of hBN.[71,75–82] In collaboration with Cui, we have been successful in growing polymer chains from exfoliated hBN by applying a technique for surface-initiated polymerization. Our polymer-grafted hBN can be uniformly dispersed in a polymer matrix. Visually comparing composites formed with grafted versus ungrafted hBN clearly demonstrates the improved dispersibility and tensile testing demonstrates improved mechanical properties. Starting with hydroxylated hBN (BNO) that has been functionalized with a diisocyanate we attached an initiator for ATRP and grew PMMA. While we chose to work with PMMA in this study, due to the thermal and chemical stability of BN, we see no reason why our technique could not work for any monomer or conditions currently being utilized for surface-initiated ATRP. Composites of ungrafted hBN/PMMA displayed similar properties to polymer/graphene nanosheet composites that have shown increases in Young's modulus along with decreases in elongation and

toughness[83] while composites using PMMA grafted BNO showed improvements in Young's modulus as well as elongation and toughness.

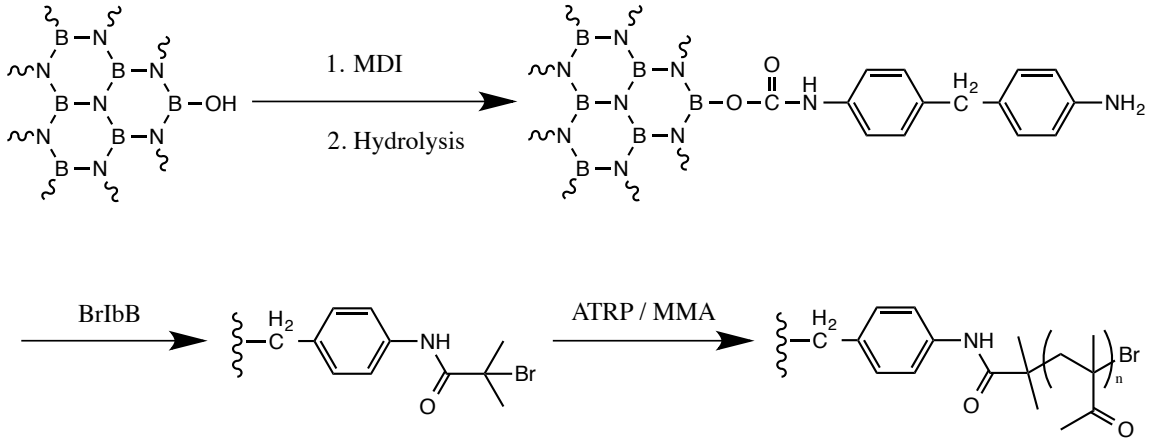

Figure 24: Reaction scheme for grafting PMMA from boron nitride oxide.

3.2 Functionalization of Boron Nitride: Our reaction scheme is illustrated in **figure 24**. Excess 4,4'-methylene di-p-phenyl diisocyanate (MDI) was added to BNO prepared by Cui using techniques described previously[75]. Excess MDI was used to avoid linking of BNO sheets by the difunctional molecule. Next, we hydrolysed the free isocyanate of MDI functionalized BNO (BN-MDI) to produce a primary amine (BN-NH_2). BN-NH_2 that was reacted with BrIbB to generate a surface bound ATRP initiator. FTIR analysis shown in **figure 25** confirms that initiator was bound to the nanosheets.

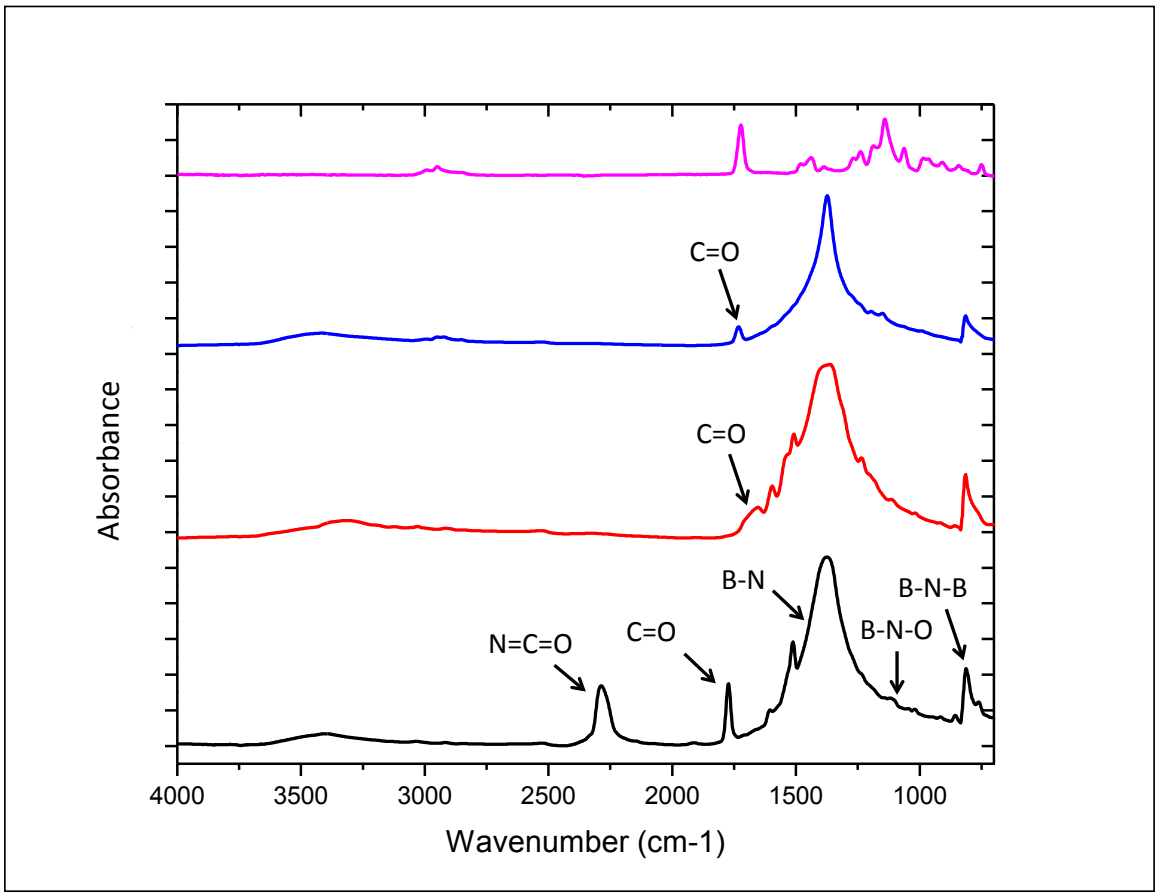

Figure 25: FTIR spectra of functionalized BN-MDI. BN-NH_2 (black) showed unreacted isocyanate at 2250cm^{-1}, a carbonyl peak corresponding to the carbamate formed by reaction of -B-OH with -N=C=O at 1760cm^{-1}, and B-N broad stretch centered at 1400cm^{-1}. Amine peaks are faint between 3250 and 3500cm^{-1}. BN-Br (red) shows a new carbonyl stretch 1670cm^{-1}. BN-PMMA (blue) shows a carbonyl peak at 1710cm^{-1} corresponding to PMMA. The spectrum in pink is the filtrate, which contained mostly PMMA.

3.3 Polymerization from Boron Nitride: Polymerizations were set up in a nitrogen atmosphere glovebox. BN-Br was added to a solution of CuBr, $CuBr_2$ and acetone followed by MMA and stirred at room temperature. PMMA grafted boron nitride (BN-PMMA) was collected by vacuum filtration and rinsed with THF and re-filtered several times to remove unbound PMMA. PMMA was confirmed by FTIR. Polymer in the filtrate was precipitated in methanol. GPC analysis of polymer that came out with rinsing gave a Mn of 174kg/mol and PDI of 2.52. We took this to be roughly similar to polymer grown from the surface of boron nitride. The same polymerization conditions were used to synthesize control PMMA

by adding an appropriate molar amount of BrIbB rather than BN-Br to achieve a similar MW to that of the rinse polymer. GPC analysis of control PMMA gave Mn of 199kg/mol and PDI of 1.15. See **appendix 2**.

3.4 Characterization of PMMA Grafted Boron Nitride and Composite: Further characterization and formation of a BN-PMMA/PMMA composite was performed by our collaborator, Zhenhua Cui. Herein, we decribe results from our upcoming publication[84] however, we do not include figures as these will be included in our collaborator's dissertation.

Thermogravimetric analysis (TGA) was used to find the weight percentage of PMMA in BN-PMMA. Control PMMA began to degrade at after 250°C and was completely degraded by 280°C. BN-PMMA began to degrade earlier at slightly below 200°C and was completely degraded at approximately the same temperature as the control. It was determined that PMMA made up 53% by weight of the BN-PMMA.

SEM analysis shows a clear difference between BNO and BN-PMMA. BN-PMMA has smooth edges and a polymer-like appearance while BNO has more sharp edges and individual sheets are clearly discernible from one another. Mixing BNO and ungrafted PMMA in THF and precipitating into methanol gives SEM images that appear to show BNO structure with phase separated clumps of PMMA.

Samples of BNO or BN-PMMA were added to a solution of PMMA in THF and cast onto glass slides. The BNO sample aggregates forming BNO rich domains while the BN-PMMA sample remains a well-dispersed homogeneous composite.

Tensile testing was performed to determine mechanical properties of a PMMA composite with 1% by weight BN-PMMA. For comparison, pure PMMA and 1% by weight hBN composite controls were also made. Compared with pure PMMA, the BN-PMMA composite shows improvements of 6.2% in Young's modulus, 13% in elongation, and 31% in work toughness while the hBN composite shows decreases in elongation and work toughness and only a 1.8% increase in Young's modulus.

3.5 Discussion and Conclusion: We attribute the increases in toughness and modulus of the composite to the modulus of hBN, the dispersion of nanosheets, and the strength of the interaction between boronitride and the PMMA matrix. hBN has a high modulus[85] that contributes to the force needed to deform the composite. The homogeneous dispersion of hBN achieved using BN-PMMA takes greater advantage of this property than when heterogeneous hBN rich domains are formed using ungrafted material. The compatibility of the PMMA in BN-PMMA with the PMMA matrix increases the interaction between BNO and the matrix. Similar impacts on mechanical properties have been reported for well dispersed boron nitride nanosheet composites.[76]

Improvements to elongation can also be attributed to enhanced dispersion of BN-PMMA and compatibility due to covalently attached PMMA allowing greater deformation prior to failure. The pBN/PMMA composite showed reduced elongation prior to failure in comparison to pure PMMA. The shear field generated by elongating the sample can cause aggregated hBN to break apart initiating a crack. Additionaly, hBN rich domains have weaker interactions with the rest of the composite. The non-uniformity of the composite gives sites for cracks to initiate.

The composites we have formed represent a step forward in compatibilizing thermally conductive, electrically insulating nanofillers for polymer composites. Our approach is a scalable method for the production of well-dispersed boron nitride nanocomposites with physical properties that are as good or better than the pure polymer.

3.6 Experimental

Materials: 2-bromoisobutyryl bromide (BrIbB, Acros, 98%), copper (I) bromide (Strem Chemicals, 98%), copper (II) bromide (Fisher, reagent grade), 4-dimethylaminopyridine (DMAP, Aldrich, 99%), dimethlyformamide (DMF, Fisher, certified ACS grade), N,N,N',N",N"-pentamethyldiethylenetriamine (PMDETA, Aldrich, 99+%), methanol (Aldrich, 99.8%), and tetrahydrofuran (THF, Fisher, histological grade) were used without further purification. Acetone (Fisher, histological grade) was dried with $CaSO_4$ then distilled and stored over 3Å molecular sieves. Methyl methacrylate (Aldrich, 99%) was rinsed three times with 5%wt. $NaOH_{(aq)}$ to remove monomethyl ether hydroquinone, three times with distilled water to remove NaOH, then dried with $CaCl_2$, distilled under reduced pressure, and stored over CaH_2 at -32^oC. 1-methyl-2-pyrollidinone (NMP, Fisher, laboratory grade) was dried with CaH_2 then distilled under reduced pressure. Triethylamine (Acros, 99%) was dried with $CaSO_4$, distilled under reduced pressure, then stored over CaH_2.

Functionalization: 700mg BN-MDI was dispersed into approximately 5ml DMF then added drop-wise to approximately 100ml diH_2O while stirring at room temperature. Drop-wise addition and a large dilution was used to avoid the reaction between BN-MDI and BN-NH_2 which would form urea linkages. The mixture was degased while stirring and allowed to sit overnight. The resultant white powder was collected by vacuum filtration and dried

under vacuum. 590mg BN-NH_2 was added to a solution of 15ml NMP, 0.18ml triethylamine and 72mg DMAP in a scintillation vial. This mixture was chilled to 0°C on an ice bath then 0.30ml BrIbB was added under a stream of nitrogen. The vial was sealed and the mixture was allowed to come to room temperature and stirred overnight. The powder was collected by vacuum filtration and rinsed with methanol then dried under vacuum.

Polymerization: In a nitrogen atmosphere glovebox, 300mg BN-Br was added to a solution of 108mg copper (I) bromide (0.753mmol), 16mg copper (II) bromide (0.071mmol), 0.172ml PMDETA (0.824mmol), and 8.0ml acetone followed by 8.0ml MMA. The mixture was stirred at room temperature for 19 hours after which the solution became viscous and was diluted with THF. The powder was collected by vacuum filtration and the polymer in the filtrate was precipitated in methanol. The powder was rinsed with THF and re-filtered serveral time before drying under vacuum.

FTIR: Fourier transform infrared spectroscopy (FTIR) was performed using a Magna-IR 560 spectrometer with an infrared microscope accessory. Samples were prepared by drying in a vacuum oven and were pressed between diamond plates to allow transmission of infrared beam.

Additional characterization performed by Cui.[84]

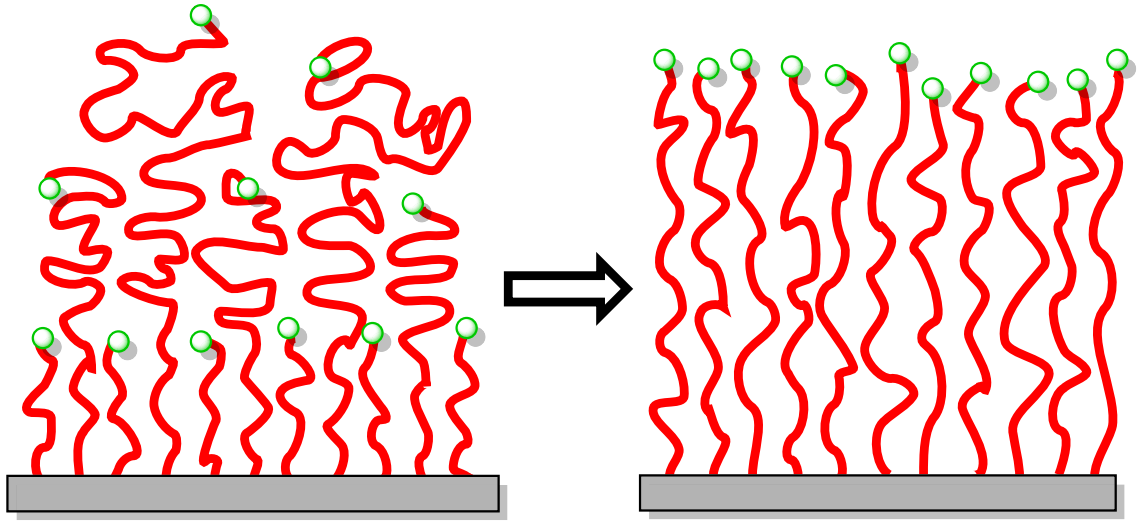

Figure 26: Depiction of improvement in brush polydispersity.

4.1 Sources of Nonuniformity and Potential Applications of Uniform Brushes: : Brush uniformity can be effected by chain termination but can also be a symptom of monomer density gradient. Any non-uniformity in the brush may hinder the diffusion of monomer to shorter chains allowing longer chains to grow preferentially. This phenomenon may be exacerbated by positive feedback. The polydispersity arising from this phenomenon is manifest towards top of the brush where shorter chains are hidden and the ends of longer chains may adopt a "mushroom" conformation. Multiple studies suggest that brush density is decreased with distance from the base.[27,28,86] **Figures 27-29** summarize work from such studies. Decreases in chain density reduce chain stretching and orientation at the surface relative to the body of the brush. Therefore, we propose that improved uniformity in polymer brushes (as represented in **figure 26**) should increase stretching and orientational order at chain ends thus leading to enhancements of properties discussed in section 1.3 such as increased glass transition temperature, improved colloidal stability, and size exclusion properties.

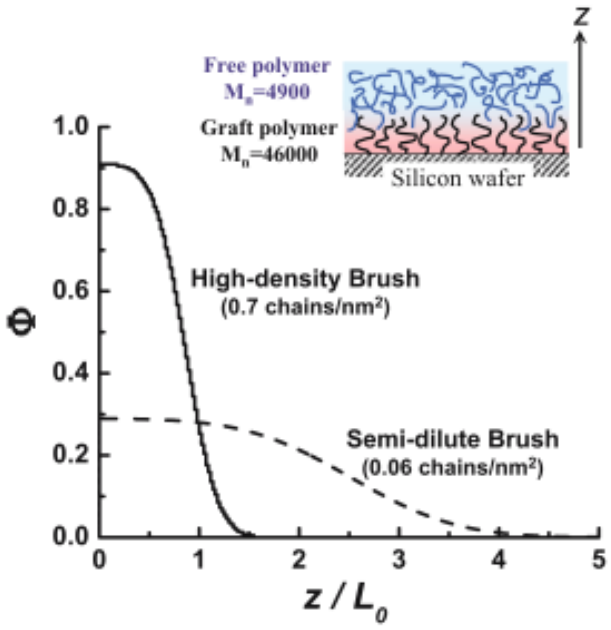

Figure 27: Work by Yamamoto, Tsujii, and Fukuda investigated brush density with distance from surface for low and high-density brushes. Neutron reflectivity was used to detemine misciblity of deuterated PMMA oligomers with PMMA brushes. Swelling of brush with oligomer was used to determine density.[86]

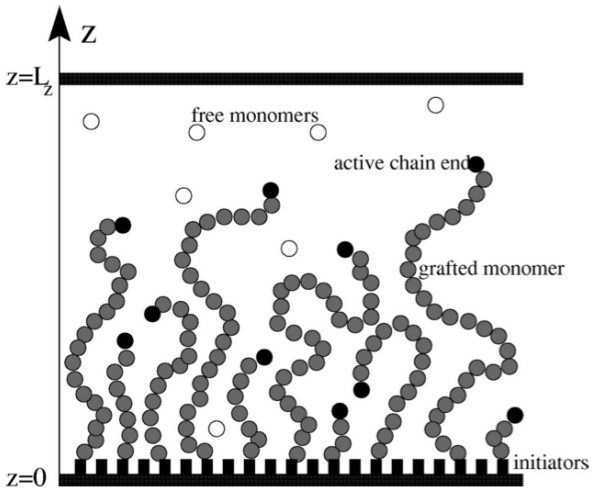

Figure 28: Computational work by Milchev, Whitmer, and Landau on living brush polymerization. It was found that the polydispersity of living polymer in the brush decayed much slower than in a corresponding bulk polymerization system. This difference was attributed to the monomer density gradient within the dense brush that favored monomer addition to longer chains.[27]

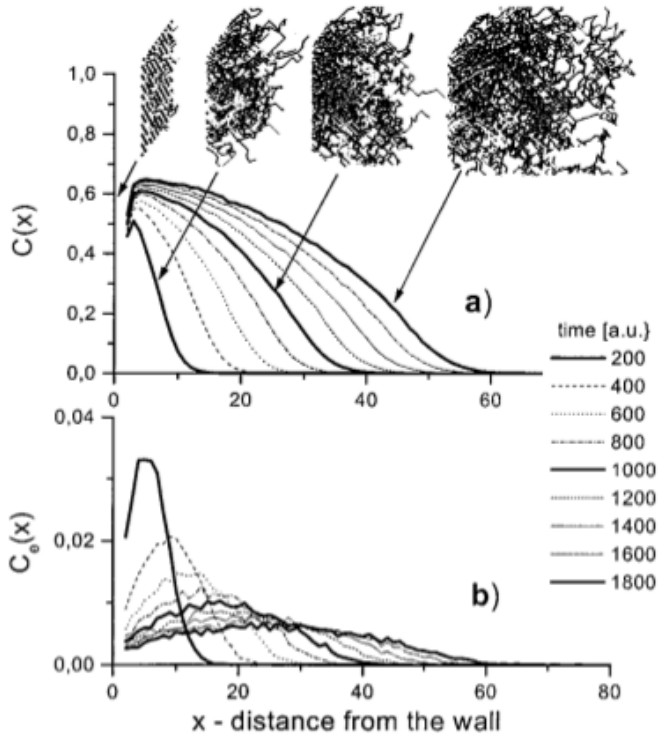

Figure 29: Computation work by Matyjaszewski et al. on growth of polymer brushes. A) Concentration of polymer chains with distance from the surface at various times. b) Concentration of chain ends with distance from the surface at various times. Grafting density was 0.25 where 1.0 corresponds to a fully packed surface. The system was designed in such a way that it most closely resembles anionic polymerization. While polydispersities were low (≤1.11) and decreased with time, the brush exhibited higher polydispersities than chains grown in solution given the same conditions. Simulations wherein grafting density was increased (>0.5) showed broader polydispersity and non-linear conversion versus time.[28]

We see improved uniformity and stretching of chain ends as potentially enhancing any function for which accessibility of chain ends is required such as further polymerization or reaction of chain ends. One application for which we see improvements in orientational order of brushes as beneficial is the use of brushes in organic electronics. Charge transport and separation is essential in photovoltaics. Polymer brushes are finding use as electron donating layers in organic photovoltaics (OPVs)[87,88] due to their conformational order improving charge transport. Huck et al. showed up to a 1000 fold enhancement in current density for poly(triphenylamine acrylate) brushes compared with spin-coated films of the same thickness.[89] Their work is summarized in **figure 30**. They attributed this enhancement

to the vertical stretching of chains in the brush. Spin-coated films are more likely to exhibit chain alignment in the plane of the film, which necessitates more inter-chain hopping of charges, therefore significantly impeding charge transport normal to the plane of the film.[89]

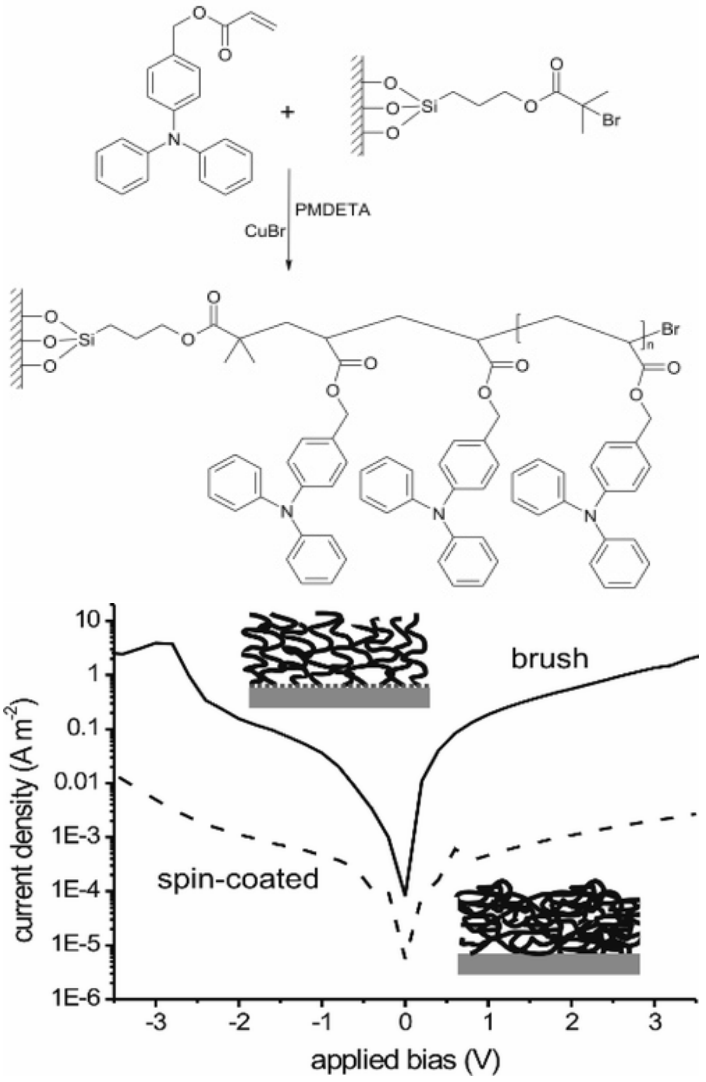

Figure 30: Huck et al. grew polytriphenylamine acrylate (PTPAA) brushes from ITO. Grafting density was estimated at 0.14 chains/nm^2. Brushes demonstrated a greater current density versus spin-coated films. Applied bias in a sandwich structure device of ITO/PTPAA/PEDOT:PSS/Au. The PTPAA layer was 80nm.[89]

Charge separation in photovoltaics occurs at the interface of the electron donating and accepting layers. An exciton must travel to this interface and be split by the energy difference of the lowest unoccupied molecular orbital (LUMO) of the two layers. Exciton

lifetime is very short before electron-hole recombination. It is essential that excitons reach the donor-acceptor interface prior to recombination to generate current. Enhanced orientational order throughout the brush, including at the interface where the effects of polydispersity are likely to manifest, should enhance current through OPVs.

In section 4.2 below, we illustrate techniques that may lead to the production of more uniform brushes. For the application of OPVs it is necessary that the brushes be semiconducting. To this end, monomers with highly conjugated pendant groups such as triphenylamine acrylate or monomers that generate conjugated main-chain polymers such as acetylene might be employed. We have also identified several monomers (structures in **appendix 3**) that can be polymerized by ROMP and may be suitable for production of semiconducting brushes.

4.2 Strategies for Producing Uniform Brushes: We have considered techniques with the potential to eliminate the problem of monomer density gradient as a contributor to brush nonuniformity. We invision two general strategies towards eliminating this source of polydispersity. First, having the source of monomer eminate from the base of the brush rather than the top, and second having chains grow from their base like grass rather than having the active end at the top of the brush. Using either of these approaches (illustrated in **figure 31**) should avoid giving longer chains preferential acess to monomer.

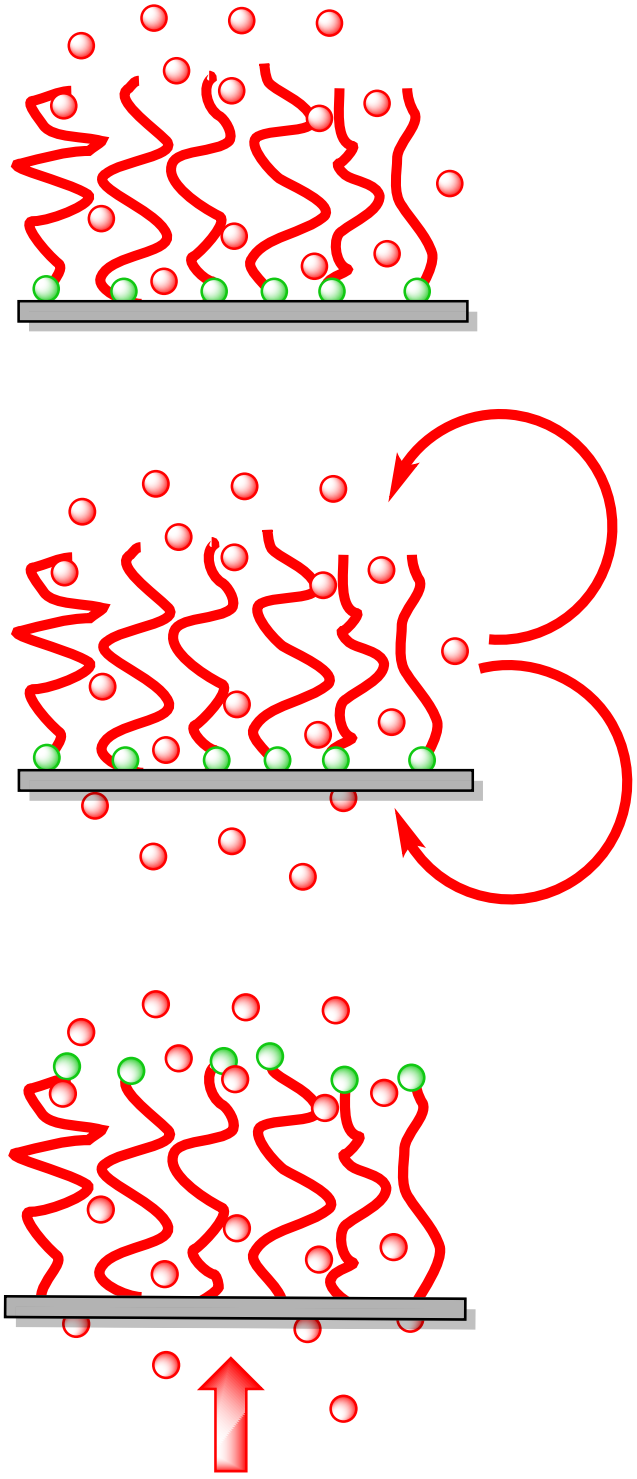

Figure 31: Representation of chains growing by monomer insertion at the base (top), monomer flowing through the brush from the base (bottom), and a combination of both strategies (center).

4.3 Brush Growth from Dialysis Tubing: To grow brushes wherein monomer is fed up from the bottom of the brush, we have attempted to grow from cellulose dialysis tubing using ATRP. We have functionalized the dialysis tubing similarly to our approach for functionalizing nylon but without needing a hydroxymethylation step because of the hydroxyl groups already present in cellulose. **Figure 32** shows functionalization and polymerization from cellulose dialysis tubing.

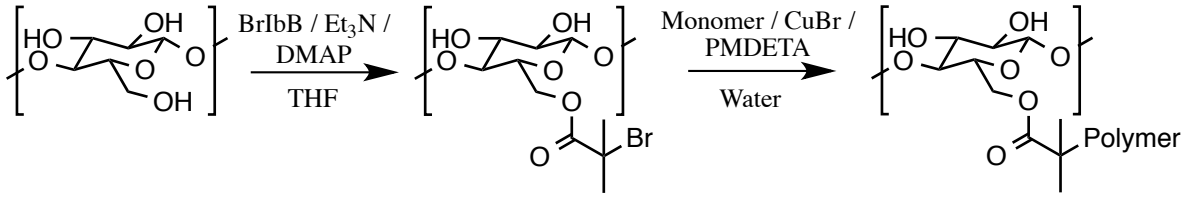

Figure 32: Reaction scheme for fucntionalization of and polymerization from cellulose dialysis tubing. BrIbB is used to generate an ATRP initiator. BrIbB is shown attaching at the most accessible hydroxyl group but may also attach to others.

Once we attached an ATRP initiator we performed our polymerizations in degassed distilled water using the molar ratios in **table 5**. We began with only water and monomer inside of the dialysis tubing. Water was a necessary solvent to allow the dialysis tubing to function properly. We used the water soluble monomers shown in **figure 33**, N-hydroxymethyl acrylamide (NHAA) and poly(ethylene glycol) methacrylate (PEG-meth). Polymerizations where dialysis took place were typically done in 100ml or 150ml water to accommodate the dimensions of the dialysis tubing and clips. As controls, we performed polymerizations on a smaller scale using squares of dialysis tubing. In these trials, monomer was in solution and the tubing was not clamped at either end. The volume was also one tenth

that of the polymerizations where dialysis occurred. ATR-FTIR analysis (shown in **figure 34**) was used to verify functionalization by initiator and polymer growth.

Table 4: Molar ratios for ATRP and ARGET ATRP.

	Monomer	CuBr	$CuBr_2$	PMDETA	N_2H_2
Normal ATRP	~30mmol / 100 equiv	0.30mmol / 1.0 equiv	0.0mmol	0.30mmol / 1.0 equiv	0.0mmol
ARGET ATRP	~4.5mmol / 100 equiv	0.0mmol	0.90mmol / 20 equiv	0.90mmol / 20 equiv	0.30mmol / 6.7 equiv

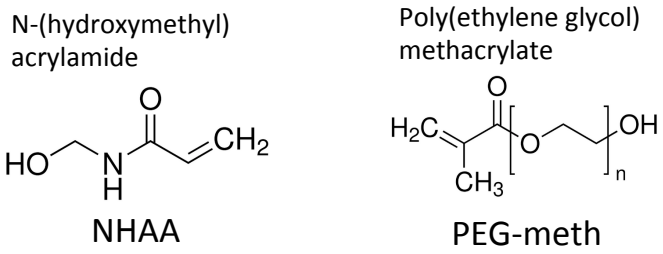

Figure 33: Structures of monomers used for ATRP from dialysis tubing.

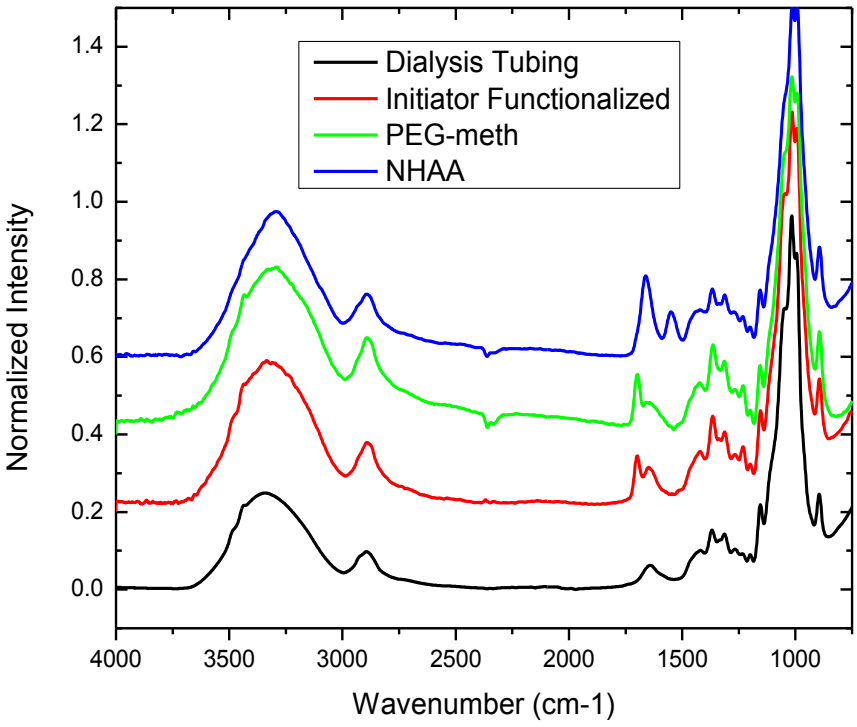

Figure 34: FTIR spectra of dialysis tubing unfunctionalized, after addition of initiator, and after polymerization of PEG-meth and NHAA.

After polymerization we observed the tubing to darken in color and the inner solution to match the color of the outer solution as seen in **figure 35**. Using ATR-FTIR we were able to see that polymer grew on both sides of the tubing however peaks corresponding to polymer appeared stronger from the interior. Generally the interior of the tubing also contained free polymer so these more intense peaks may be due to absorbed free polymer that was not fully rinsed from the tubing. We could also observe polymer by SEM although it was often difficult to detect. The controls generally grew more polymer. We believe that in addition to having fewer constraints on polymerization (monomer not required to diffuse through a membrane), the control benefited from higher monomer and catalyst concentrations and a more effective degassing step owing to the lower volume of solvent

used. We had better results using the activators regenerated by electron transfer (ARGET) ATRP with the PEG-meth monomer. ARGET ATRP uses a reducing agent such as hydrazine or tin(II)-ethyl hexanoate to form the activating catalyst in situ and is more tolerant to dissolved oxygen in the solution.

Figure 35: Dialysis tubing post polymerization. Initially the solution inside is only water and monomer and is colorless. During polymerization, copper salts diffuse into the tubing.

SEM analysis showed what might be pores in the dialysis tubing. Unmodified tubing shown in **figure 36** shows structures approximately 2µm in length, 100-200nm in width and all oriented in the same direction. We suspect these pore-like structures are responsible for the apparent ordering of grafted polymer seen throughout SEM images in **figures 37**, **38**, **40** and **43**. We also tried using toluene as a solvent in which to functionalize tubing with BrIbB. Tubing prepared in toluene was seen to grow more polymer as seen in **figures 38** and **39**. We do not see a reason why the functionalization reaction should be favored in toluene, rather, we suspect the toluene may have been more dry than the THF as it is a less hydroscopic solvent.

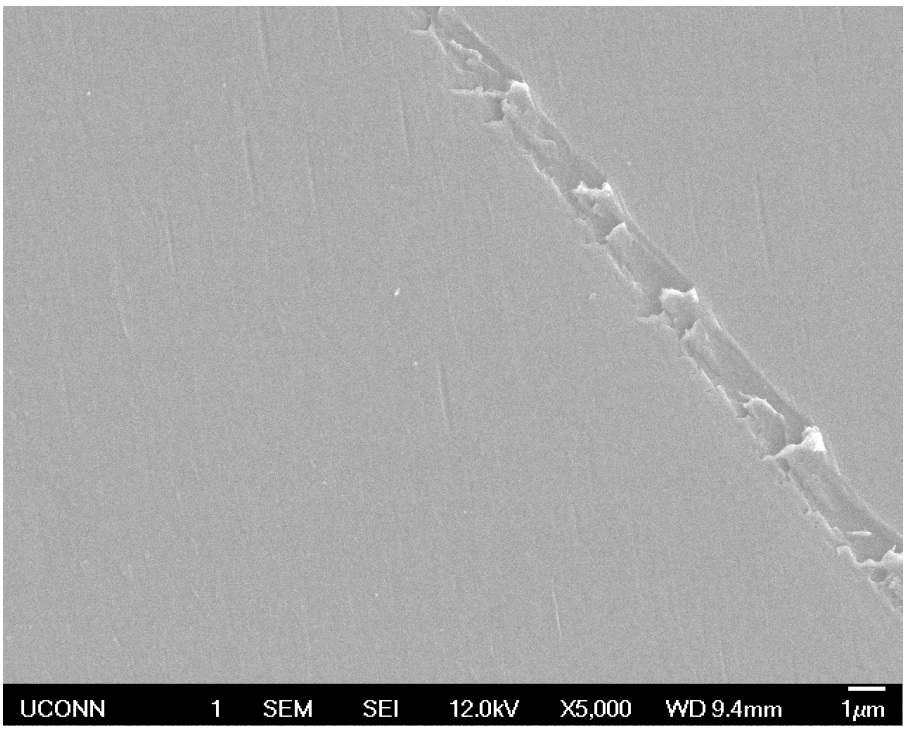

Figure 36: SEM image of unmodified dialysis tubing. The diagonal scratch was a defect used for focusing purposes and was not typical of the sample.

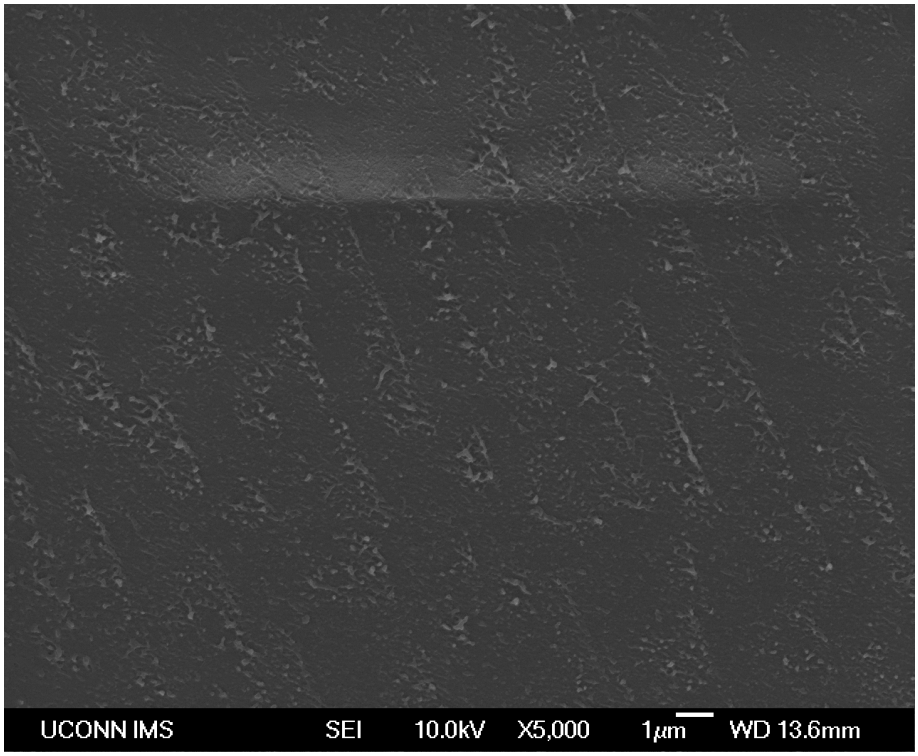

Figure 37: SEM image of dialysis tubing after polymerization of NHAA at room temperature for one day. The tubing was cut into peices and not clamped such that monomer had to diffuse out.

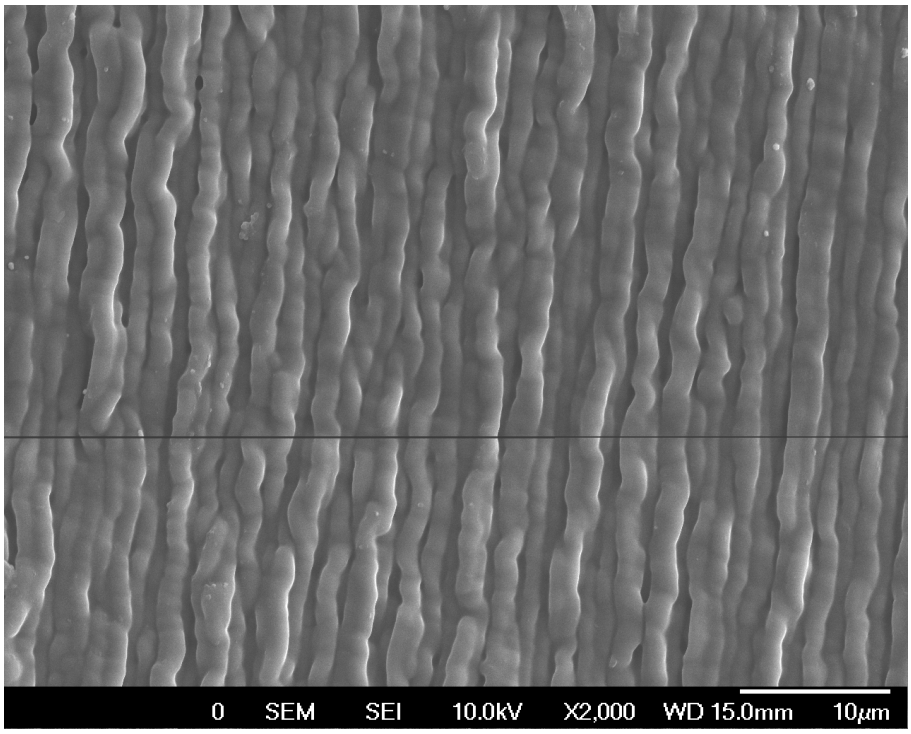

Figure 38: SEM image of dialysis tubing after polymerization of NHAA at room temperature for one day. Functionalization of tubing was done in toluene rather than THF, which apparently gave better coverage of initiator. The tubing was cut into pieces and not clamped such that monomer had to diffuse out.

Figure 39: Image of dialysis tubing after polymerization of NHAA at room temperature for one day. Functionalization of tubing was done in toluene rather than THF, which apparently gave better coverage of initiator. The tubing was cut into pieces and not clamped such that monomer had to diffuse out. Picture taken with optical microscope at low magnification.

Much less polymer was observed to form when monomer was inside the clamped tubing at the start of the polymerization. We observed a viscous polymer solution inside of

the tubing after polymerization. Polymer was observed on the interior but not exterior of the tubing when using NHAA in the dialysis polymerization. We suspect from **figure 42** that NHAA polymerized in pores of the tubing and trapped remaining monomer from escaping. Dialysis polymerization of the PEG-meth monomer using ARGET conditions described in **table 5,** yielded polymer on both sides of the tubing as shown in **figures 44** and **45**. We suspect that due to the lower concentration of activator in ARGET compared with conventional NHAA, the rate of polymerization was slower allowing more monomer to diffuse through the tubing before being polymerized and potentially clogging pores.

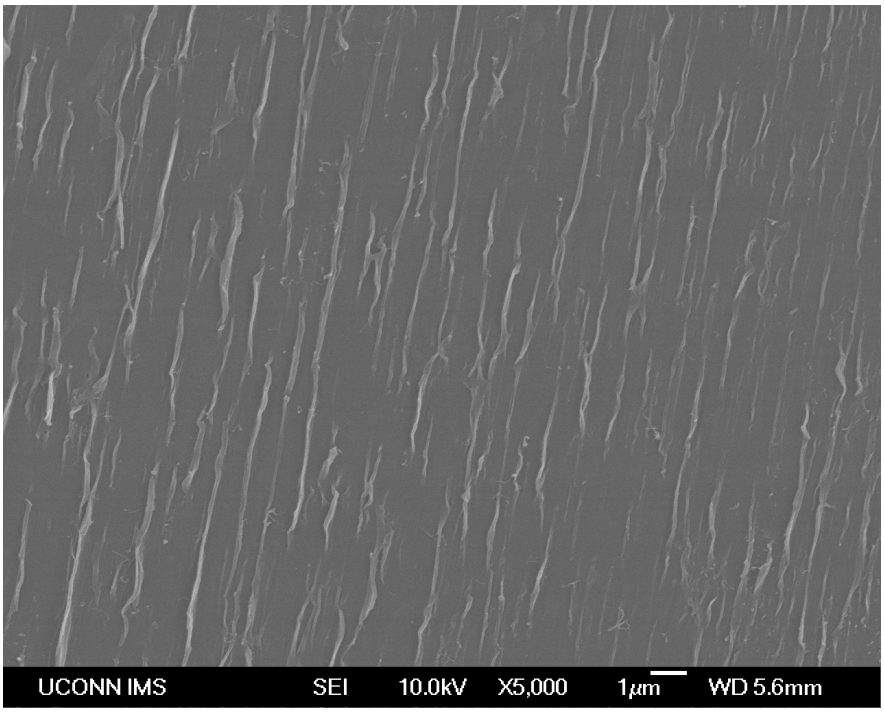

Figure 40: SEM image of interior of dialysis tubing after polymerization of NHAA at room temperature for one day. The tubing filled with monomer and water and clamped at both ends before being placed into reaction vessel.

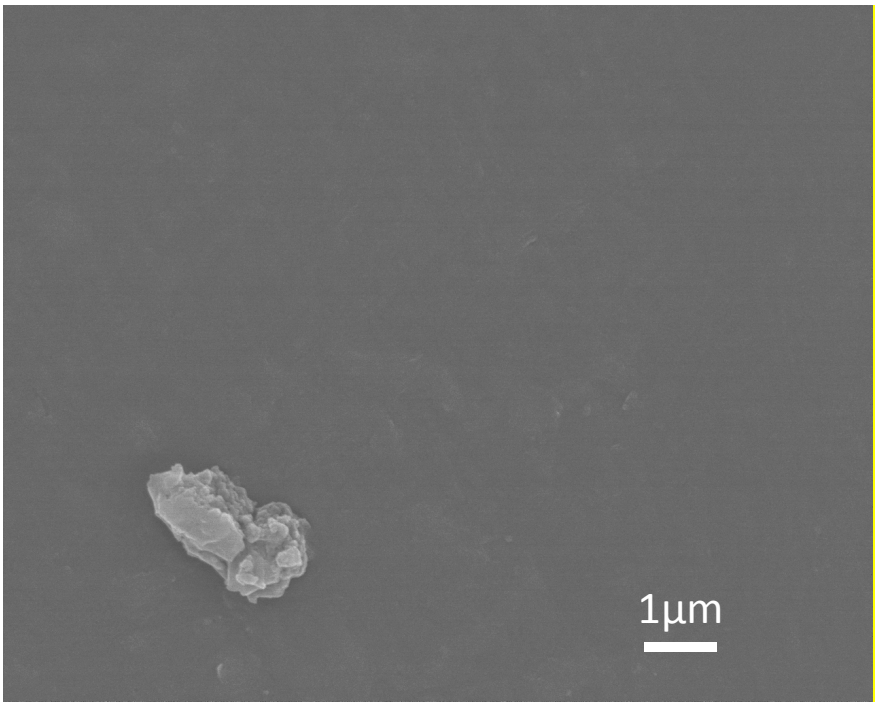

Figure 41: SEM image of exterior of dialysis tubing after polymerization of NHAA at room temperature for one day. The tubing filled with monomer and water and clamped at both ends before being placed into reaction vessel. The structure in the bottom left was used to focus the image but was not common throughout the sample. Magnification is 10,000 times.

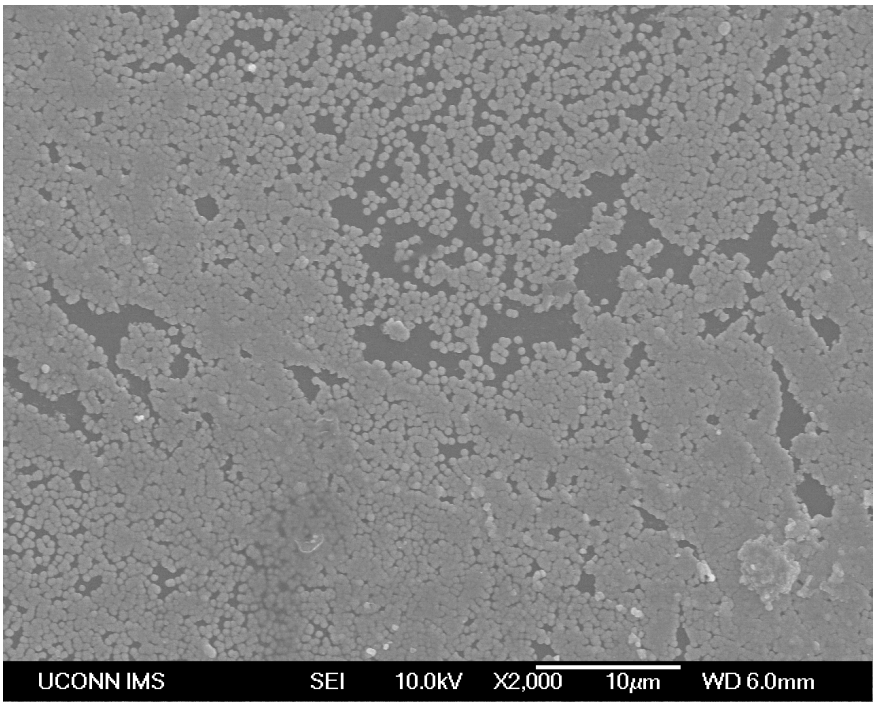

Figure 42: SEM image of interior of dialysis tubing after polymerization of PEG-meth at room temperature for one day. The tubing filled with monomer and water and clamped at both ends before being placed into reaction vessel. The ARGET technique was used.

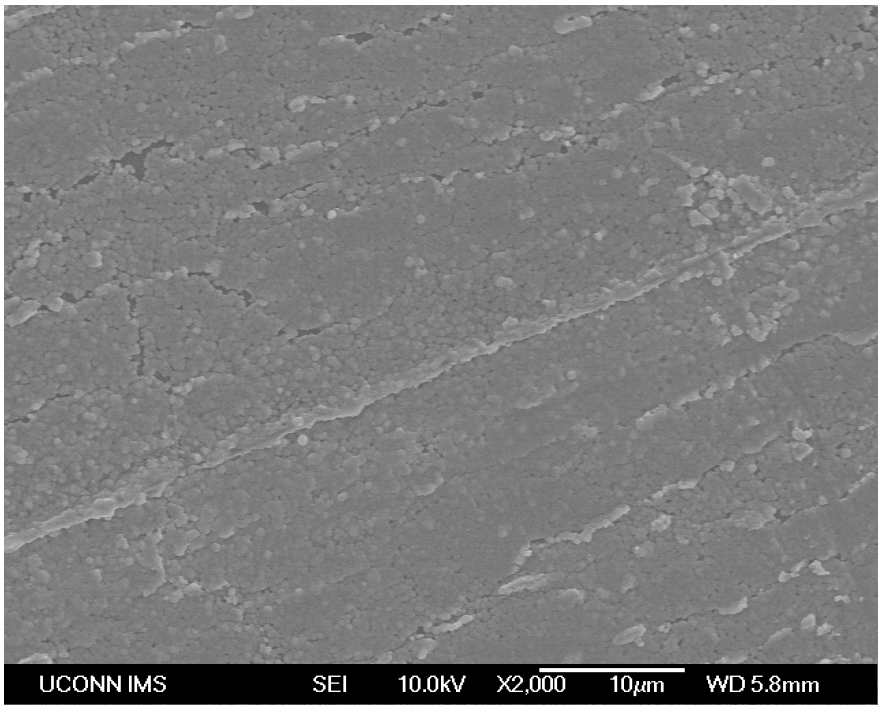

Figure 43: SEM image of exterior of dialysis tubing after polymerization of PEG-meth at room temperature for one day. The tubing filled with monomer and water and clamped at both ends before being placed into reaction vessel. The ARGET technique was used.

A great deal of work is still needed to evaluate the dialysis polymerization technique. Difficulties producing any detectable polymer with the dialysis technique stagnated attempts to evaluate the effects of varying conditions or to perform kinetic studies. We would like to investigate any differences in polymer brushes grown with and without the dialysis technique. Atomic force microscopy would be our choice for measuring frictional coefficients as well as to investigate the force needed to compress the brushes. We would anticipate a brush with a more uniform surface to have a lower friction coefficient and to require more force to compress than a brush with a polydisperse surface.

4.4 Experimental

Materials: 3500 dalton molecular weight cut off regenerated cellulose dialysis tubing (Fisherbrand), N-(hydroxymethyl)acrylamide (TCI 98%), 2-bromoisobutyryl bromide (BrIbB, Acros, 98%), copper (I) bromide (Strem Chemicals, 98%), copper (II) bromide (Fisher, reagent grade), N,N,N',N",N"-pentamethyldiethylenetriamine (PMDETA, Aldrich, 99+%), hydrazine hydrate (Acros, 64%), 4-(dimethylamino)pyridine (DMAP, Aldrich, ≥99%), methanol (Aldrich, 99.8%), acetone (Fisher, histological grade), were used as purchased without further purification. Poly(ethylene glycol)methacryate (Aldrich) was passed through a column to remove monomethyl ether hydroquinone before use. Triethylamine (Acros, 99%) and tetrahydrofuran (THF, Fisher, histological grade) were dried with $CaSO_4$, distilled under reduced pressure, then stored over CaH_2.

Dialysis Tubing Functionalization: We consulted work by Lindqvist and Malmstrom for the functionalization of cellulose.[90] Tubing was rinsed with acetone and THF and dried under vacuum prior to reaction. Tubing was suspended in dry THF or toluene (10ml) with triethylamine (0.12ml) and a catalytic amount of DMAP. The vial was sealed and chilled $<0^oC$ prior to addition of BrIbB (0.10ml). The reaction was allowed to come to room temperature and stirred three hours. Precipitation of triethylamine acid salt was observed. Reactions were decanted and tubing was rinsed with THF, acetone, and methanol before drying under vacuum.

ARGET Dialysis Technique: Doubly distilled water (100ml) in a round bottom flask was degased by aspirator then bubbled with argon. $CuBr_2$ (0.90mmol), PMDETA (0.90mmol), and $N_2H_{4(aq)}$ (0.30mmol) was added. Initiator functionalized dialysis tubing was clamped at one end and filled with a solution of 2.0ml PEG-meth and water that had been degased. The

tubing was sealed and added to the flask, which was sealed under argon. The reaction was stirred at room temperature overnight. The solution was decanted and tubing unclamped and allowed to soak in water overnight then rinsed with water and THF and dried.

Dialysis Technique: Doubly distilled water (150ml) in a round bottom flask was degased by aspirator then bubbled with argon. CuBr (0.042g, 0.30mmol), and PMDETA (0.063ml, 0.30mmol) were added. Initiator functionalized dialysis tubing was clamped at one end and filled with a solution of NHAA (3.03g, 30mmol) and water that had been degased with argon. The tubing was sealed and added to the flask, which was sealed under argon. The reaction was stirred at room temperature overnight. The solution was decanted and tubing unclamped and allowed to soak in water overnight then rinsed with water and THF and dried.

Non-Dialysis Technique: NHAA (3.03g, 30mmol), CuBr (0.042g, 0.30mmol), and PMDETA (0.063ml, 0.30mmol) were added to 15ml distilled water and three freeze-pump-thaw cycles were performed to degas the solution. The solution was stirred until homogeneous then several pieces of initiator functionalized dialysis tubing were added and two more freeze-pump-thaw cycles were performed before allowing to stir overnight. The solution was decanted and tubing was rinsed with water and THF and dried.

FTIR: Performed using the same instrumentation and techniques as listed in section 2.7.

Electron Microscopy: Performed using the same instrumentation and techniques as listed in section 2.7.

4.5 Brush Growth via ROMP: To synthesize brushes that grow from their base we have investigated synthetic strategies for attaching a ROMP catalyst to a surface. With the metal carbene immobilized at the surface, monomer would insert at the base of the chain. **Figure 44** illustrates addition of a monomer by ROMP to a chain that is surface-bound though a Grubbs catalyst. We were unable to employ these strategies for growing brushes but present here our preliminary work.

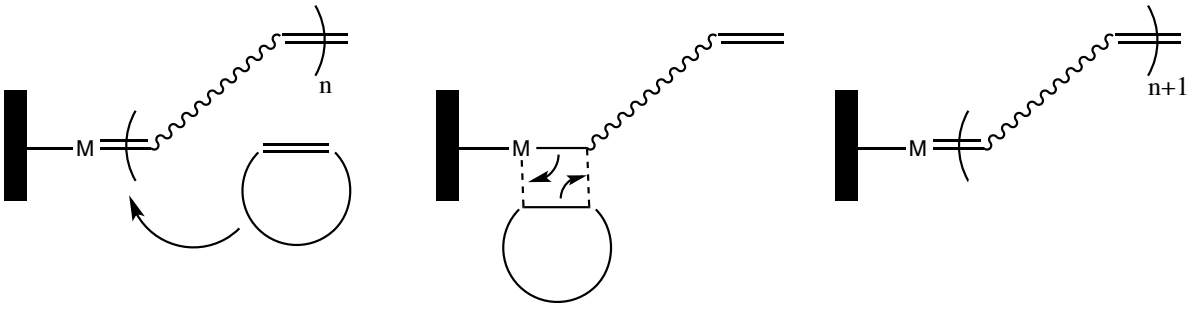

Figure 44: Representation of monomer addition by ROMP to a chain in a polymer brush.

We attempted an ion exchange strategy employed previously by Buschmann et al.[91] Perflouroglutaric anhydride (PFGA) is reacted with a surface baring an amine. Next sodium hydroxide and silver nitrate are used to create the silver carboxylate. In the presence of the second generation Hoveyda-Grubbs catalyst, the carboxylate should bind to the ruthenium center and one of the chlorine ligands should come off and precipitate with one of the silver cations as silver chloride. **Figure 45** shows our desired reaction scheme.

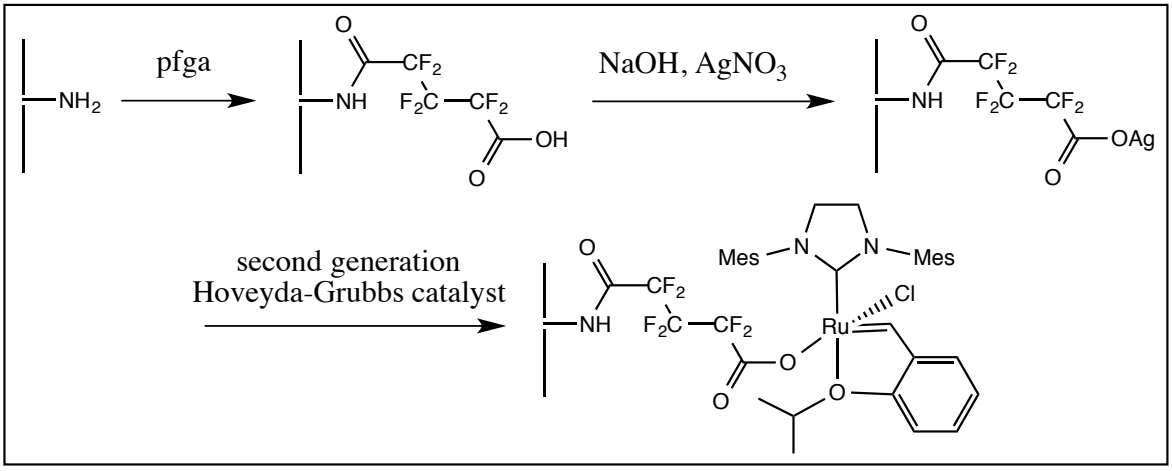

Figure 45: Reaction scheme for attachment of Grubbs catalyst to nylon membrane by ion exchange. Strategy based upon work by Buschmann et al.[92]

We have attempted to use nylon membranes as our surface. To generate primary amines for reaction with PFGA, we experimented with various concentrations, reaction times, and temperatures for the hydrolysis of amide bonds by stirring in aqueous sodium hydroxide solutions. We stirred nylon membranes in 3.0M $NaOH_{(aq)}$ for 30 minutes at gentle reflux then rinsed with water until rinse solution was neutral. Membranes were dried under vacuum. Next, membranes were stirred at room temperature in dry THF and PFGA (5%vol.) for one hour then dried. To form the silver salt, membranes were rinsed briefly with 0.1M $NaOH_{(aq)}$, then water, and finally stirred in 0.1M $AgNO_{3(aq)}$. We were able to observe attachment of PFGA by a carbonyl stretch in FTIR as seen in **figure 46**, however, this peak was often lost after rinses with 0.1M $NaOH_{(aq)}$ and water. In instances when the peak remained, we attempted to attach the Grubbs catalyst by stirring a dilute solution of catalyst in dry dichloromethane (~0.2%wt.). We were unable to detect attachment of the catalyst by FTIR. Infrequently, membranes adopted a light green color that persisted after rinsing. We stirred these membranes in solutions of norbornene and were able to produce polymer in solution, however, FTIR of membranes after rinsing with THF showed no polymer on the

membranes. We believe that any catalyst on the membranes was only physically adsorbed. If we were to revisit this strategy we would begin with a hydroxymethylation reaction to generate a primary alcohol rather than attempting to generate a primary amine via base hydrolysis.

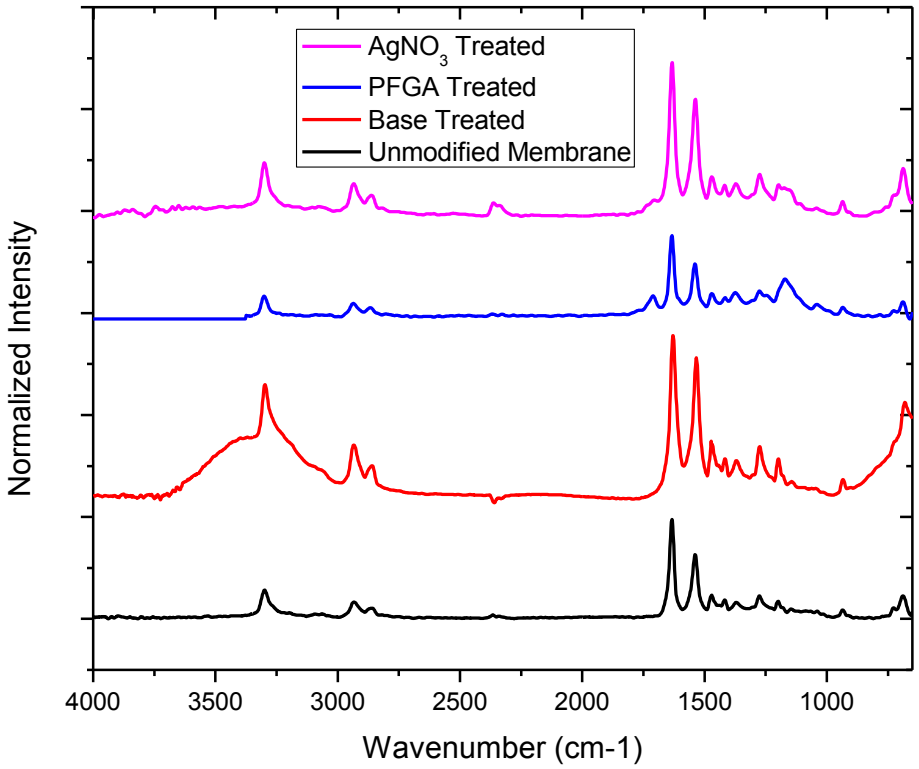

Figure 46: FTIR spectra of membranes prepared for ion-exchange attachment of Grubbs catalyst. After base treatment the filters were seen to be more hydrophilic. A new carbonyl stretch was seen after functionalization with PFGA that was partially lost after formation of silver carboxylate. Generally membranes gave FTIR spectra similar to an unmodified membrane after silver nitrate treatment and rinsing or after attempts to attach Grubbs catalyst.

A second strategy we pursued is summarized in **figure 47**. Synthesis of a N-heterocyclic carbene (NHC) ligand has been reported separately by Grubbs[93] and Blechert.[91] A nucleophilic substitution reaction is used to react 2,3-dibromo-1-propanol with 2,4,6-trimethylaniline. Next, the resulting molecule is reacted with

trimethyl orthoformate to generate the NHC. This ligand can displace a tricyclohexylphosphine ligand and bind to the ruthenium center of a Grubbs catalyst.

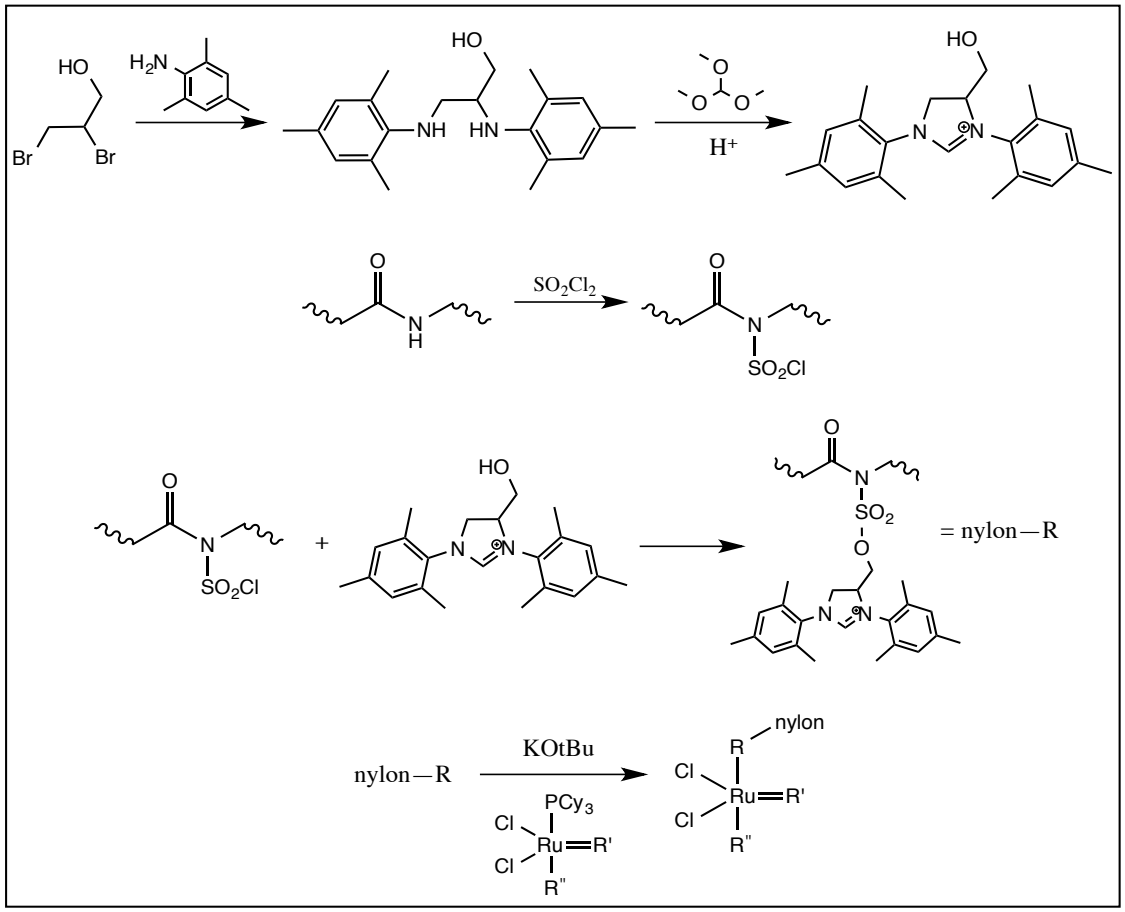

Figure 47: Reaction scheme for attachment of Grubbs catalyst to nylon membrane via ligand exchange. Ligand synthesis and exchange based upon separate work by Grubbs[93] and Blechert.[91] Sulfuryl chloride coupling based upon work by Ford and Grant.[94]

To pair this ligand to a nylon membrane we have followed the techniques of Ford and Grant developed for coupling amines, isocyanaytes, and alcohols to polyamide supports using sulfuryl chloride chemistry.[94] **Figure 55** shows FTIR of a nylon membrane after reaction with sulfuryl chloride. It was necessary to slightly modify conditions used by Ford and Grant as we found that membranes lost their structure with high concentrations of sulfuryl chloride or after extended exposure. We were able to form the intermediate, 2,3-

dimesitylamine-1-propanol. 2,4,5-trimethylamaline (12.4ml, 88mmol) was stirred in dry methanol (15ml) as 2,3-dibromo-1-propanol (4.11ml, 40mmol) was added dropwise. The reaction was fitted with a $CaCl_2$ drying tube and stirred overnight at reflux. The product was purified by rinsing with ethanol. **Figure 49** shows the NMR spectrum of 2,3-dimesitylamine-1-propanol.

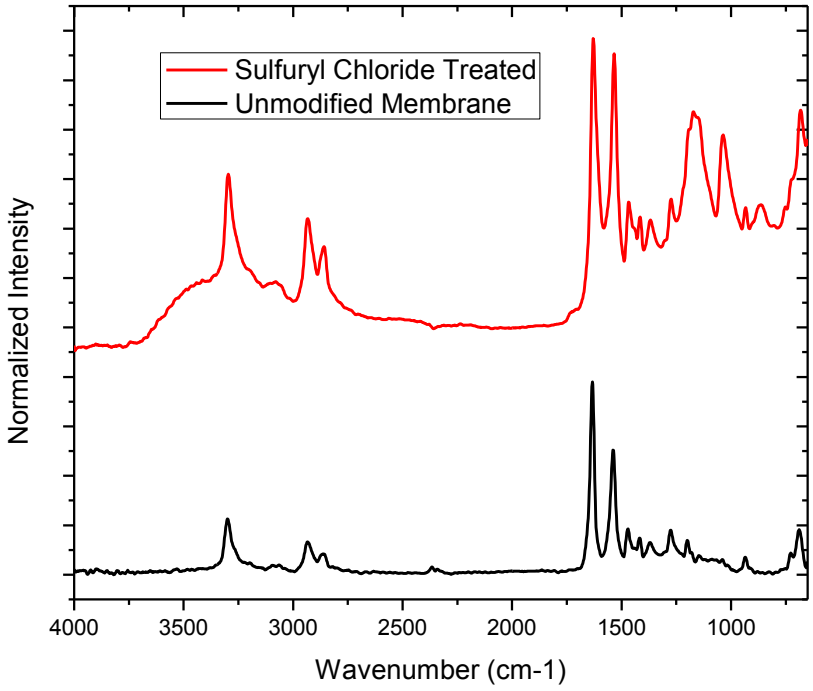

Figure 48: FTIR of sulfuryl chloride treated membranes. Peaks from the imparted sulfonyl chloride moiety are seen from 1000-1250cm^{-1}.

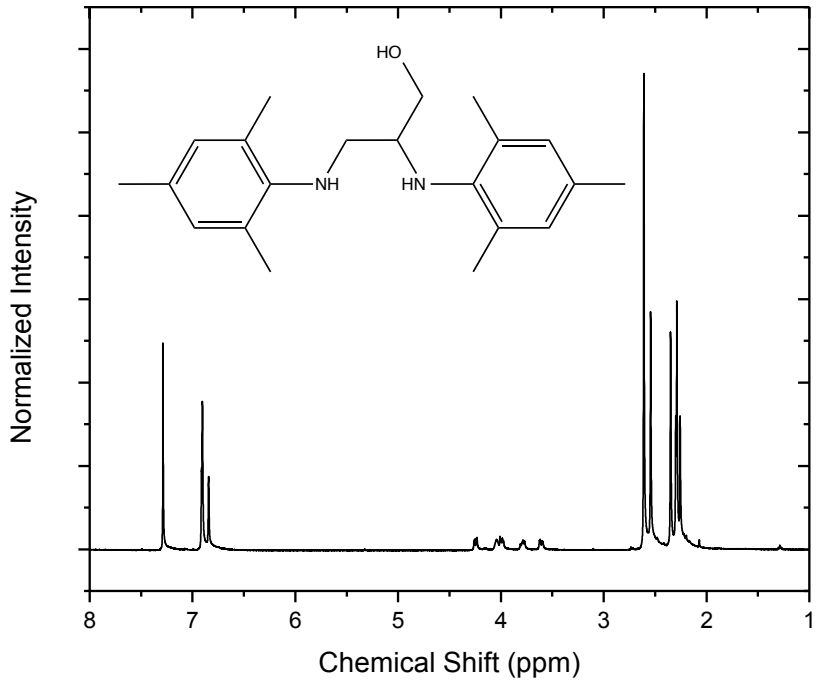

Figure 49: NMR of 2,3-dimesitylamine-1-propanol.

We attempted to form the NHC ligand but could not obtain a pure product or couple the ligand to a nylon membrane through the sulfuryl chloride technique. 2,3-dimesitylamine-1-propanol was suspended in dry methanol and concentrated HCl was added to dissolve the sample. The reaction was then heated to dryness and the solid was rinsed with water several times then dried in vacuum oven. The product was dissolved in trimethylorthoformate with a catalytic amount of formic acid and heated to dryness with stirring. **Figure 50** shows the least complex NMR spectrum we were able to obtain in our attempt to synthesize the NHC.

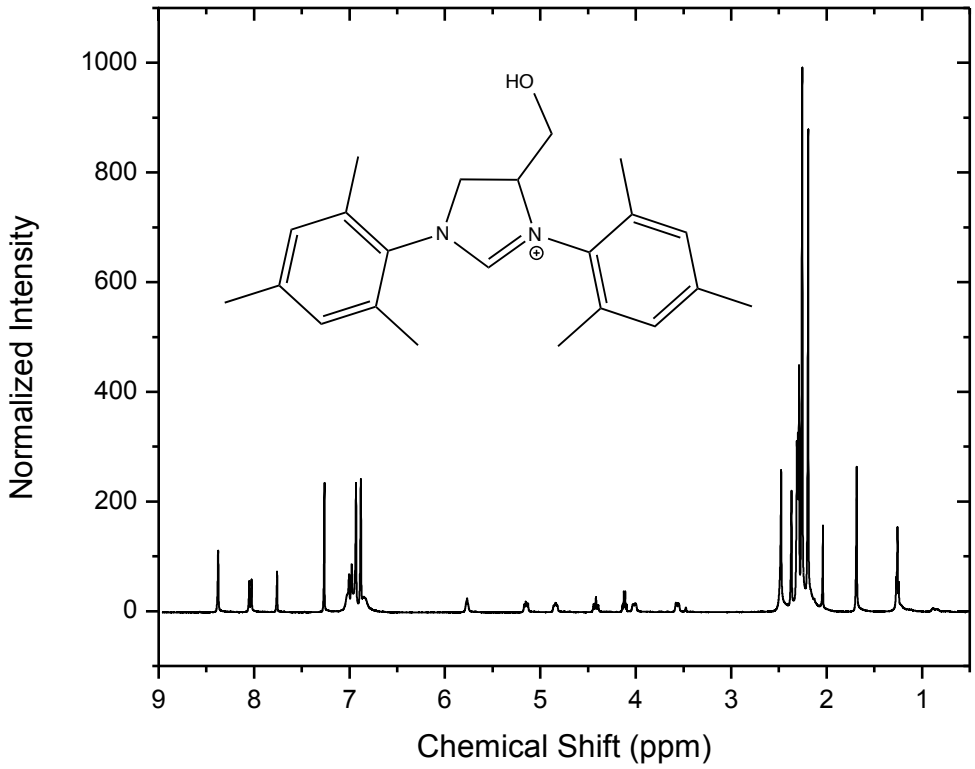

Figure 50: NMR of NHC ligand.Product not pure.

The final strategy we considered was based on bis(dicyclohexylphosphinomethyl) amine ligand synthesis by Russell et al.[95] as well as work by Astruc[96] for catalyst binding by these ligands. The proposed reaction scheme is shown in **figure 51**. We attempted to generate the starting material dicyclohexylphosphine by reduction of tricyclohexylphosphine but were unable to obtain the product with the purity needed to proceed with this strategy.

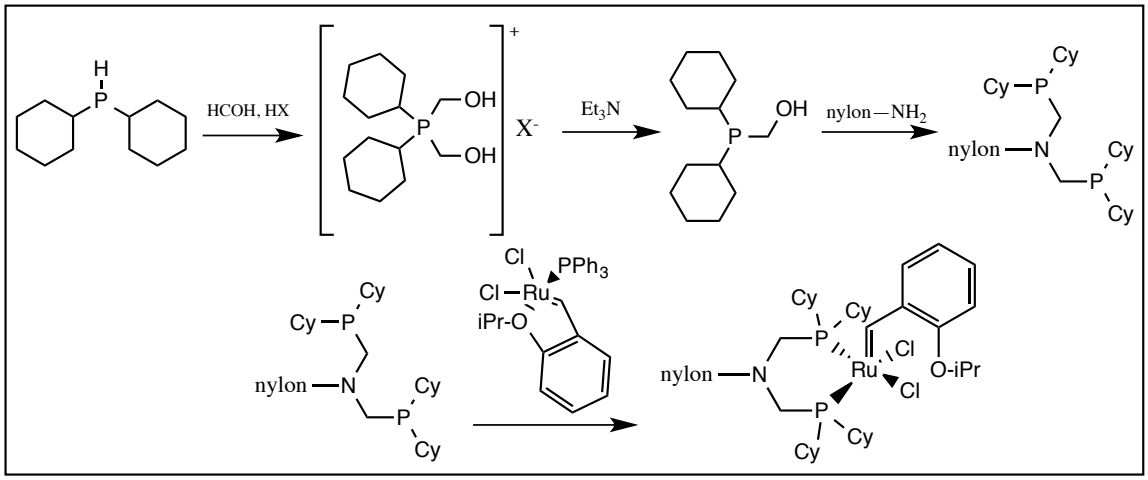

Figure 51: Reaction scheme for attachement of ROMP catalyst by exchange of triphenylphosphine and isopropyl ether ligands for bis(dicyclohexylphosphinomethyl)amine. Generation of bis(dicyclohexylphosphinomethyl)amine ligand on nylon based on work by Russell et al.[95] **Attachment to ROMP catalyst based on work by Astruc.**[96]

PART 2 – Bottlebrushes and Self-Assembly

Chapter 5 – Synthesis and Characterization of Bottlebrush Copolymers

5.1 Introduction: We have synthesized triblock bottlebrush copolymers composed of a polystyrene (PS) and polyisoprene (PI) linear BCP backbone having poly(ethylene oxide) (PEO) chains extending from the PI block. Our chosen architecture was inspired by the work of Semenov who proposed that a long hydrophobic block, or "H" block attached to polar "P" units separated by short H blocks might lead to the formation of "protein-like" copolymers that collapse to form unimolecular micelles given appropriate solvent conditions.[97] **Figure 52** depicts a polymer of our chosen architecture collapsing to a unimolecular micelle with the addition of selective solvent. We have chosen THF/water as our solvent system as the two solvents are miscible but have very different interactions with the blocks of our polymer. PEO is soluble in both solvents while the PSPI backbone is soluble in THF but highly insoluble in water. We dissolve polymers in THF then slowly add water. This lowers solvent quality for PS causing the volume of PS blocks to reduce in order to minimize the high-energy interfacial area between PS and the solvent. While it does not appear that we have formed unimolecular micelles, we have observed self-assembly with increasing water content. Background on self-assembly of aphiphilic polymers in selective solvent is discussed in **section 1.4**. We find that the distribution of PEO into many short arms or few long arms determines the structures that are accessible through self-assembly and appears to alter the structure of micelle coronas.

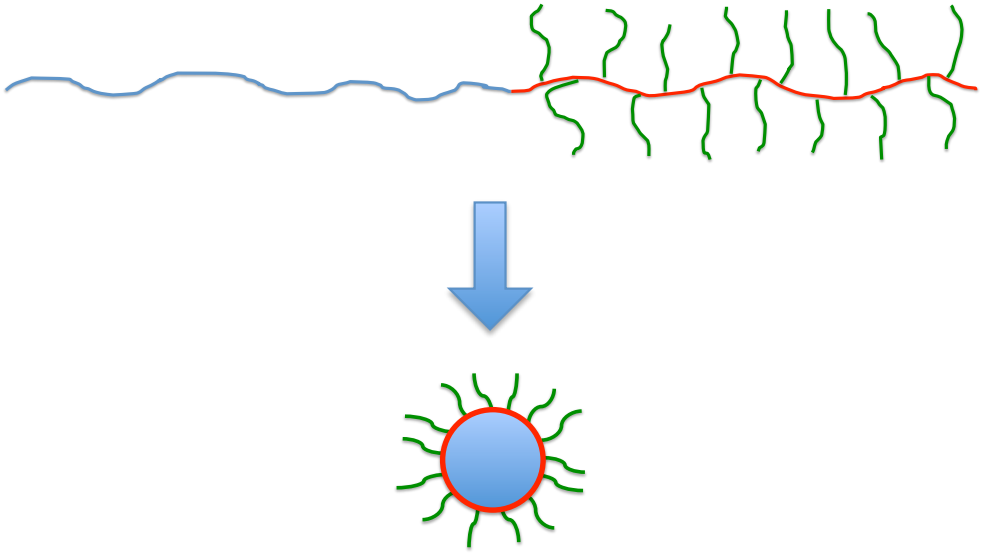

Figure 52: Representation of desired unimolecular collapse by addition of selective solvent. PS, PI, and PEO are respresented as blue, red, and green respectively.

5.2 Synthesis of Bottlebrush Copolymers: PS-*b*-PI was synthesized anionically by sequential monomer addition following nucleophilic initiation. The polymerization was terminated by methanol. Anionic polymerization (discussed in **section1.5**) afforded a high degree of control over MW and PDI. We obtained PS_{392}-*b*-PI_{134} with a PDI of 1.05, which we used for all subsequent hydroboration and grafting. Hydroboration and oxidative workup were used to generate hydroxyl groups along the PI block. Hydroboration was chosen for its ability to substitute double bonds in an anti-Markovian fashion. Anti-Markovian substitution allows the hydroxyl groups to be more sterically accessible for the grafting of ethylene oxide. The mechanism of hydroboration is shown in **figure 53**.We hydroborated our polymer to varying extents by changing the reaction stoichiometry to control the density of PEO grafts on our PSPI backbone. Polymers 1 and 2 were synthesized from PSPI for which we attempted to hydroborate 100% of double bonds. Polymer 3 was synthesized from PSPI for which we attempted to hydroborate 10% of double bonds. Polymers 4 and 5 were synthesized from PSPI for which we attempted to hydroborate 5% of double bonds. After

hydroboration, the polymers hardened and caked together and were difficult to dissolve in THF. Initially we had difficulty growing PEO from the hydroborated polymers. Eventually we determined that boric acid was the most likely hindrance to initiation and polymerization. We removed excess boric acid by breaking our polymer down to a coarse powder with a mortar and pestle, suspending in methanol, and codistilling off methanol and boric acid under reduced pressure. Afterwards the polymers dissolved easily into THF and upon reprecipitation, formed a light powder.

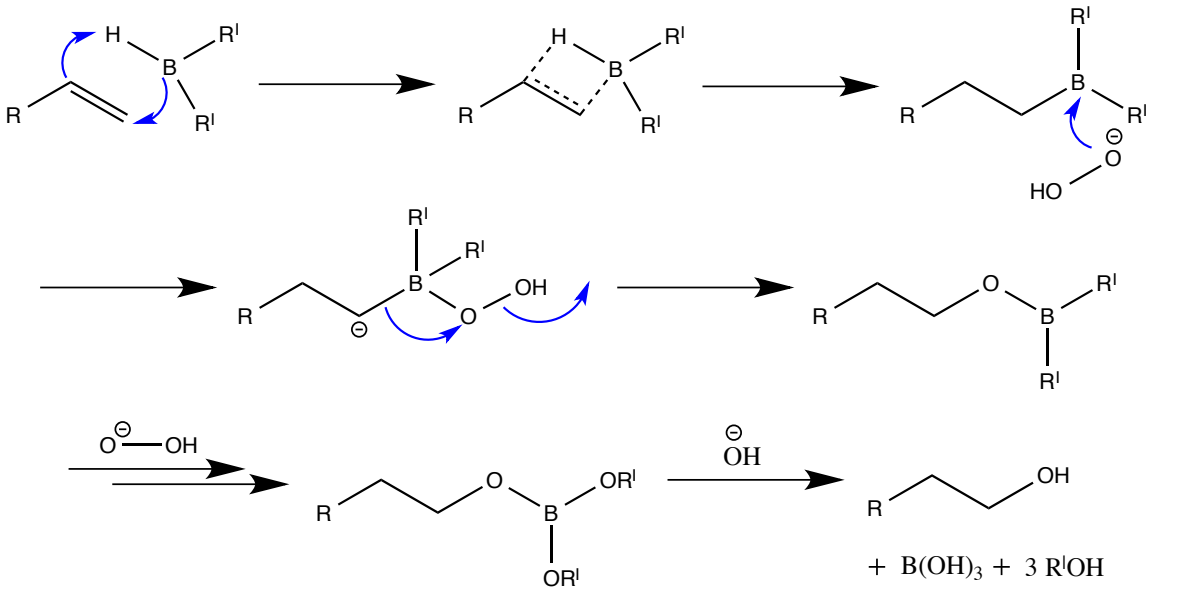

Figure 53: Hydroboration mechanism.

Ethylene oxide was polymerized from the hydroxyl groups generated on the PI block by an anionic ring opening mechanism following initiation by electron transfer using potassium naphthalide. THF was used rather than a hydrocarbon solvent for grafting ethylene oxide in order to solubilize the potassium cation thus stabilizing the anion–radical initiator. Potassium was used rather than lithium because, although lithium-based initiators initiate ethylene oxide, the lithium cation binds too tightly with alkoxides to allow

propagation. Termination by methanol confered hydroxide chain ends to the PEO grafts. **Figure 54** shows the reaction scheme that was followed.

MW was determined by a combination of GPC and NMR. Just prior to the addition of isoprene the reaction was sampled to determine the MW of the PS block using GPC by comparing the retention time of our polymer against a standard curve constructed from narrow PS standards. MWs of PI and PEO were determined by NMR. The integrations of PI and PEO peaks were compared with the integration of PS peaks to calculate DP of each block. PDI was determined by GPC. NMR and GPC spectra are shown in **figures 55**, **56** and in **appendices 4** and **5**. Number of individual PEO grafts and their DP were determined by reaction with the acid bromide, IbB and subsequent NMR analysis shown in **figure 58** and **appendix 4**. **Figure 57** depicts the reaction between the chain ends of PEO grafts and IbB. **Figure 59** depicts the architectures of the polymers that were synthesized based on our analyses. Our polymers were additionally characterized by dynamic light scattering (DLS), static light scattering (SLS), and transmission electron microscopy (TEM) to determine sizes and structures formed in THF, water, and solvent mixtures. We also varied temperatures used for DLS. We saw that the formation of spherical and cylindrical micelles, vesicles, and intermediate structures was dependent on bottlebrush block ratio and architecture as well as the water content of the solvent. In certain cases temperature driven transitions in particle size were observed.

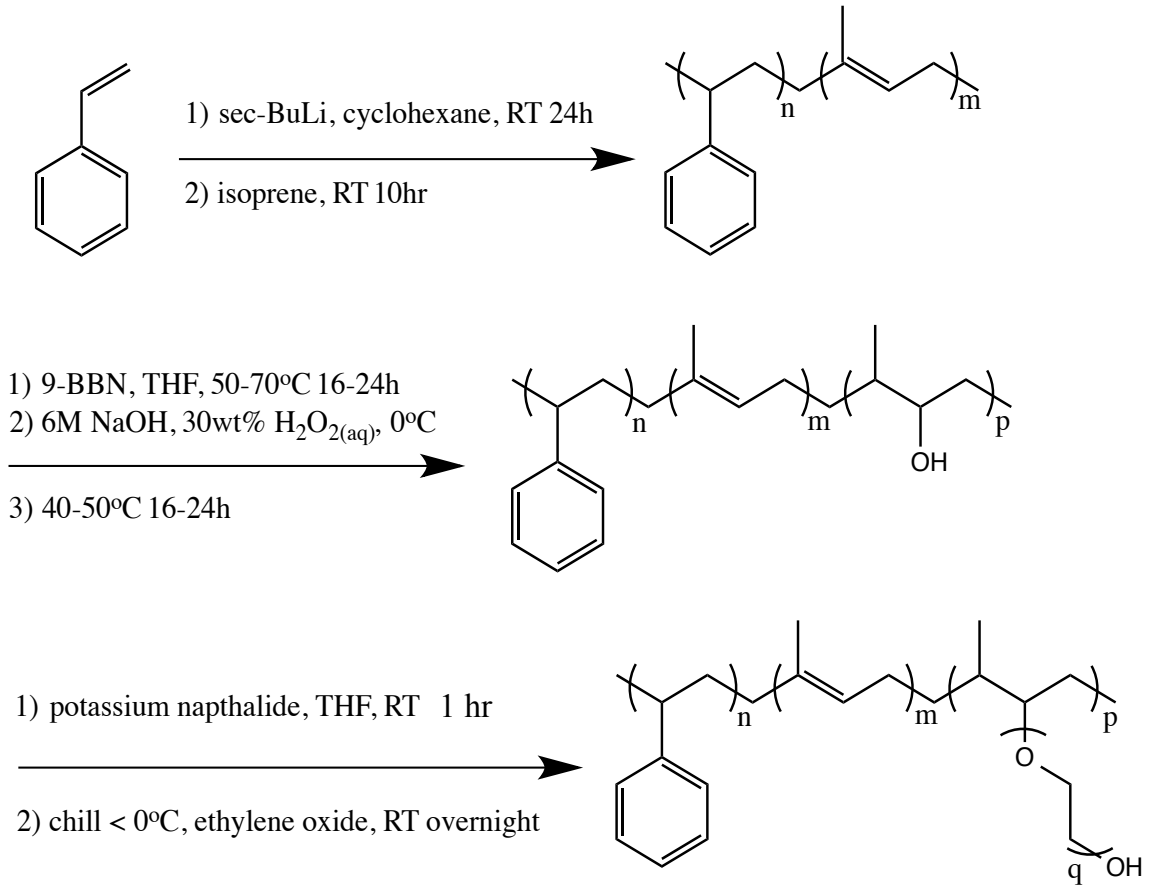

Figure 54: Synthetic scheme for PS-*b*-PI-*g*-PEO copolymer.

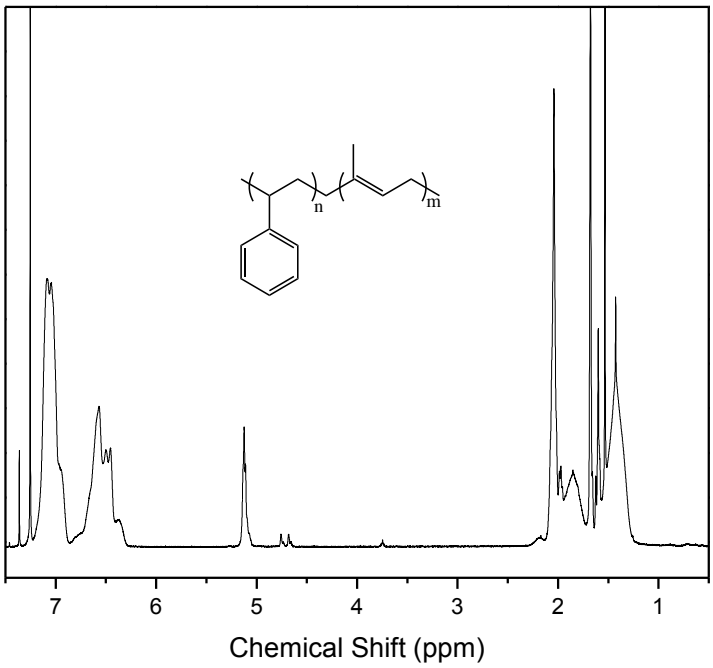

Figure 55: H¹-NMR of PS-*b*-PI linear block copolymer.

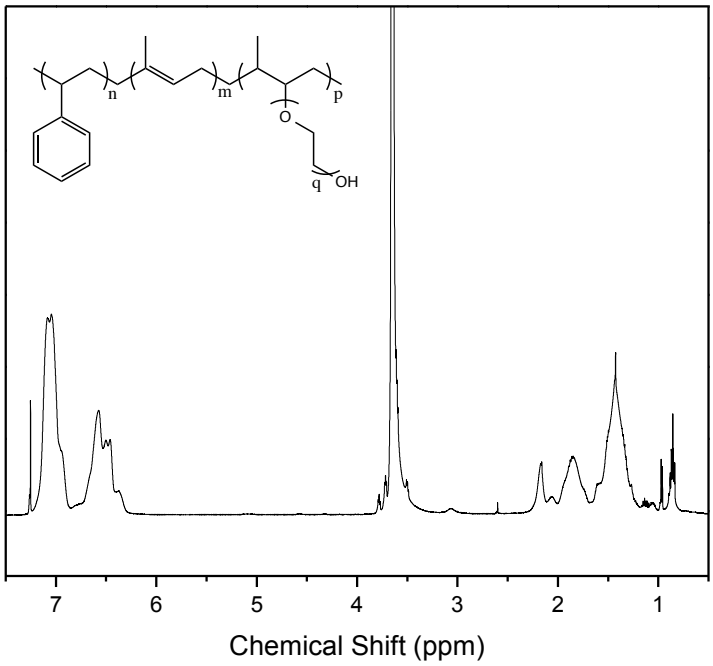

Figure 56: H¹-NMR of PS-b-PI-g-PEO bottlebrush. Polymer 1 pictured. Additional polymer H¹-NMR in appendix 4.

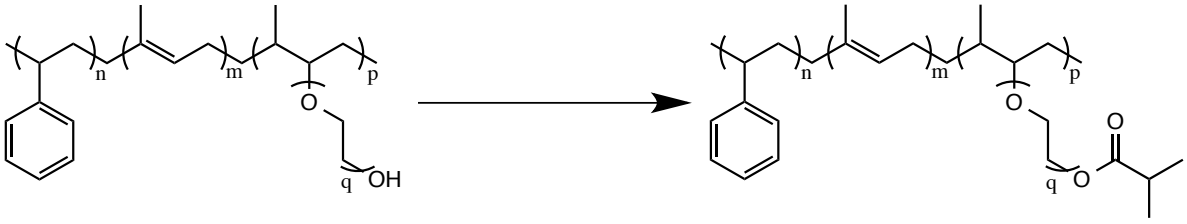

Figure 57: Functionalization of PS-*b*-PI-*g*-PEO copolymers with IbB.

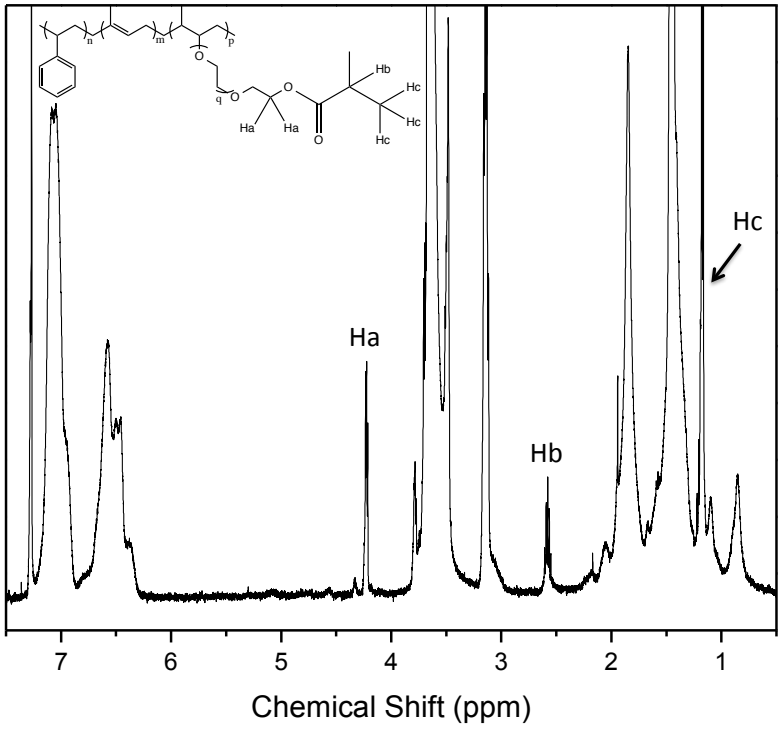

Figure 58: H¹-NMR of IbB functionalized polymer. Polymer 1 pictured. Additional H¹-NMR in appendix. The peak at ~3.2ppm is from hydrolyzed IbB that has not been reacted with the polymer. An acid peak is observed above 9ppm for this molecule.

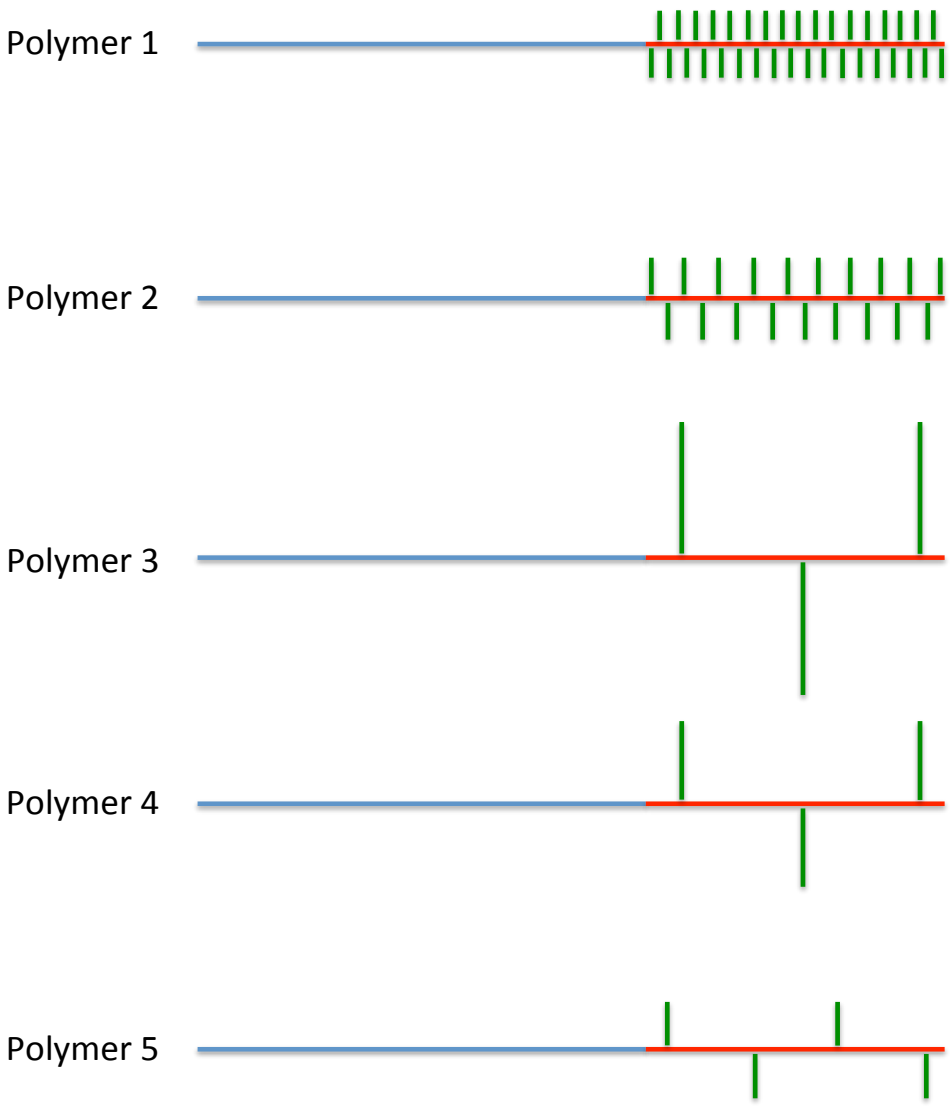

Figure 59: Architecture of PS-*b*-PI-*g*-PEO bottlebrush polymers synthesized.

Table 5: DP and number of grafts and polydispersity of polymers. All polymers were based on the same PS_{392}-b-PI_{134} backbone having a PDI of 1.05.

Polymer	Total PEO DP	Grafts	Graft DP	Polymer PDI
1	710	35	20	1.09
2	465	19	25	1.09
3	485	3	162	1.13
4	287	3	96	1.24
5	210	4	53	1.17

We produced densely and sparsely grafted bottlebrushes. Grafting density along PI roughly followed our targeted degrees of hydroboration in that polymers 1 and 2 were densely grafted and polymers 3, 4, and 5 were sparsely grafted. However, our results show that we grew far fewer PEO grafts than expected based on targeted extents of hydroboration and while polymer 3 was intended to grow more grafts than polymers 4 and 5, all three polymers grew approximately the same number of grafts. PDI after grafting increased slightly for densely grafted bottlebrushes and to a greater extent for sparsely grafted bottlebrushes. We see variation in hydroboration as a major source of polydispersity as hydroboration is responsible for PEO initiation sites. The difference of a single graft added to or removed from densely grafted bottlebrushes has far less of an effect than adding or removing a single graft from sparsely grafted bottlebrushes.

5.3 Self-Assembly of Bottlebrush Copolymers:

Table 6: Dimensions of self-assembled structures and micelle aggregation numbers. Diameter and R_{core} measurements were made using ImageJ and TEM images. R_{corona} was calculated by subtracting R_{core} from R_h as measured by DLS. Aggregation numbers were calculated using equation 4 below.

Polymer	R_{core} (nm)	R_{corona} (nm)	N_{agg} (spherical micelle)	Sphere Diameter (nm)	Rod Diameter (nm)	Vesicle Diameter (nm)
1	18	25	< 320	35±4 PDI: 1.01	n/a	n/a
2	21	31	< 510	41±6 PDI: 1.02	62±7 PDI: 1.01	n/a
3	27	36	< 950	54±11 PDI: 1.04	n/a	282±90 PDI: 1.10
4	20	38	< 360	39±6 PDI: 1.02	69±8 PDI: 1.01	n/a
5	23	17	< 590	46±7 PDI: 1.02	57±5 PDI: 1.01	432±112 PDI: 1.07

$$\frac{4\pi\rho R_{\text{core}}^{3}}{3} = N_{\text{agg}}\frac{M_{\text{W core block}}}{N_{\text{A}}}$$

Equation 4: Micelle aggregation number.[98] **$Mw_{\text{core block}}$ was taken as that of the PS block for Polymer 1 and 2 and that of PS_{392}-b-PI_{134} for Polymer 3, 4, and 5. Bulk density of the core (ρ) was taken to be less than that of bulk PS (<0.969g/cm^3).**[67] **For this reason we report our N_{agg} values with a "less than" symbol.**

TEM: Polymers 1 and 2, which were densely grafted, were only observed to form spherical micelles and, in the case of polymer 2, few short cylindrical micelles. TEM images of polymer 1 and 2 are shown in **figures 60** and **61** respectively. Both showed very few, large dark spheres. We believe these may be the result of sample preparation if a proportion of chains were not able to properly orient and self-assemble for kinetic reasons. We are not surprised that polymer 1 forms only spherical micelles because it has a large proportion of PEO relative to PSPI reducing its packing parameter and favoring structures with highly curved interfaces. While all our polymers formed spherical micelles, polymer 1 formed the smallest thus having the most highly curved interface.

We were not able to observe the PEO corona for the self-assembled structures of any of our polymers because we did not perform cryogenic TEM. However, we determined coronal thickness as the difference in size measured by TEM and DLS.

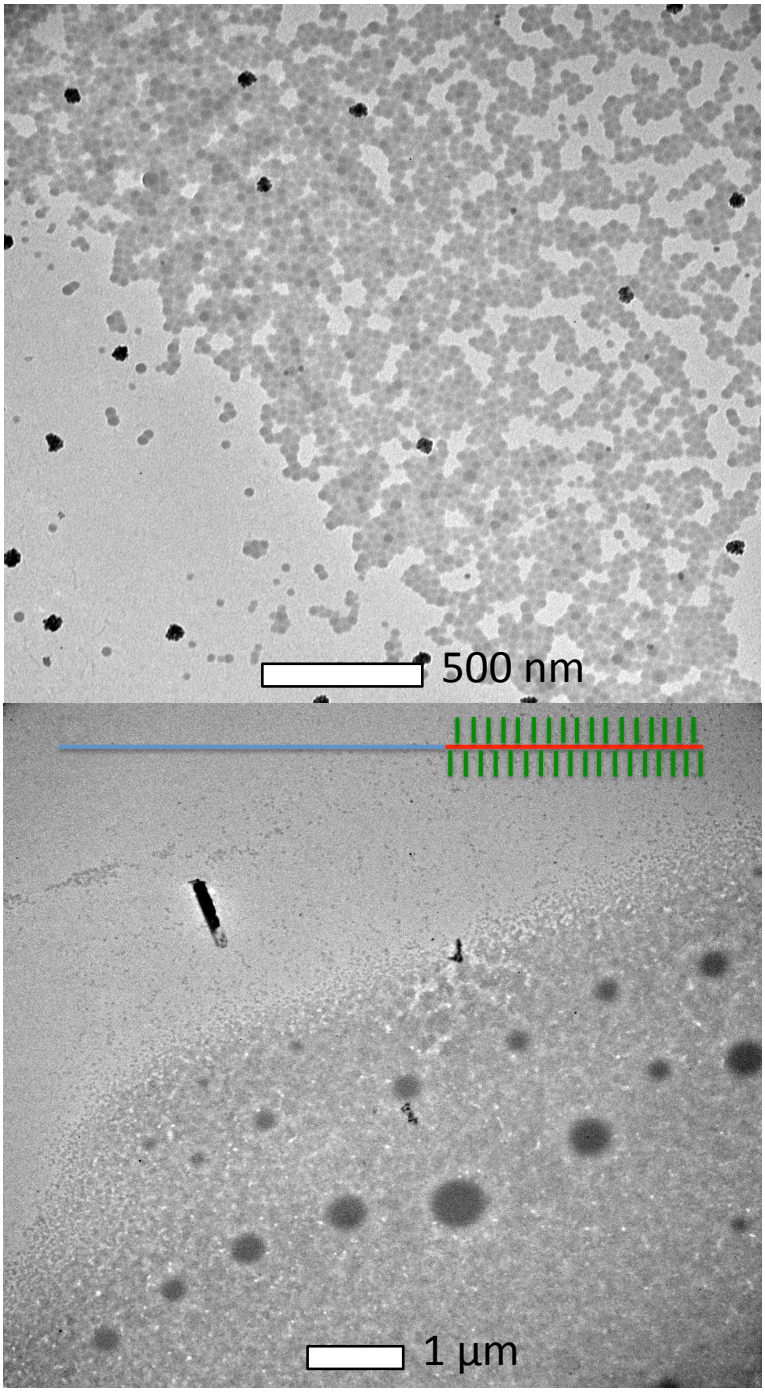

Figure 60: Images of polymer 1 self-assembled structures in water. The above image is typical of the sample. The image below showing large dark spheres highlights these uncommon structures.

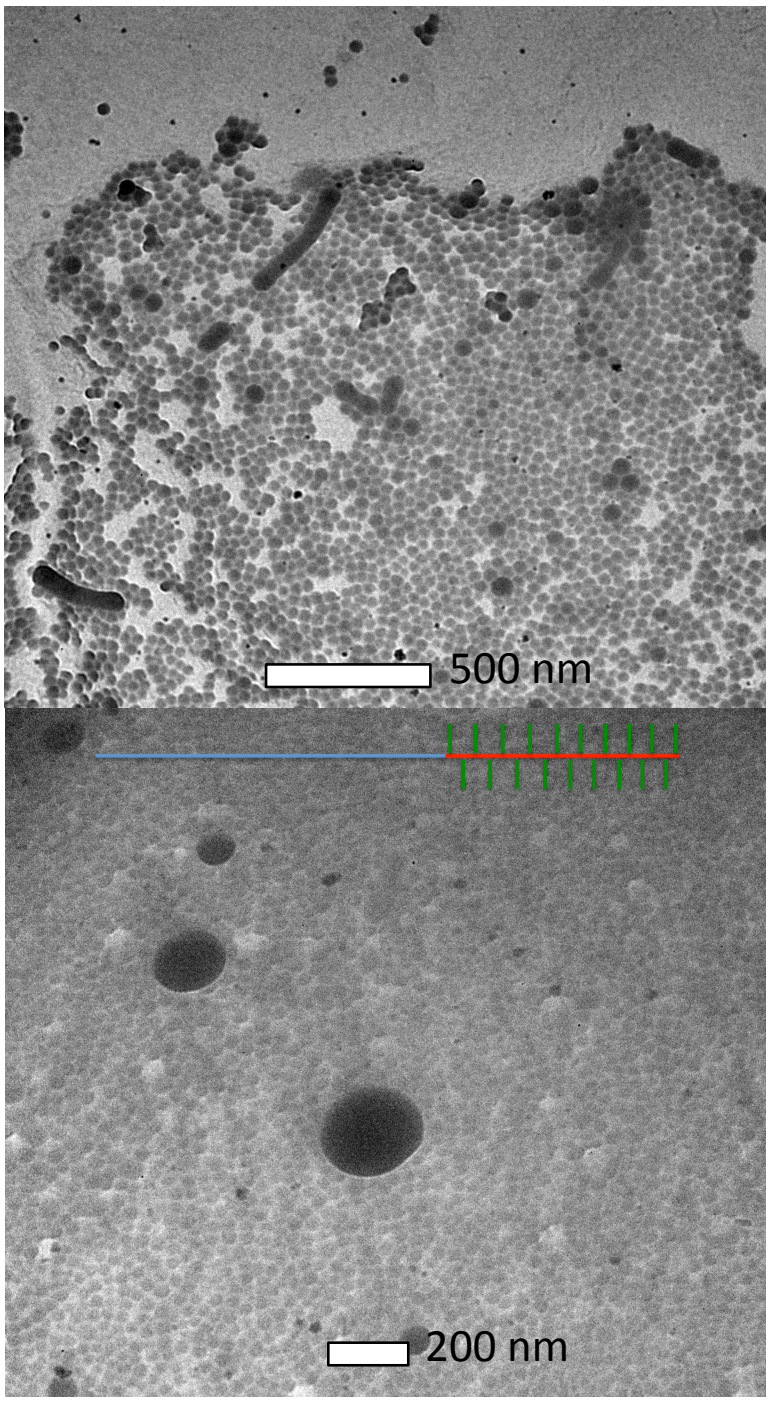

Figure 61: Images of polymer 2 self-assembled structures in water. The image above is typical of the sample. The image below showing large dark spheres highlights these uncommon structures.

Polymer 3 formed only spherical micelles and vesicles in water. TEM images of polymer 3 are seen in **figure 62**. We were surprised not to observe cylindrical micelles. We predict the architecture of our polymers may hinder formation of cylindrical micelles. Like polymer 5, the vesicles formed were not simple bilayer structures. Vesicles were complex, often appearing to have vesicle-in-vesicle morphology. Some appeared to have multiple incased vesicles analogous to Russian dolls.

Polymer 4 formed mostly spherical micelles with fewer cylindrical micelles and did not form vesicles. **Figure 63** shows TEM images of polymer 4 self-assembled in water. We were surprised not to see vesicles, as polymer 4 is structurally similar to polymers 3 and 5 and should have a packing parameter intermediate of the two. Polymer 4 has the highest PDI, which may play a role in this observation.

Polymer 5 was the only polymer to form spherical and cylindrical micelles as well as vesicles. We expected polymer 5 to form vesicles because it has the least PEO of any of our polymers. **Figure 64** shows TEM images of polymer 5 self-assembled in water. Many cylindrical micelles appeared in a transitional state towards becoming vesicles as seen below in **figure 65**. We believe that with even more careful sample preparation polymer 5 may form more vesicles relative to cylindrical micelles.

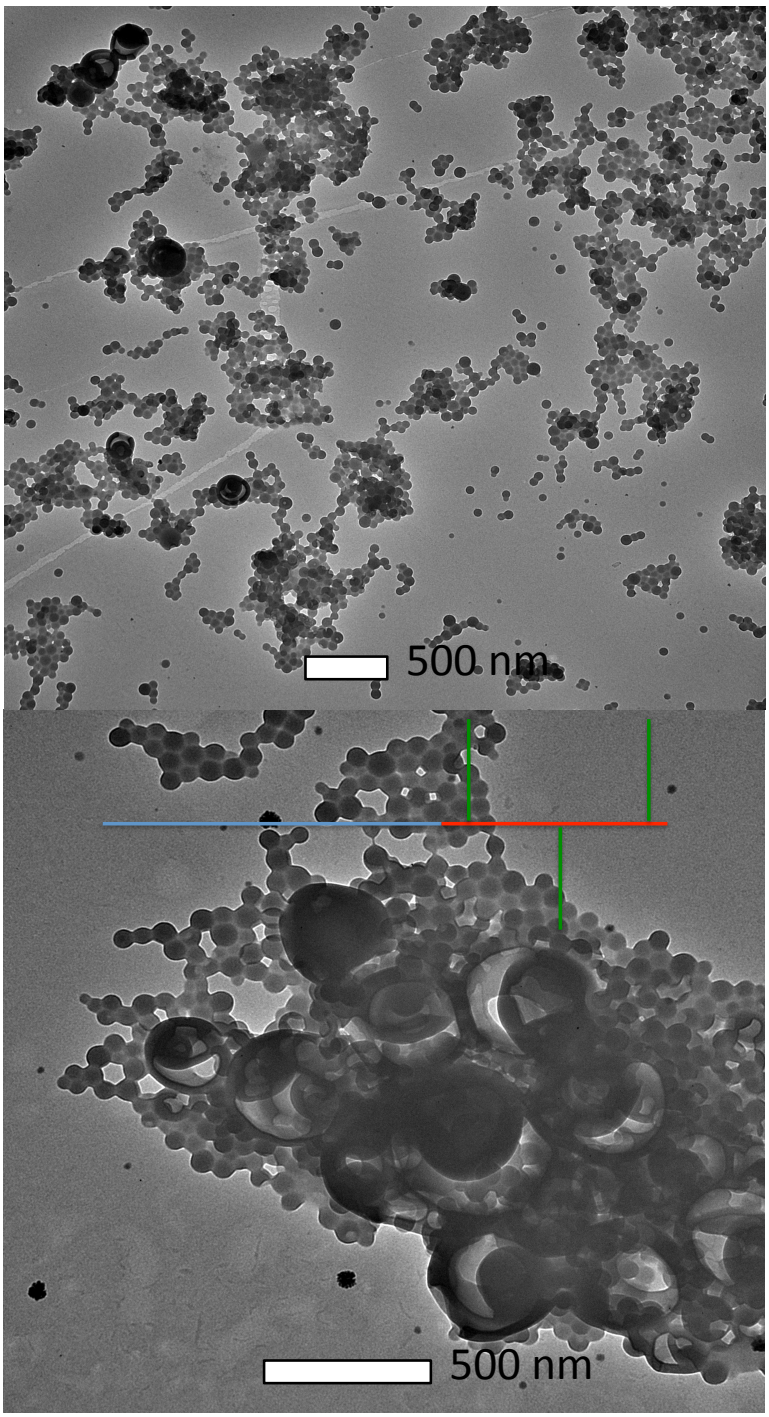

Figure 62: Images of polymer 3 self-assembled structures in water.

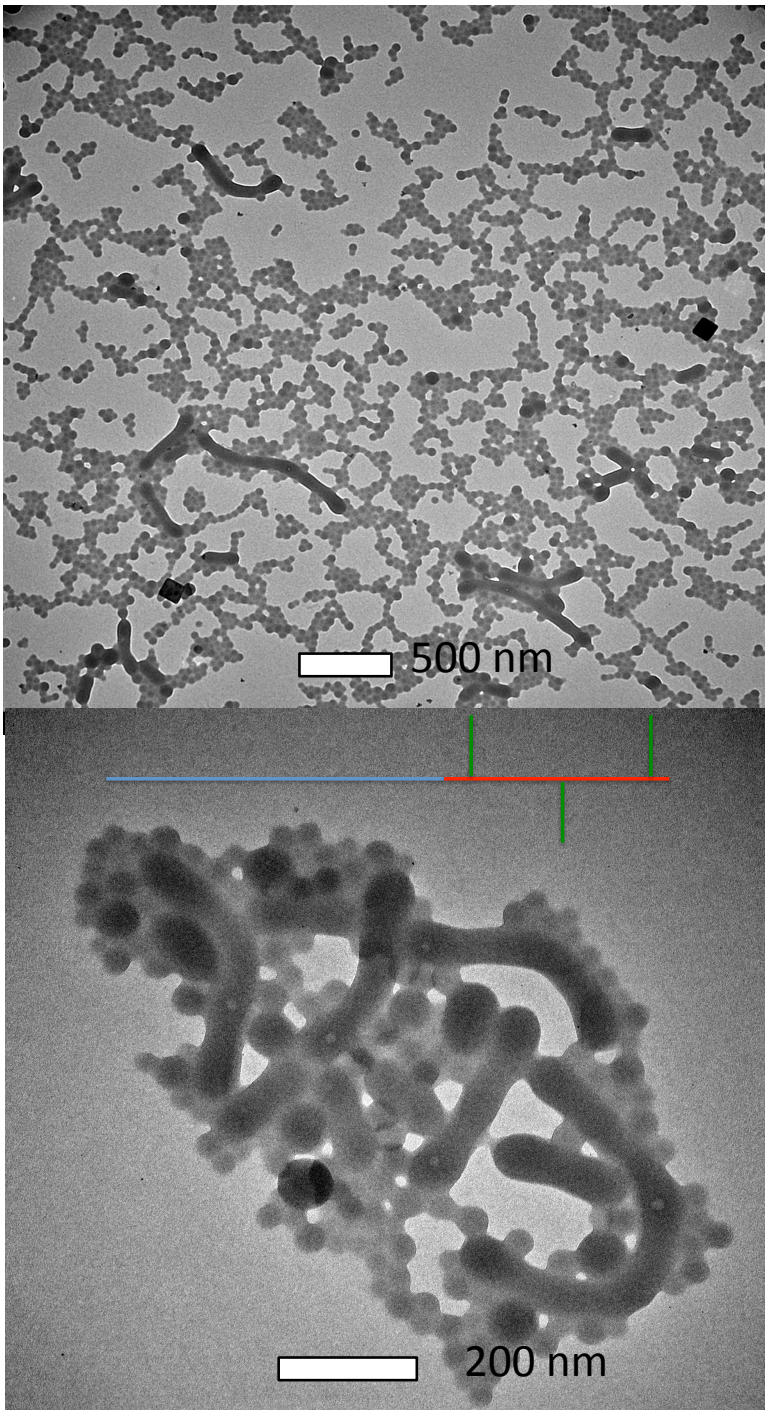

Figure 63: Images of polymer 4 self-assembled structures in water.

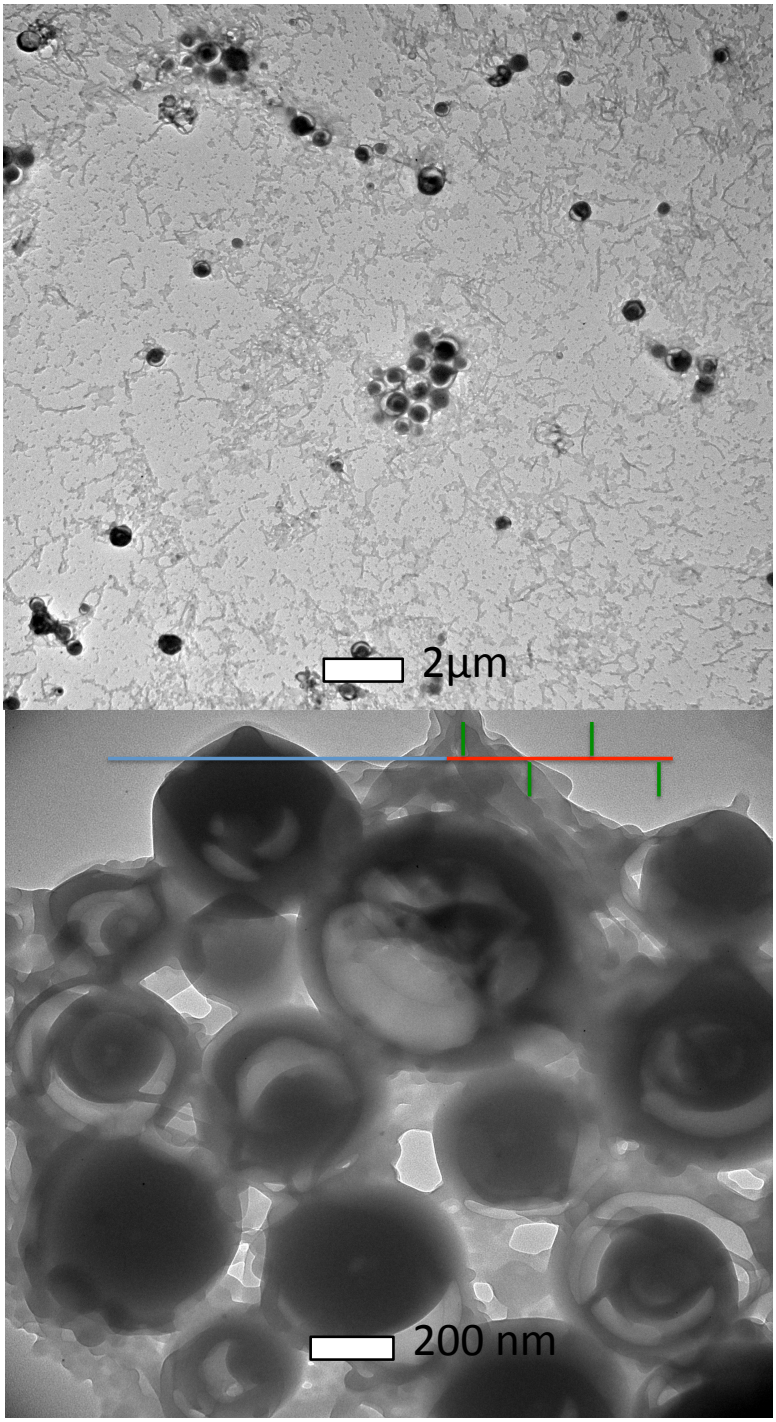

Figure 64: Images of polymer 5 self-assembled structures in water.

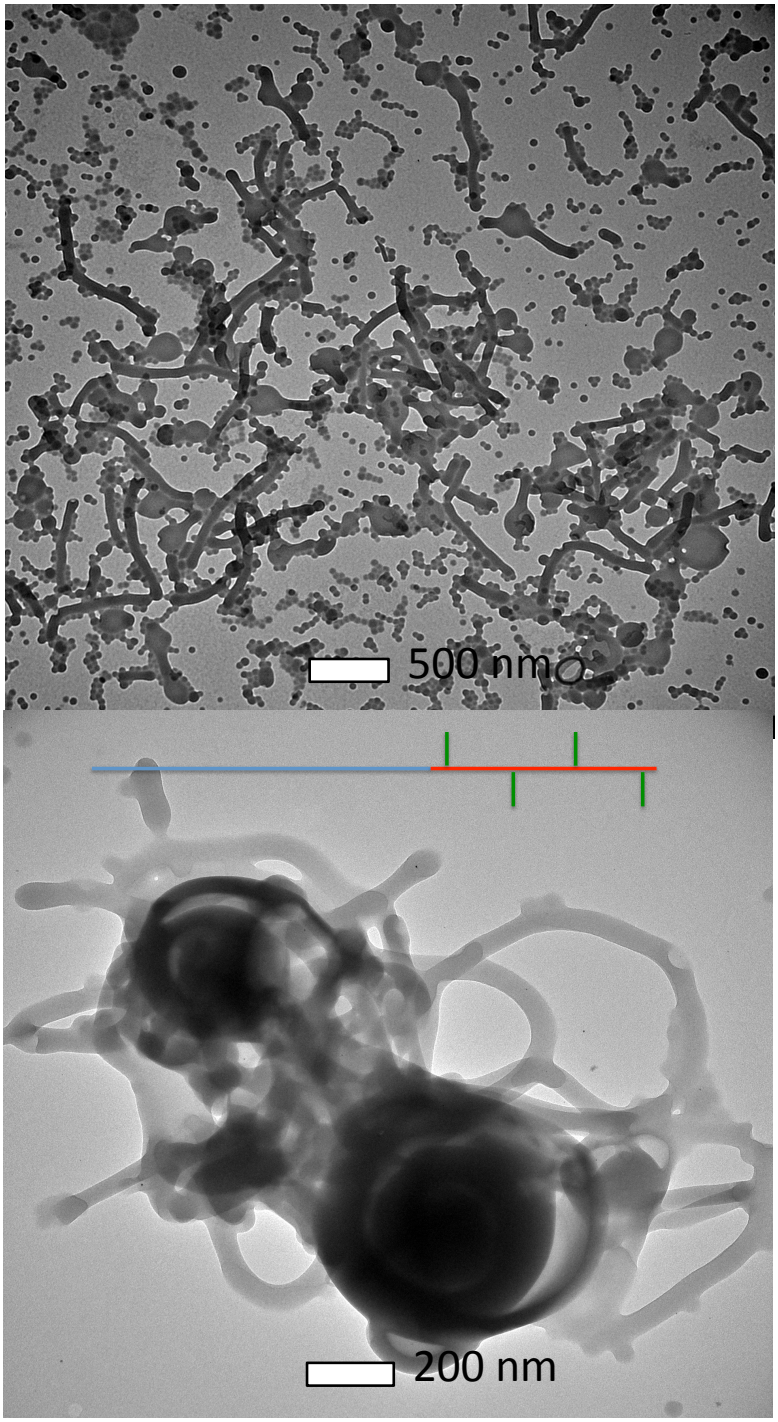

Figure 65: Images of Polymer 5 self-assembled structures in transitional states between cylindrical micelles and vesicles.

DLS: In our nonselective solvent, THF, polymer coil size scaled roughly with total MW aside from polymer 4, which is fairly polydisperse. We also observed aggregates in THF that may or may not be micelle in structure. We observed the sizes of these aggregates and their peak area relative to single chain coils to generally decrease with decreasing polymer concentration. All polymers form micelles in water. The same polymers that do not show vesicles under TEM do not show hydrodynamic radius (R_h) values associated with vesicle size. Micelle R_h values scaled with PEO graft DP for sparsely grafted polymers. We expected this trend, as micelle corona thickness is dependent upon the DP of the hydrophilic block.

Table 7: Hydrodynamic radius results from DLS of polymers at 0.20%wt. in THF and water. R_h values for polymer 2 in THF could not be determined by software because peaks in the distribution function were unresolved so values were estimated visually from peak locations. R_h values for polymer 2 in parentheses were obtained by using a coarse filter to prepare samples.

Polymer	R_h in THF (coil)	R_h in THF (aggregate)	R_h in Water (Micelle)	R_h in Water (Vessicle/Aggregate)
1	7.6 nm	87.9 nm	43.1 nm	N/A
2	7±0.5 nm	45±5 nm	51.9 (64.3 nm)	N/A (434 nm)
3	6.6 nm	90.2 nm	63.2 nm	523.0 nm
4	7.5 nm	122.3 nm	58.2 nm	N/A
5	6.3 nm	105.5 nm	39.6 nm	186.0 nm

DLS With Temperature: In our non-selective solvent, THF, temperature had little effect on polymer coil size, as seen in **figure 66**. We expect all polymer chains to exist as single coils at this concentration of water and polymer. The larger size observed for polymer 5 in pure THF was calculated from non-prominent but distinct peaks in the distribution function. It was difficult to observe a relaxation time in the correlation function corresponding to these sizes upon visual inspection. Furthermore, the larger sizes were only observed at half of the sampled temperatures and varied greatly in R_h with no trend with respect to temperature. We do not take these data points to be an indication of ordered self-assembled structures in our sample. Rather, they may correspond to transient aggregates.

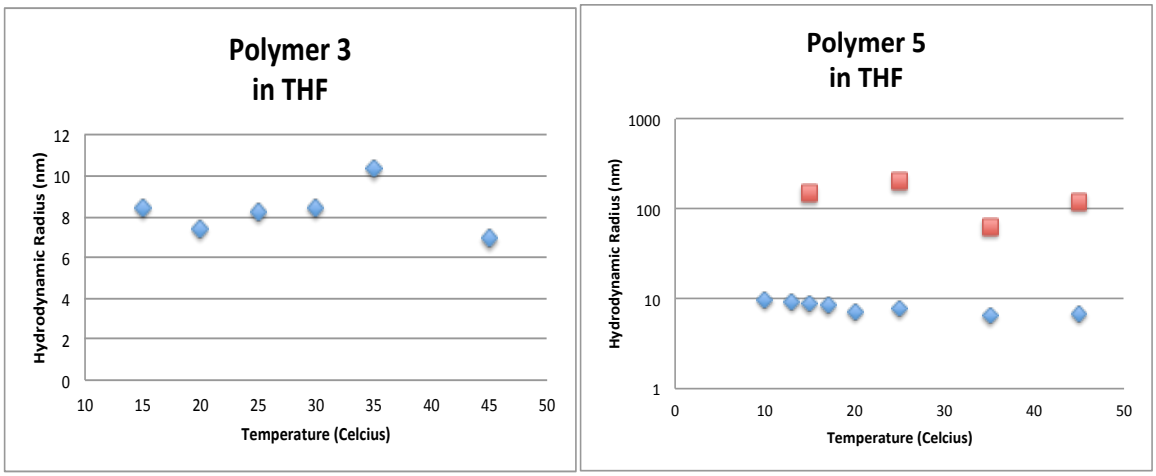

Figure 66: Hydrodynamic radii of polymers 3 and 5 in pure THF with changing temperature. Square points correspond to a secondary (lower intensity) particle size in the distribution.

At intermediate water concentrations we see two particle sizes, as seen in **figure 67**. Small hydrodynamic radii are of single chain coils and their sizes do not change with temperature. Large particles are on the order of what we have observed by TEM for similar water concentrations (**figure 68**). At 25°C, multiple relaxation times were observed for polymer 5 indicating the coexistence of not only single chain coils and large particles, but large particles of various morphologies. TEM of intermediate water concentration shows

several different structures in this range for polymer 5 as seen in **figure 68**. Large particles became smaller as temperature increased and, for polymer 3, disappeared at higher temperatures. This indicates that self-assembly is temperature responsive. Aggregate sizes, morphologies, or both respond to changing temperature. Also, single coils were not observed at the lowest temperatures investigated. We are not sure if this is a result of ordered self-assembly or agglomeration.

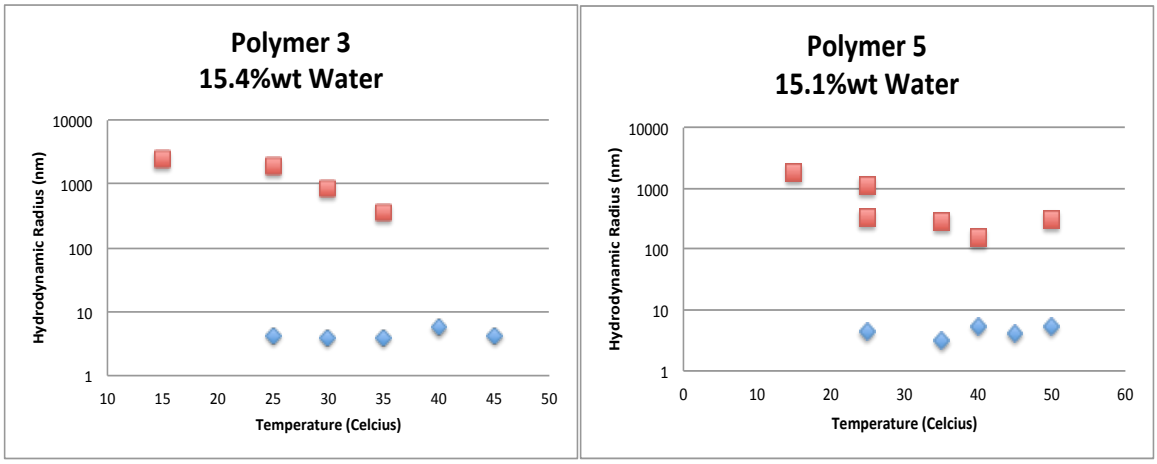

Figure 67: Hydrodynamic radii of polymers 3 and 5 in solutions of 15.4wt% and 15.1wt% water in THF respectively with changing temperature. Square points correspond to a secondary (lower intensity) particle size in the distribution.

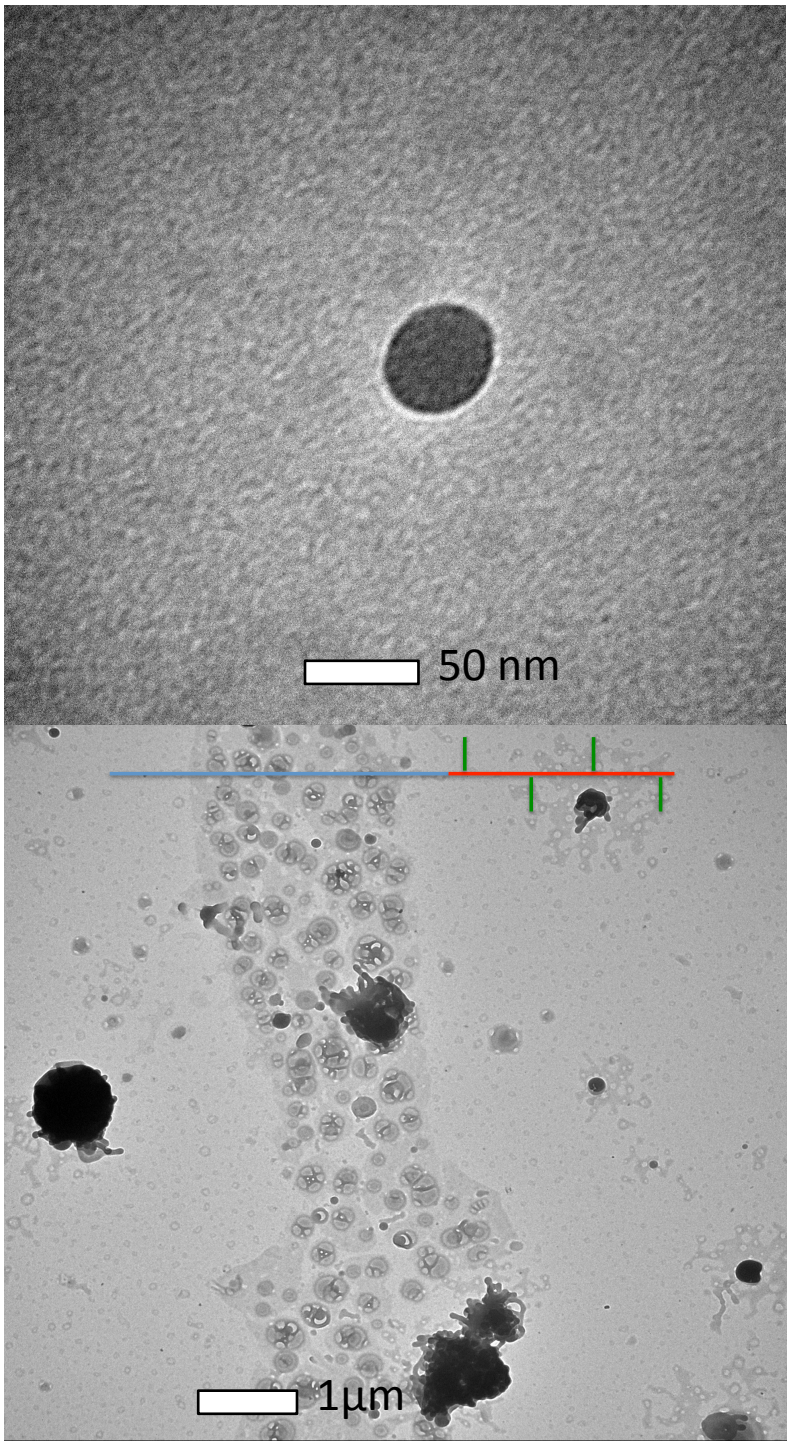

Figure 68: Images of Polymer 5 self-assembled structures at 15%wt. water.

At higher water concentrations we did not observe single chain coils. At ambient or slightly elevated temperature we see very large particles. Sizes are concurrent with some of the structures observed by TEM at this water concentration as seen in **figure 70**. The TEM of polymer 5 shows bundles of bicontinuous cylindrical micelles. The decrease in size at elevated temperature may correspond to a breakup of these bundles. We were not able to observe a transition to single chain coils by increasing temperature indicating that single chain particles may not be accessible at certain water contents.

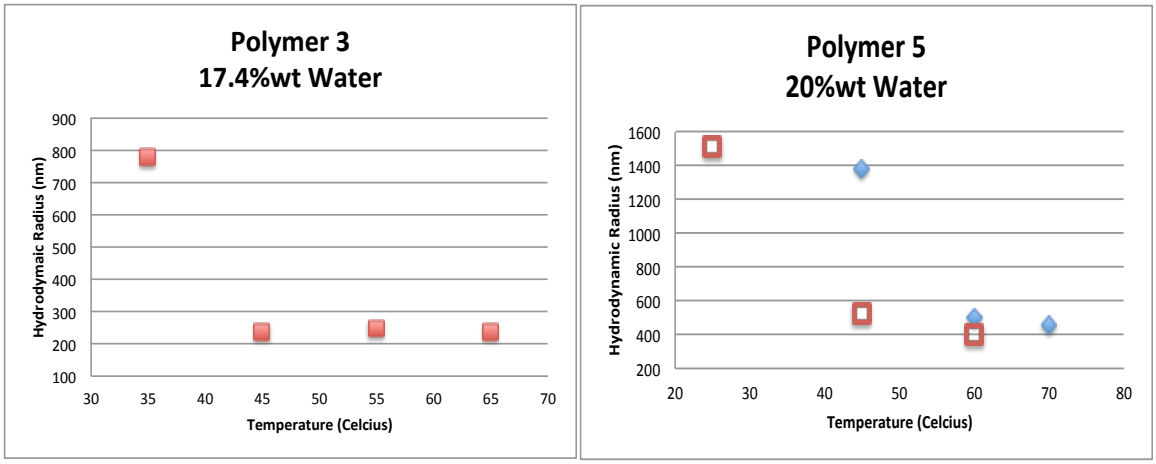

Figure 69: Hydrodynamic radii of polymers 3 and 5 in solutions of 17.4wt% and 20.0wt% water in THF respectively with changing temperature. For polymer 5, Square red points represent data taken one day after blue points. Solution sat at room temperature between taking first and second data set.

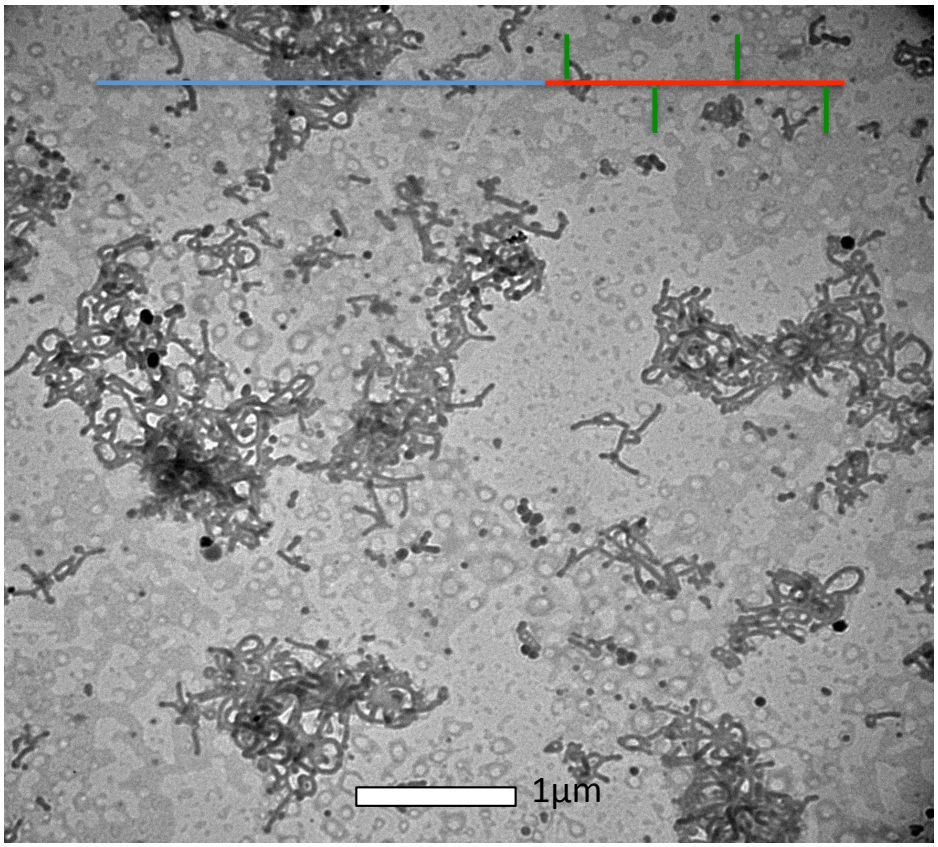

Figure 70: Image of Polymer 5 self-assembled structures at 20%wt. water.

DLS With Concentration (CWC/CMC): We attempted to measure critical water content (CWC) was measured by DLS. We have noticed that THF solutions of our polymers become turbid at generally between 10%wt. and 15%wt. water. To measure CWC we performed DLS for solutions made at 0.2%wt. polymer and varied water concentration while measuring scattering intensity. Unfortunately our results were inconclusive. We have observed that at intermediate water concentrations, samples that are initially turbid will become clear but polymer residue will adhere to the glass ampule. This reduces polymer concentration in solution and thus scattering intensity. At higher water concentrations polymer comes back into solution and solutions become turbid once again. Because of this phenomenon, although we observed aggregates by the correlation functions, samples at

intermediate water contents such as 15%wt. and 17%wt. water gave low scattering intensities.

To address whether the aggregates seen in pure THF might be micelle in nature, we attempted to measure a critical micelle concentrations (CMC) by DLS, observing scattering intensity as samples were progressively diluted. We observed no clear discontinuous change in scattering intensity indicating that there was no break up of micelle structures. See Appendix 6 for CWC and THF CMC plots.

SLS: Static light scattering (SLS) was performed for polymer 1, however, we had difficulty with sample preparation and measuring an accurate *d*n/*d*c. The results were not consistent with the rest of our experiments. SLS results have been included in the appendix.

DCA: We measured CMC of polymers 1 and 3 by dynamic contact angle (DCA) as polymer concentration was reduced in water. We expect that, above CMC, surface tension should be constant regardless of changes in polymer concentration but below CMC, surface tension should increase with decreasing polymer concentration. We observed surface tension to change very little above 0.020%wt. polymer, as seen in **figure 71**. The values correspond to 2.6μM and 2.8μM for polymers 1 and 3 respectively. At lower concentrations surface tension increased quickly. These values are in line with typical CMC values for polymeric micelles which are in the 10^{-6}-10^{-7} molar range.[99,100] More data points are needed to get precise CMC values.

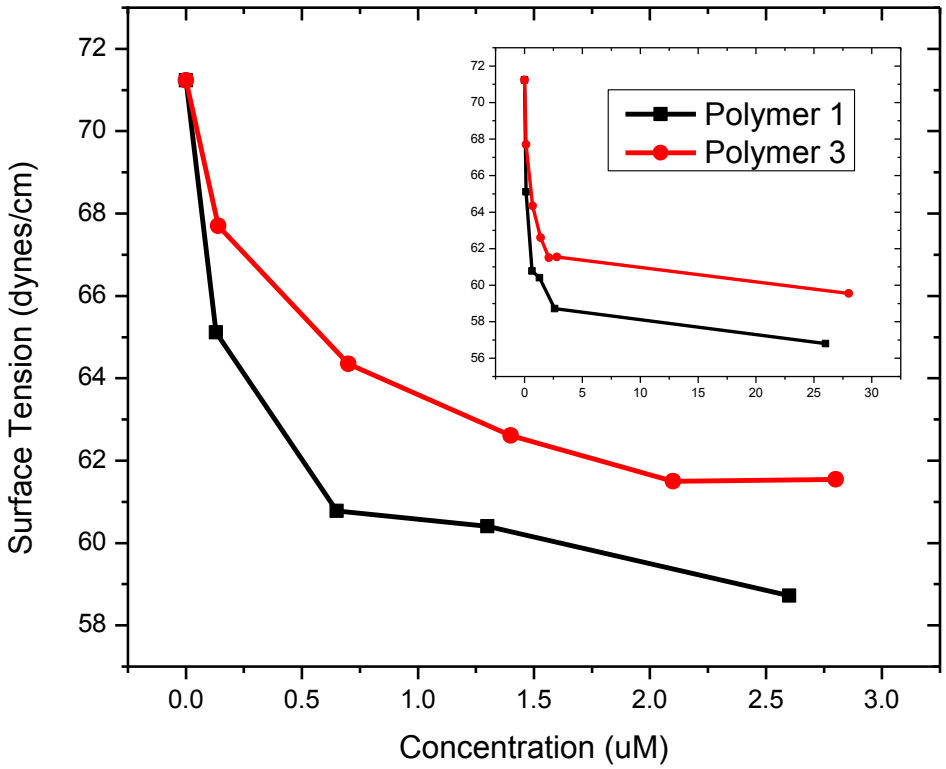

Figure 71: DCA analysis of polymer 1 and 3 in water. Inset, the full plot includes the 0.20%wt. polymer concentration (26 and 28μM for polymers 1 and 3 respectively).

5.4 Discussion and Conclusion: We did not observe the formation of unimolecular micelles. As we increased water concentration we were able to observe decreased sizes of individual polymer chains that coexisted with larger aggregates. However, we believe these were coils and not micelle in conformation because they were not stable to further increases in water concentration. We suspect that unimolecular micelles are achievable using our general bottlebrush architecture. It is likely that the bottlebrush portion of our densely grafted polymers was too rigid to encapsulate the hydrophobic PS chain. Our sparsely grafted polymers likely did not have enough grafts to adequately cover and stabilize a spherical micelle. In future study we would like to synthesize polymers with an intermediate

number of grafts to achieve unimolecular micelles. We would also like to experiment with using much lower polymer concentrations as this may favor the formation of unimolecular versus aggregate structures.

DCA analysis was initially performed on polymer 1 in hopes of indicating unimolecular micelle formation. In the case of unimolecular micelles we would expect to detect no CMC as the formation of micelles would have no concentration dependence. Detection of a CMC, as seen in **figure 71**, for both polymers 1 and 3 shows that micelles are in fact not unimolecular. We focused on the very low concentration range of 10^{7}–10^{6}M as high MW self-assembling block copolymers have shown CMC values in this region.[99,100] While we would need more data points to get precise CMC values, polymers 1 and 3 appear to show CMCs in the 10^{7}–10^{6}M range. Low CMC values indicate micelle stability so we see our micelles as being fairly stable on the same order as other reported micelles formed by high MW amphiphilic polymers.

Other than polymer 5, our polymers did not form many cylindrical micelles and those that did form were generally short. Polymer 5 formed many long cylindrical micelles coexisting with spheres and vesicles in water, however, upon close inspection many of these cylindrical micelles appeared to be in a transitional phase towards the formation of vesicle type structures. The observation that, at 20%wt. water, polymer 5 formed many cylindrical micelles but no vesicles and did form many vesicles at 100%wt. water indicates that the vesicle morphology is favored at higher water content. TEM also reveals the lowest proportion of spherical micelles for Polymer 5. This is not surprising as Polymer 5 has the lowest total PEO DP, therefore the greatest packing parameter so morphologies with high interfacial curvature should be less stable. We believe that with different sample preparation

we could induce a total transition to vesicle morphology for polymer 5. We see TEM results for polymer 5, as well as the coexistence of multiple morphologies seen for polymers 3 and 4, as indication that our sample preparation may not produce structures with under total thermodynamic control. In the future we would like to prepare solutions at an even slower rate of water addition to totally avoid kinetic trapping of intermediate structures.

We formed complex vesicles that appeared concentric as well as continuous. Outer vesicles appeared to evolve or spiral out from inner vesicles is many cases. We hypothesize that the architecture of our polymers does not allow simple phase segregation of hydrophilic and hydrophobic blocks, which may lead to the complexity seen in our vesicles. However, we realize that kinetic trapping may have had a hand in the complexity in the vesicles we observed.

Based solely on total PEO DP and the fact that polymer 3 forms vesicles, we should expect to see vesicles formed by polymers 2, 4 and 5 using packing parameter arguments. Comparing polymer 2 and 3, which have approximately the same total PEO DP shows the effect that architecture has on the self-assembly of our polymers. The densely grafted polymer 2 does not appear to be able to form vesicle structures while the sparsely grafted polymer 3 readily forms vesicles. We speculate that although polymers 2 and 3 have approximately the same total hydrophilic fraction, dividing the hydrophilic component into a greater number of grafts causes it to take up a greater total volume thus decreasing the effective packing parameter. Another way to consider the situation is that if, in densely grafted polymers 1 and 2, PI is effectively excluded from contributing to the polymer's hydrophobic volume due to its inflexibility, the total hydrophobic volume is decreased therefore again decreasing the packing parameter.

Temperature was seen to have little effect on the size of single chain coils but a large effect on the formation of aggregates. At intermediate water concentrations we were able to induce the appearance or disappearance of aggregates by lowering or raising temperature respectively. We assume that this effect is due to improvements in solvent quality at higher temperatures as none of the blocks in our polymers are considered to be especially temperature sensitive.

Micelle Coronas: The thickness of micelle coronas (R_{corona}) can be measured by subtracting the radius of micelles as measured by TEM from the R_h obtained from DLS.[98] **Table 9** shows the results of this calculation to find R_{corona}.

Table 8: Grafting density at surface of micelle core. Surface density of PI or PEO chains was calculated based on N_{agg} values and the micelle core surface areas calculated from R_{core} (see table 7). See appendix 9 for the equations used in calculating R_{max} and R_F values.

Polymer	R_{corona} (nm)	PI R_{max} (nm)	Grafts	Graft DP	Graft R_{max} (nm)	Graft R_F (nm)	Surface Density PI (chains/nm^2)	Surface Density PEO (chains/nm^2)
1	25	68	35	20	7.7	< 3.3	< 0.084	< 2.9
2	31	68	19	25	9.6	< 3.8	< 0.096	< 1.8
3	36	68	3	162	62	< 11	< 0.10	< 0.31
4	38	68	3	96	37	< 8.4	< 0.075	< 0.23
5	17	68	4	53	20	< 5.8	< 0.089	< 0.36

Consideration of our PEO Graft DP along with R_{corona}, we conclude that the micelles formed by densely grafted polymers (polymer 1 and 2) must have bottlebrush coronas where PI is excluded from the micellar core and extends the length of the corona. **Figure 72** depicts what the corona may look like.

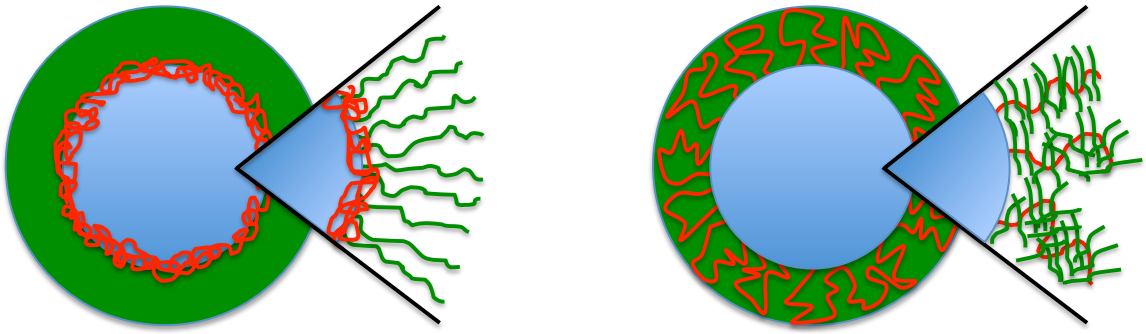

Figure 72: Proposed morphologies of micelles formed by sparsely grafted (left) and densely grafted (right) polymers.

We support this hypothesis with multiple lines of reasoning based upon parameters we have calculated and reported in **table 9** above. First, based on the number of grafts we have measured for polymer 1 and 2 and total PEO DP, Graft DP is too small to extend R_{corona} even in their fully extended conformations (Graft R_{max}). Realistically, were the corona composed of these PEO grafts, we would expect R_{corona} to be some thickness greater than the unperturbed coil size (Graft R_F) but less than Graft R_{max} with thickness increasing with coronal density. Second, given Graft R_F and the number of grafts, repulsions among adjacent grafts should cause extension of the PI block such that inclusion of the short PI segments between PEO grafts into the micelle core would incur and energetic penalty destabilizing to the micelle. Third, calculation of coronal density (at the surface of the core) based on micelle aggregation number and surface area of the core yields unreasonable values if we consider the corona to be composed of solely PEO grafts. Values approaching 1.0 chain/nm^2 are rarely reported in polymer brush literature. Such high coronal density values would be destabilizing to micelle formation. Corona density measured as extended PI chains is in a very reasonable range considering common polymer brush densities.

In contrast to our densely grafted polymers, calculations for our polymers with few grafts (polymer 3, 4, 5) suggest that the micelle corona can be composed of only PEO grafts.

Most likely, the corona does not contain PI because of the high energy hydrophobic interactions that the long segments of PI between PEO grafts would have with water. Calculating coronal density assuming it to be comprised of solely PEO gives numbers typical of a densely grafted polymer brush for which chains would be highly extended. This is consistent with our calculations of R_{corona}, which are close to Graft R_{max}. Graft R_{max} of polymer 3 is furthest from its R_{corona} however The disparity seem reasonable as we do not expect chains to be fully extended especially as effective grafting density decreases with distance from the micelle core. Since the grafts of polymer 3 are longer than those of polymer 4 or 5 we should expect the largest disparity between R_{corona} and R_{max}.

Micelle morphologies such as those we have proposed for our densely grafted polymers have been recently reported by Rzayev et al. who synthesized amphiphilic bottlebrush polymers.[60] Their polymers were traditional bottlebrushes that were grafted over the entire length of the backbone but one half of backbone was grafted with hydrophobic chains and the other half with hydrophilic chains. They were able to form spherical and cylindrical micelles as well as some irregular vesicles and flat bilayers by varying the hydrophobic and hydrophilic graft lengths. Our work is, to our knowledge, the first study reporting micelles of this architecture formed by the self-assembly of bottlebrushes having linear hydrophobic tails.

Considering the micelle corona thicknesses of the densely grafted polymers allows us to infer what factors affect extension of the PI backbones. Polymer 2 formed micelles with thicker coronas than polymer 1 although they both had the same PI DP. First, we calculated the surface density of PI to be approximately 14% greater for polymer 2 micelles than polymer 1 micelles. Increased grafting density should cause extension of the chains.

Secondly, polymer 2 has fewer and longer grafts as compared with polymer 1. These longer grafts of polymer 2 have a graft R_F approximately 15% greater than grafts of polymer 1. We see denser grafting of polymer 1 as causing stretching of PI due to intrapolymer excluded volume interactions and increased graft R_F of polymer 2 as causing stretching of PI due to interpolymer excluded volume interactions. Unfortunately, while we see the increased corona thickness of polymer 2 as a result of interpolymer interactions, we cannot distinguish whether graft R_F or surface density of PI chains is a greater contributor to PI extension.

We are confused as to why polymer 4 does not appear to form vesicles given its total PEO DP and architecture. We suspect the high PDI of polymer 4 as compared with our other polymers is responsible. We are aware that self-assembled structures may be destabilized by polydispersity in the solvophobic block but polydispersity in the solvophilic block has not been shown to hinder assembly. Rather, studies show that polydispersity in the solvophilic block can generate smaller vesicles as shorter chains generally situate on the interior of the vesicle and longer chains on the exterior thereby allowing a tighter curvature.[101,102] These studies used linear BCPs so our observations for polymer 4 may highlight another way in which the self-assembly of bottlebrushes is unique. We speculate that, if a certain fraction of polymer 4 is more densely grafted such that PI is extended into the corona as for polymers 1 and 2, that fraction may be unstable towards the formation of vesicles and cause stabilization of the micelle morphology. If the energy penalty is great enough, micelles may not transition to vesicles. **Figure 73** below depicts a speculative representation of how micelles formed by polymer 4 may look with a corona composed partially of extended densely grafted PI chains. We may test this hypothesis in the future by mixing various ratios of densely and sparsely grafted bottlebrushes and observing by TEM

what structures are formed.

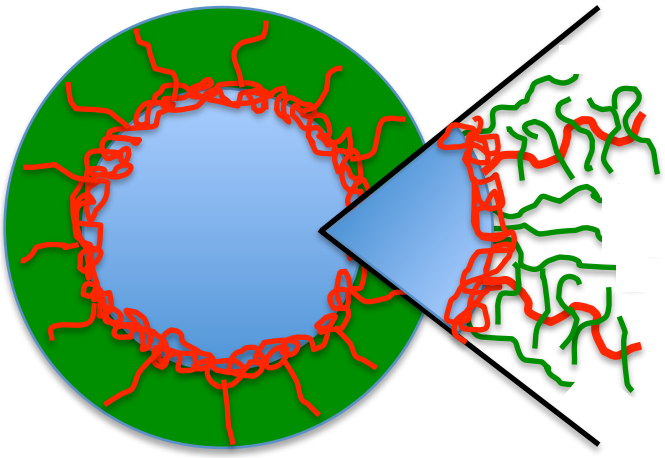

Figure 73: Potential structure of a micelle formed by both densely and sparsely grafted bottlebrushes.

5.5 Experimental

Polymer Synthesis: Reagents were purchased from Fisher Scientific. Cyclohexane (Fisher, 99.9%), Isoprene (Aldrich, 99%), and Styrene (Aldrich, ≥99%) were dried, degassed and distilled under vacuum then brought into a N_2 filled glovebox prior to use. Cyclohexane and isoprene were dried with sec-butyl lithium (Acros, 1.3M in cyclohexane/hexane(92/8)). Styrene was dried with di-n-butylmagnesium (Acros, 0.5M in heptane). All glassware was oven dried before entering the glovebox. A round-bottomed flask was charged with a stir-bar and dry cyclohexane. To assure solvent was entirely dry, a small amount of 1.3M sec-butyl lithium (approximately 0.1%volume of cyclohexane) was added to the flask that was then stoppered and shaken vigorously for several seconds. While stirring, styrene was added to the flask and solution became faintly yellow. Polymerization was initiated by the addition of 1.3M sec-butyl lithium and solution became orange. After 20 hours of stirring in the glovebox at room temperature an aliquot was removed for GPC. Isoprene was added and

solution became a pale yellow. After another 10 hours stirring at room temperature the flask was removed from the glovebox and polymerization was terminated with methanol (Aldrich, ≥99%). Polymer was precipitated into methanol, collected by vacuum filtration and dried in a vacuum oven after which GPC and ^{1}H-NMR spectra were taken. Hydroboration of the poly(styrene)-*b*-poly(isoprene) (PSPI) copolymer was set up in the glovebox. The polymer was dissolved in THF (Fisher, histological grade) that had been dried by refluxing with and distilling from sodium. Next 9-borabicyclo[3.3.1]nonane (Aldrich, 0.5M in THF) (9-BBN) was added. Heating and oxidative workup were performed outside of the glovebox using NaOH (Fisher, pellets) and H_2O_2 (fisher, 30%wt) solutions degassed by repeated aspirating and backfilling with N_2. The procedure reported by Ramakrishnan[26] was followed to achieve various extents of hydroboration. Hydroborated polymer was precipitated into methanol, collected by vacuum filtration and dried in a vacuum oven after which GPC and ^{1}H-NMR spectra were taken. Boric acid was removed by suspending manually breaking down the polymer to a powder, suspending in methanol, then removing methanol under reduced pressure by rotovap,

Growth of ethylene oxide grafts was performed in the glovebox. Potassium naphthalide was made up in the glovebox within a week of use using dry THF, naphthalene (Aldrich, ≥99%), and excess potassium. Ethylene oxide was distilled and condensed on the vacuum line and kept at as a liquid at -34^{o}C in the glovebox freezer. Hydroborated polymer was placed in a scintillation vial with a stir-bar and fitted with a PTFE lined cap then dissolved in dry THF and potassium napthalide was added. Solution became dark green and was stirred at room temperature for > 1 hour. Solution was chilled in the glovebox freezer at -34^{o}C for 15-30 minutes then removed and ethylene oxide was added using a chilled

syringe. Solution was sealed and stirred at room temerature for 20+ hours during which time it became lighter yellow/orange. Polymerization was terminated with methanol then precipitated into diethyl ether. Precipitation was generally incomplete and polymer was collected by reducing with air then drying in a vacuum oven before taking GPC and ^{1}H-NMR spectra. To remove poly(ethylene oxide) (PEO) homopolymer, polymers were stirred in distilled water and insoluble portions were collected by vacuum filtration. NMR of soluble fraction confirmed homo-PEO. Polymers were esterified by dissolving 0.050g into 5.0ml $CHCl_3$ and 0.4ml triethylamine then adding 0.15ml IbB and allowing to stir overnight at room temperature. Following precipitation and drying, the number of grafts was determined by NMR.

GPC: Gel permeation chromatography (GPC) was used to determine PDI of all polymers synthesized and M_n of PS blocks. Samples were prepared by dissolving polymer in THF, then passing through 0.45μm syringe filter. Samples were run in THF mobile phase at a flow rate of 2 ml/min. Autosampler and column oven were set to 40^{o}C. Column set consisted of one 100k, two 10k and one 500 angstrom Jordi Gel fluorinated DVB columns and a Varian 380-LC Evaporative Light Scattering Detector (ELSD) was used for detection. MW was determined by comparison with a standard curve calculated from narrow PS standards.

NMR: Performed using the same instrumentation and techniques as listed in section 2.7.

DLS: Dynamic Light Scattering (DLS) for samples taken without temperature variation was performed with an ALV/CGS-3 compact goniometer system on a ALV-7004 digital real time correlator integrated in ALV/LSE-6004 light scattering electronics at a fixed scattering angle of 90^{o}**.** The CONTIN analysis method was used. The instrument was equipped with a

laser source having a λ of 632.8nm and a temperature controlled sample cell filled with toluene kept at 25 °C. Temperature variable DLS was performed with a BI-200SM goniometer (Brookhaven Instruments) using a 2.5 W Ar laser light source (Model Innova 70-3 from Coherent) operating at 514.5 nm and a BI-9000 AT digital correlator (Brookhaven Instruments). Samples were prepared by dissolving polymer in THF then adding distilled water to attain the desired weight fraction. Excess THF was added as necessary to attain a consistent weight fraction of polymer in solution for all samples. Samples of 100% water were prepared by slowly adding water to a THF/polymer solution at a rate less than 1%wt./minute and agitating to ensure mixing until the solution became turbid. Next the solution was dialyzed against distilled water to remove all THF. Samples were filtered through 0.45μm filters. For measurements in which temperature was varied, hydrodynamic radii were determined by using the Stokes-Einstein equation and calculated diffusion coefficients.

$$D = \frac{k_B T}{6\pi \eta r}$$

Equation 5: Stokes-Einstein equation.

Diffusion Coefficients were determined by measuring multiple angles and building plots of q^2 versus $1/\tau$. See appendix 6 for diffusion coefficient plots. We made glass ampules that the samples were prepared in. The samples were then frozen using liquid nitrogen and a torch was used to seal the ampules under vacuum. A circulating water bath was used to control temperature. Sample refractive index, n_D, and viscosity, η, were calculated using experimental data on water/THF mixtures reported by Aminabhavi[28] assuming a linear trend between data points. All samples were dilute in polymer (0.2%wt.) so we took n_D of the solutions to be the same as the water/THF mixtures.

TEM: Transmission electron microscopy (TEM) was preformed with polymer dissolved in THF and water at 0.2%wt. Samples were drop cast on a 400 mesh TEM grid coated with a 3 nm thick carbon layer and allowed to dry. Images were taken on FEI Tecnai T12 S/TEM at 120KV.

DCA: Dynamic contact angle (DCA) measurements was performed on a Chan DCA-322 dynamic contact angle analyzer using the plate probe method to measure surface tension for which,

$$\gamma = F - F_b / L$$

Equation 6: Surface tension.

where γ is surface tension, F is force pulling the plate out from solution, F_b is the buoyancy correction, and L is the wetted length. Samples were prepared in water by successive dilutions.

***d*n/*d*c:** Polymer *d*n/*d*c was measured using a Brookhaven Instruments BI-DNDCW. Samples were prepared in water by successive dilution. Calibration was done with aqueous potassium chloride solutions.

SLS: Static light scattering (SLS) was performed on the same system as DLS and samples were made up in water by successive dilution and kept at 25^{o}C during measurements. ALV/Static and Dynamic Plot software was used to create Zimm plots and a toluene standard was used for calculation of excess Rayleigh ratio.

Chapter 6: Summary and Future Work

Two types of polymer brushes have been discussed. Polymer brushes grown from surfaces are an active area of research and have many applications both currently in use and under development. We have discussed many of these applications in some detail. Our work growing PMMA brushes from nylon membranes via ATRP has shown that, during the growth of dense brushes, a considerable fraction of oligomeric chains stop growing early during the polymerization and do not reach high MWs. We attribute this phenomenon mainly to termination that occurs when chains are short and there is a particularly high local concentration of radical chain ends. We have also noted, as has been previously reported, that when polymer is grown concurrently in solution, solution grown polymer grows to higher MW and shows lower PDI than surface grown polymer. This is largely due to the fact that monomer must diffuse into the brush to react with chain ends. We would like to see whether we observe the same phenomena with different polymerization systems and further explore the relationship between grafting density and formation of oligomeric grafts as well as system kinetics.

Various techniques having the potential to grow more uniform polymer brushes have been discussed and we have presented our work thus far towards realizing these techniques. Our work has been very preliminary. We would like to attach a dense coverage of Grubbs catalyst to a solid support and explore the growth of polymer brushes as monomer is inserted to the base of the chains by ROMP. Polymer brushes with more uniform surfaces may have favorable tribological properties that would be appealing to exploit for the production of low friction surfaces.

The application of polymer brushes as compatibilizers for nanofillers was studied. We grew PMMA brushes from functionalized BNO via ATRP. This allowed BNO to be dispersed more uniformly throughout a composite with PMMA. Our collaborator Zhenhua Cui, found that these composites showed improved mechanical properties compared with neat PMMA and composites using BNO that was not PMMA grafted. We would like to further our studies by attempting to grow other polymers from BNO for compatibility in other polymer matrices. We would also like to show that our technique is appropriate for scaling up.

We have studied the self-assembly of amphiphilic bottlebrush polymers. Our polymers formed various structures including spherical and cylindrical micelles as well as vesicles in water as a selective solvent. Complex intermediate structures were formed in water/THF mixed solvents and we observed self-assembly to be somewhat temperature dependent, which is expected as solvent quality can change with temperature. The architecture and PEO content of various polymers was seen to effect the formation of certain structures. Our calculations indicate that bottlebrushes that are densely grafted form micelles with structurally different coronas than sparsely grafted bottlebrushes. Cryogenic TEM could be used to confirm. We attribute this phenomenon to differences in flexibility of the hydrophobic backbone when grafted to various degrees. We would like to perform studies with our polymers to determine how micelles with structurally different coronas perform in the encapsulation of hydrophobic molecules. In order to make our polymers appropriate for use in biological encapsulation applications we would consider using a biodegradable polymer as our hydrophobic block. In hopes of forming unimolecular micelles, we would like to make more bottlebrush polymers of similar architecture. We believe an intermediate

degree of grafting between our densely and sparsely grafted polymers may confer the appropriate backbone flexibility as well as micelle surface coverage by hydrophilic polymer in order to stabilize unimolecular micelles.

References

(1) Jeon, S. .; Lee, J. .; Andrade, J. .; De Gennes, P. . *J. Colloid Interface Sci.* **1991**, *142*, 149–158.

(2) Li, L.; Chen, S.; Zheng, J.; Ratner, B. D.; Jiang, S. *J. Phys. Chem. B* **2005**, *109*, 2934–2941.

(3) Rühe, J.; Yano, R.; Lee, J.-S.; Köberle, P.; Knoll, W.; Offenhäusser, A. *J. Biomater. Sci. Polym. Ed.* **1999**, *10*, 859–874.

(4) Hersel, U.; Dahmen, C.; Kessler, H. *Biomaterials* **2003**, *24*, 4385–4415.

(5) Sakata, H.; Kobayashi, M.; Otsuka, H.; Takahara, A. *Polym. J.* **2005**, *37*, 767–775.

(6) Kobayashi, M.; Terayama, Y.; Hosaka, N.; Kaido, M.; Suzuki, A.; Yamada, N.; Torikai, N.; Ishihara, K.; Takahara, A. *Soft Matter* **2007**, *3*, 740–746.

(7) Snaith, H. J.; Whiting, G. L.; Sun, B.; Greenham, N. C.; Huck, W. T. S.; Friend, R. H. *Nano Lett.* **2005**, *5*, 1653–1657.

(8) Paoprasert, P.; Spalenka, J. W.; Peterson, D. L.; Ruther, R. E.; Hamers, R. J.; Evans, P. G.; Gopalan, P. *J. Mater. Chem.* **2010**, *20*, 2651–2658.

(9) Maillard, D.; Kumar, S. K.; Rungta, A.; Benicewicz, B. C.; Prud'homme, R. E. *Nano Lett.* **2011**, *11*, 4569–4573.

(10) Ohno, K.; Ma, Y.; Huang, Y.; Mori, C.; Yahata, Y.; Tsujii, Y.; Maschmeyer, T.; Moraes, J.; Perrier, S. *Macromolecules* **2011**, *44*, 8944–8953.

(11) Lee, H.; Pietrasik, J.; Sheiko, S. S.; Matyjaszewski, K. *Prog. Polym. Sci.* **2010**, *35*, 24–44.

(12) Barbey, R.; Lavanant, L.; Paripovic, D.; Schüwer, N.; Sugnaux, C.; Tugulu, S.; Klok, H.-A. *Chem. Rev.* **2009**, *109*, 5437–5527.

(13) Zhao, B.; Brittain, W. J. *Prog. Polym. Sci.* **2000**, *25*, 677–710.

(14) Prucker, O.; Ru, J. *Macromolecules* **1998**, *31*, 592–601.

(15) Kang, C.; Crockett, R. M.; Spencer, N. D. *Macromolecules* **2014**, *47*, 269–275.

(16) Behling, R. E.; Williams, B. a.; Staade, B. L.; Wolf, L. M.; Cochran, E. W. *Macromolecules* **2009**, *42*, 1867–1872.

(17) Marutani, E.; Yamamoto, S.; Ninjbadgar, T.; Tsujii, Y.; Fukuda, T.; Takano, M. *Polymer (Guildf).* **2004**, *45*, 2231–2235.

(18) Brittain, W. J.; Minko, S. *J. Polym. Sci. Part A Polym. Chem.* **2007**, *45*, 3505–3512.

(19) Ma, H.; Hyun, J.; Stiller, P.; Chilkoti, A. *Adv. Mater.* **2004**, *16*, 338–341.

(20) Bergbreiter, D. E.; Tao, G. *J. Polym. Sci. Part A Polym. Chem.* **2000**, *38*, 3944–3953.

(21) Huang, W.; Baker, G. L.; Bruening, M. L. *Angew. Chemie Int. Ed.* **2001**, *40*, 1510–1512.

(22) Wang, J.-Y.; Chen, W.; Liu, A.-H.; Lu, G.; Zhang, G.; Zhang, J.-H.; Yang, B. *J. Am. Chem. Soc.* **2002**, *124*, 13358–13359.

(23) Lego, B.; Skene, W. G.; Giasson, S. *Macromol. Symp.* **2010**, *297*, 65–68.

(24) Kim, J.; Huang, W.; Miller, M. D.; Baker, G. L.; Bruening, M. L. *J. Polym. Sci. Part A Polym. Chem.* **2002**, *41*, 386–394.

(25) Tsujii, Y.; Ohno, K.; Yamamoto, S.; Goto, A. In *Surface Initiated Polymerization I*; Jordan, R., Ed.; Springer: Berlin Heidelberg, 2006; pp. 1–45.

(26) Babu, K.; Dhamodharan, R. *Nanoscale Res. Lett.* **2009**, *4*, 1090–1102.

(27) Milchev, a.; Wittmer, J. P.; Landau, D. P. *J. Chem. Phys.* **2000**, *112*, 1606.

(28) Matyjaszewski, K.; Miller, P. J.; Shukla, N.; Immaraporn, B.; Gelman, A.; Luokala, B. B.; Siclovan, T. M.; Kickelbick, G.; Vallant, T.; Hoffmann, H.; Pakula, T. *Macromolecules* **1999**, *32*, 8716–8724.

(29) Yamamoto, S.; Tsujii, Y.; Fukuda, T. *Macromolecules* **2002**, *35*, 6077–6079.

(30) Liu, K.; Li, L. *Chinese J. Chem. Phys.* **2008**, *21*, 469–475.

(31) Pyun, J.; Matyjaszewski, K.; Kowalewski, T.; Savin, D.; Patterson, G.; Kickelbick, G.; Huesing, N. *J. Am. Chem. Soc.* **2001**, 9445–9446.

(32) Chen, X.; Armes, S. P. *Adv. Mater.* **2003**, *15*, 1558–1562.

(33) Nuû, S.; Böttcher, H.; Wurm, H.; Hallensleben, M. L. *Angew. Chem. Int. Ed.* **2001**, 4016–4018.

(34) Wang, Y.; Teng, X.; Wang, J.; Yang, H.; Lake, A. V; York, N. **2003**, 2–6.

(35) Currie, E. P. K.; Norde, W.; Cohen Stuart, M. a. *Tethered polymer chains: surface chemistry and their impact on colloidal and surface properties*; 2003; Vol. 100-102, pp. 205–265.

(36) Hawker, C. J.; Thomas, P. **2005**, *30*, 952–966.

(37) Giacomelli, C.; Schmidt, V.; Aissou, K.; Borsali, R. *Langmuir* **2010**, *26*, 15734–15744.

(38) Bates, F. *Annu. Rev. Phys. Chem.* **1990**, *41*, 525–557.

(39) Kataoka, K.; Harada, A.; Nagasaki, Y. *Adv. Drug Deliv. Rev.* **2001**, *47*, 113–131.

(40) Blanazs, A.; Armes, S. P.; Ryan, A. J. *Macromol. Rapid Commun.* **2009**, *30*, 267–277.

(41) Gaucher, G.; Dufresne, M.-H.; Sant, V. P.; Kang, N.; Maysinger, D.; Leroux, J.-C. *J. Control. Release* **2005**, *109*, 169–188.

(42) Kim, J.-H.; Park, K.; Nam, H. Y.; Lee, S.; Kim, K.; Kwon, I. C. *Prog. Polym. Sci.* **2007**, *32*, 1031–1053.

(43) Renggli, K.; Baumann, P.; Langowska, K.; Onaca, O.; Bruns, N.; Meier, W. *Adv. Funct. Mater.* **2011**, *21*, 1241–1259.

(44) Yang, X.; Grailer, J. J.; Pilla, S.; Steeber, D. a; Gong, S. *Bioconjug. Chem.* **2010**, *21*, 496–504.

(45) Kuchanov, S.; Pogodin, S.; ten Brinke, G.; Khokhlov, a. *Macromolecules* **2008**, *41*, 2689–2693.

(46) Iha, R. K.; Wooley, K. L.; Nystrom, A. M.; Burke, D. J.; Kade, M. J.; Hawker, C. J. *Chem. Rev.* **2009**, *109*, 5620–5686.

(47) Yuan, W.; Zhang, J.; Wei, J. *Prog. Chem.* **2011**, *23*, 760–771.

(48) Nomura, K.; Abdellatif, M. M. *Polymer (Guildf).* **2010**, *51*, 1861–1881.

(49) Le, D.; Morandi, G.; Legoupy, S.; Pascual, S.; Montembault, V.; Fontaine, L. *Eur. Polym. J.* **2013**, *49*, 972–983.

(50) Lutz, J.-F. *J. Polym. Sci. Part A Polym. Chem.* **2008**, *46*, 3459–3470.

(51) Ma, H.; Wells, M.; Beebe, T. P.; Chilkoti, A. *Adv. Funct. Mater.* **2006**, *16*, 640–648.

(52) Deshpande, M. C.; Davies, M. C.; Garnett, M. C.; Williams, P. M.; Armitage, D.; Bailey, L.; Vamvakaki, M.; Armes, S. P.; Stolnik, S. *J. Control. Release* **2004**, *97*, 143–156.

(53) Bergström, L. M. In *Application of Thermodynamics to Biological and Materials Science*; Tadashi, M., Ed.; INTECH, 2011; pp. 289–314.

(54) Liu, F.; Urban, M. W. *Prog. Polym. Sci.* **2010**, *35*, 3–23.

(55) Bawa, P.; Pillay, V.; Choonara, Y. E.; du Toit, L. C. *Biomed. Mater.* **2009**, *4*, 22001.

(56) Mai, Y.; Eisenberg, A. *Chem. Soc. Rev.* **2012**, *41*, 5969–5985.

(57) Bhargava, P.; Zheng, J. X.; Li, P.; Quirk, R. P.; Harris, F. W.; Cheng, S. Z. D. *Macromolecules* **2006**, *39*, 4880–4888.

(58) Rzayev, J. *ACS Macro Lett.* **2012**, *1*, 1146–1149.

(59) Zhang, M.; Müller, A. H. E. *J. Polym. Sci. Part A Polym. Chem.* **2005**, *43*, 3461–3481.

(60) Fenyves, R.; Schmutz, M.; Horner, I. J.; Bright, F. V.; Rzayev, J. *J. Am. Chem. Soc.* **2014**, *136*, 7762–7770.

(61) Odian, G. In *Principles of Polymerization*; John Wiley & Sons, Inc., 2004; pp. 372–463.

(62) Hadjichristidis, N.; Pitsikalis, M.; Pispas, S.; Iatrou, H. *Chem. Rev.* **2001**, *101*, 3747–3792.

(63) Huang, Wenxi; Kim, Jong-Bum; Bruening, Merlin L.; Baker, G. L. *Macromolecules* **2002**, *35*, 1175–1179.

(64) Gorman, C. B.; Petrie, R. J.; Genzer, J.; Carolina, N. *Macromolecules* **2008**, 4856–4865.

(65) Turgman-Cohen, S.; Genzer, J. *J. Am. Chem. Soc.* **2011**, *133*, 17567–17569.

(66) Shirahase, T.; Komatsu, Y.; Tominaga, Y.; Asai, S.; Sumita, M. *Polymer (Guildf).* **2006**, *47*, 4839–4844.

(67) Rubinstein, M.; Colby, R. H. *Oxford Univ. Press. New York* **2003**.

(68) Xu, F. J.; Zhao, J. P.; Kang, E. T.; Neoh, K. G.; Li, J. *Langmuir* **2007**, *23*, 8585–8592.

(69) Engler, M.; Lesniak, C.; Damasch, R.; Rusinger, B.; Eichler, J. *CFI. Ceram. forum Int.* **2007**, *84*, 49–53.

(70) Lin, Y.; Connell, J. W. *Nanoscale* **2012**, *4*, 6908–6939.

(71) Xu, M.; Liang, T.; Shi, M.; Chen, H. Graphene-like two-dimensional materials. *Chemical Reviews*, 2013, *113*, 3766–3798.

(72) Rao, C. N. R.; Nag, A. In *European Journal of Inorganic Chemistry*; 2010; pp. 4244–4250.

(73) Coleman, J. N.; Lotya, M.; O'Neill, A.; Bergin, S. D.; King, P. J.; Khan, U.; Young, K.; Gaucher, A.; De, S.; Smith, R. J.; Shvets, I. V; Arora, S. K.; Stanton, G.; Kim, H.-Y.; Lee, K.; Kim, G. T.; Duesberg, G. S.; Hallam, T.; Boland, J. J.; Wang, J. J.; Donegan, J. F.; Grunlan, J. C.; Moriarty, G.; Shmeliov, A.; Nicholls, R. J.; Perkins, J. M.; Grieveson, E. M.; Theuwissen, K.; McComb, D. W.; Nellist, P. D.; Nicolosi, V. *Science* **2011**, *331*, 568–571.

(74) Sajjad, M.; Jadwisienczak, W. M.; Feng, P. *Nanoscale* **2014**, *6*, 4577–4582.

(75) Cui, Z.; Oyer, A. J.; Glover, A. J.; Schniepp, H. C.; Adamson, D. H. *Small* **2014**, *10*, 2352–2355.

(76) Sainsbury, T.; Satti, A.; May, P.; Wang, Z.; McGovern, I.; Gun'ko, Y. K.; Coleman, J. *J. Am. Chem. Soc.* **2012**, *134*, 18758–18771.

(77) Bhimanapati, G. R.; Kozuch, D.; Robinson, J. *Nanoscale* **2014**.

(78) Chen, X.; Boulos, R. A.; Dobson, J. F.; Raston, C. L. Shear induced formation of carbon and boron nitride nano-scrolls. *Nanoscale*, 2012.

(79) Xu, M.; Fujita, D.; Chen, H.; Hanagata, N. *Nanoscale* **2011**, *3*, 2854–2858.

(80) Yuan, S.; Toury, B.; Journet, C.; Brioude, A. *Nanoscale* **2014**, *6*, 7838–7841.

(81) Nag, A.; Raidongia, K.; Hembram, K. P. S. S.; Datta, R.; Waghmare, U. V.; Rao, C. N. R. *ACS Nano* **2010**, *4*, 1539–1544.

(82) Zhi, C.; Bando, Y.; Tang, C.; Kuwahara, H.; Golberg, D. *Adv. Mater.* **2009**, *21*, 2889–2893.

(83) Potts, J. R.; Dreyer, D. R.; Bielawski, C. W.; Ruoff, R. S. *Polymer (Guildf).* **2011**, *52*, 5–25.

(84) Cui, Z.; Martinez, A.; Adamson, D. H. *Nanoscale*.

(85) Solozhenkoa, V. L. *J. Phys. Chem. Solids* **1997**, *58*, 1321–1323.

(86) Yamamoto S, Tsujii Y, Fukuda T, Torikai N, T. M. *KENS Rep. 14*, 204.

(87) Whiting, G. L.; Gb, C.; Friend, R. H.; Snaith, H.; Gb, E. (19) United States (12) Patent Application Publication (10) Pub . No .: US 2007 / 0169814 A1, 2007.

(88) Saha, S.; Baker, G. L. *J. Appl. Polym. Sci* **2015**, *41363*, 1–9.

(89) Whiting, G. L.; Snaith, H. J.; Khodabakhsh, S.; Andreasen, J. W.; Breiby, D. W.; Nielsen, M. M.; Greenham, N. C.; Friend, R. H.; Huck, W. T. S. *Nano Lett.* **2006**, *6*, 573–578.

(90) Lindqvist, J.; Malmström, E. *J. Appl. Polym. Sci.* **2006**, *100*, 4155–4162.

(91) Catalyst, I. O.; Schürer, S. C.; Gessler, S.; Buschmann, N.; Blechert, S. *Angew. Chem. Int. Ed.* **2000**, 3898–3901.

(92) Yang, L.; Mayr, M.; Wurst, K.; Buchmeiser, M. R. *Chem. - A Eur. J.* **2004**, *10*, 5761–5770.

(93) Hong, S. H.; Grubbs, R. H. *J. Am. Chem. Soc.* **2006**, *128*, 3508–3509.

(94) Ford, D. L.; Grant, R. Process of preparing polyamide supports capable of reaction with antibodies and enzymes and supports produced thereby. 0203095B1, 1991.

(95) Fawcett, J.; Hoye, P. A. T.; Kemmitt, R. D. W.; Law, D. J.; Russell, D. R. *J. Chem. Soc. Dalt. Trans.* **1993**, 2563–2568.

(96) Astruc, D.; Diallo, A. K.; Gatard, S.; Liang, L.; Ornelas, C.; Martinez, V.; Méry, D.; Ruiz, J. *Beilstein J. Org. Chem.* **2011**, *7*, 94–103.

(97) Semenov, A. N. *Macromolecules* **2004**, *37*, 226–237.

(98) Patterson, J. P.; Robin, M. P.; Chassenieux, C.; Colombani, O.; O'Reilly, R. K. *Chem. Soc. Rev.* **2014**, *43*, 2412–2425.

(99) Owen, S. C.; Chan, D. P. Y.; Shoichet, M. S. *Nano Today* **2012**, *7*, 53–65.

(100) Zamani, S.; Khoee, S. *Polym. (United Kingdom)* **2012**, *53*, 5723–5736.

(101) Rodriguez, A. R.; Choe, U.-J.; Kamei, D. T.; Deming, T. J. *Macromol. Biosci.* **2015**, *15*, 90–97.

(102) Jiang, Y.; Chen, T.; Ye, F.; Liang, H.; Shi, A. C. *Macromolecules* **2005**, *38*, 6710–6717.

(103) Jang, S.-Y.; Sotzing, G. a.; Marquez, M. *Macromolecules* **2002**, *35*, 7293–7300.

(104) Hilf, S.; Klos, J.; Char, K.; Woo, H.; Kilbinger, A. F. M. *Macromol. Rapid Commun.* **2009**, *30*, 1249–1257.

(105) Spring, A. M.; Yu, C.-Y.; Horie, M.; Turner, M. L. *Chem. Commun. (Camb).* **2009**, 2676–2678.

(106) Bazzi, H. S.; Sleiman, H. F. *Macromolecules* **2002**, *35*, 624–629.

Appendices

Appendix 1: Nylon Membrane Fiber Curvature: ImageJ was used to take measurements from an SEM image of an unfunctionalized nylon membrane. Average fiber thickness was 411±132nm. Treating fibers as smooth cylinders, curvature (K) perpendicular to the length of the fiber is the reciprocal of the radius.

$K = 4.87x10^{-3}\ nm^{-1}$

Circumference measured as 2π(radius) is 1290±414nm therefore a change of 0.279degrees/nm is experienced in the direction perpendicular to length of the fiber.

Appendix 2: Neat PMMA and BN-PMMA Filtrate GPC:

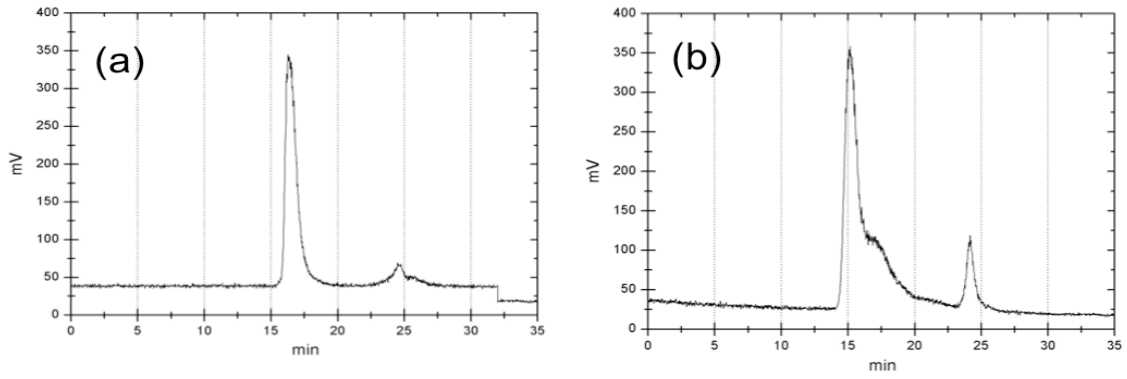

Figure 74: GPC of (a) neat PMMA, (b) BN-PMMA filtrate.

Appendix 3: Structures of Monomers for Production of Conductive Brushes by ROMP

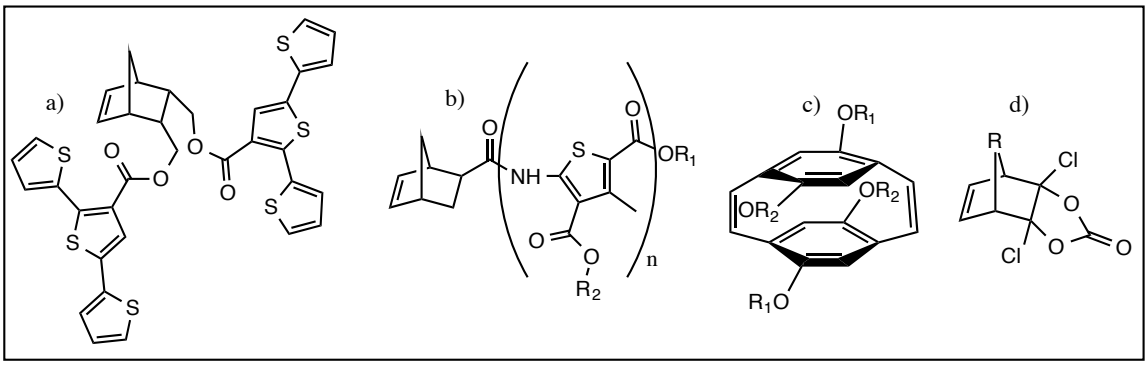

Figure 75: Potential monomers for conductive brushes by ROMP. b) Sotzing synthesized the 5-norbornene-*endo*-2,3-bis(methylene-3'-[2,2':5',2']-terhiophene acetate) monomer, which can be oxidatively crosslinked after polymerization to increase conjugation.[103] b) Kilbinger polymerized norbornene substituted oligothiophene amides with n=1,2,3.[104] Turner polymerized [2.2]paracyclophanedienes assisted by microwave, which can be UV irradiated post polymerization to give an all *trans* conformation that increases conjugation length.[105] Sleiman polymerized norbornene with a 1,2-dithiocarbonate moiety that could undergo hydrolysis and a post polymerization keto-enol tautomerization to give conjugation.[106]

Appendix 4: NMR of Bottlebrush Polymers:

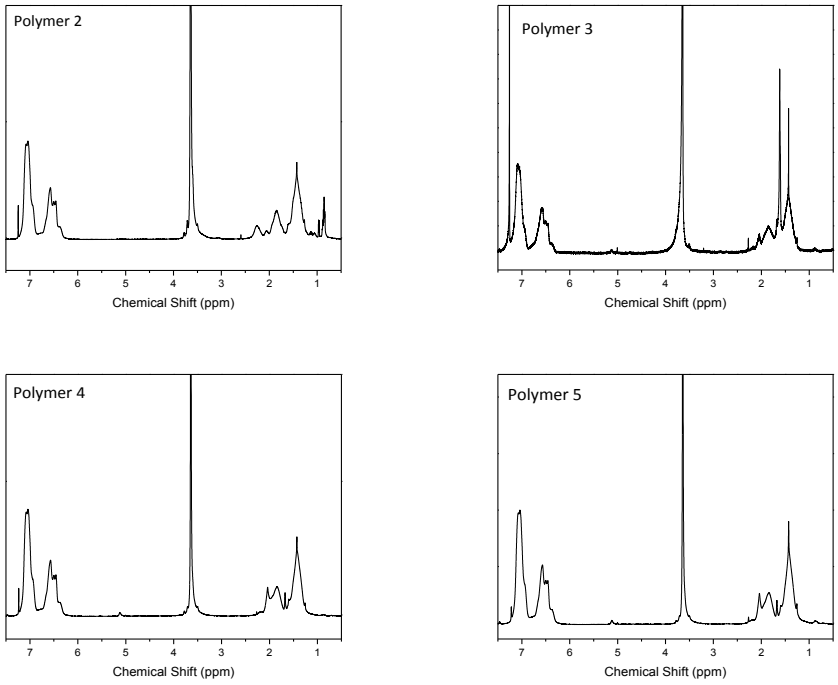

Figure 76: NMR of polymers 2-5.

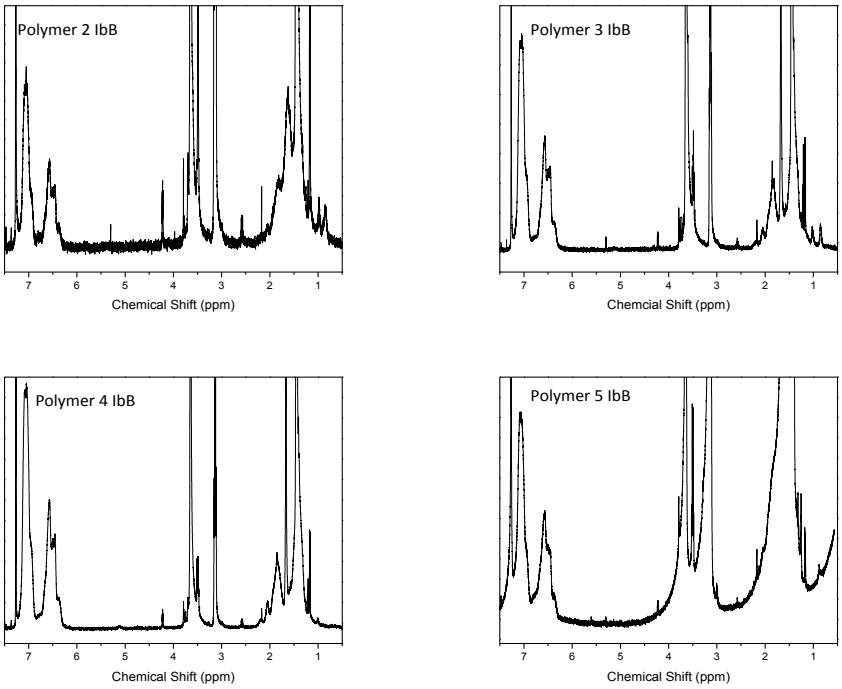

Figure 77: NMR of polymers 2-5 reacted with IbB.

Appendix 5: GPC of Bottlebrush Polymer

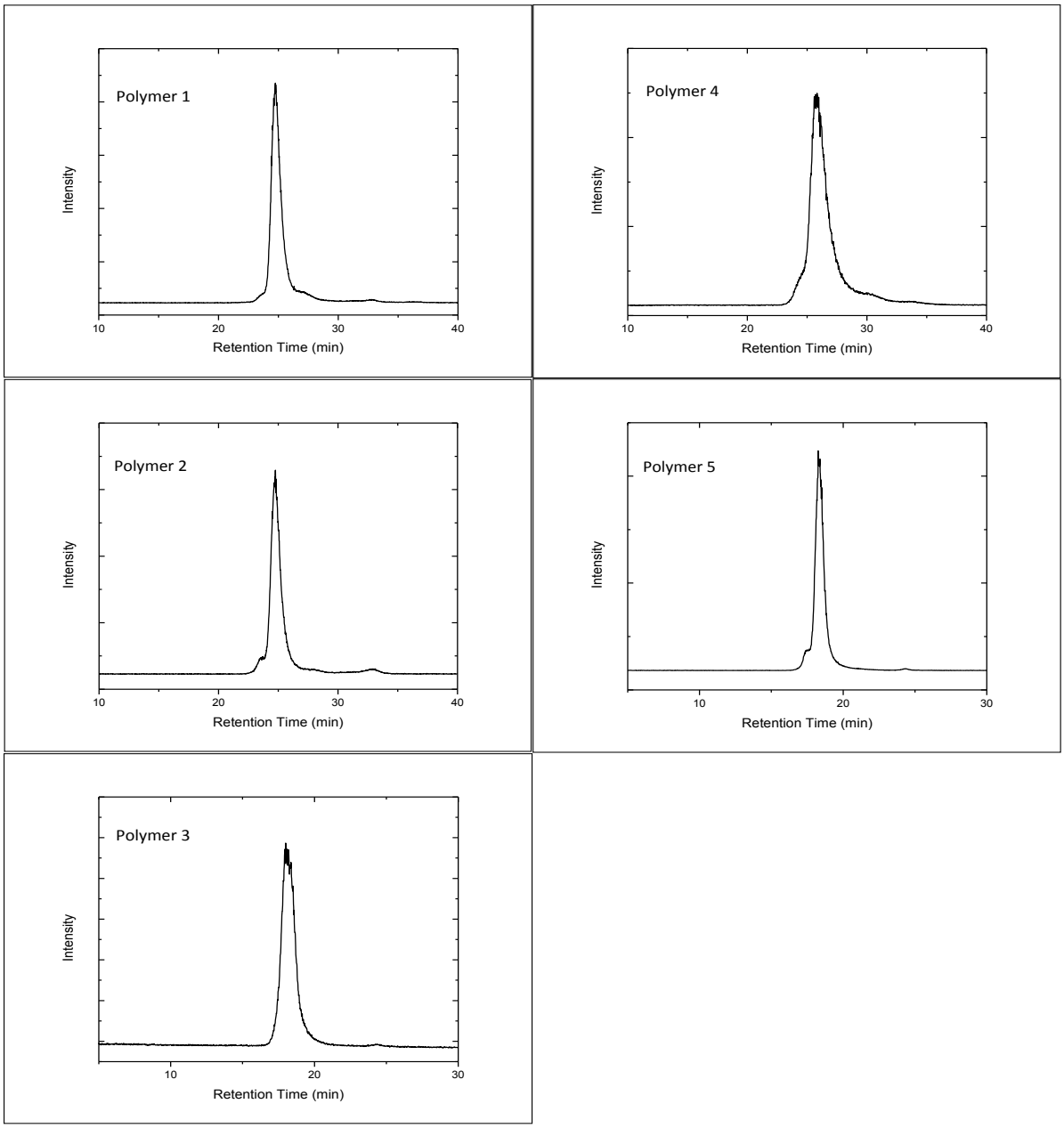

Figure 78: GPC of bottlebrush polymers. Polymers 3 and 5 used different method with a faster flow rate.

Appendix 6: Bottlebrush variable temperature DLS:

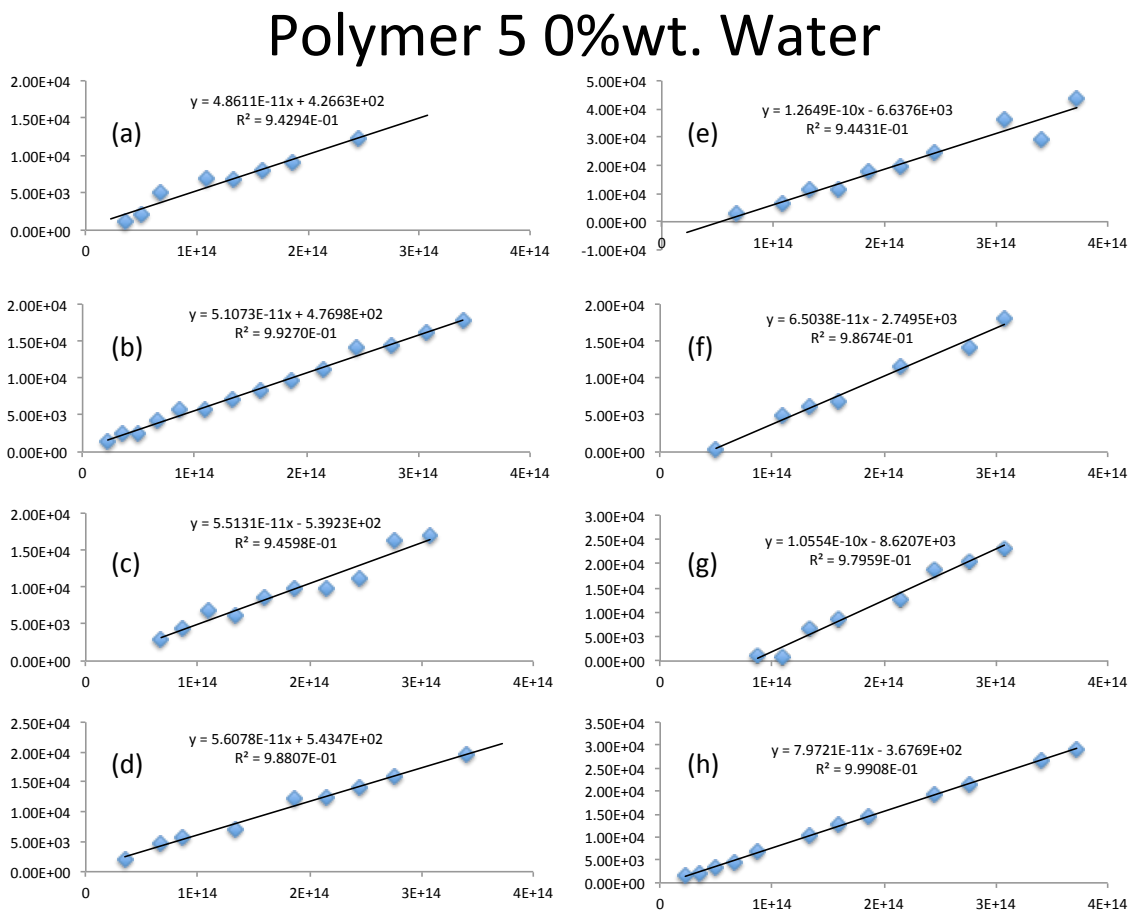

Figure 79: Plots of q^2 versus 1/tau. Slope is equal to diffusion coefficient. (a) 10°C, (b) 13°C, (c) 15°C, (d) 17°C (e) 20°C, (f) 25°C, (g) 35°C, (h) 45°C.

Polymer 5 0%wt. Water Aggregates

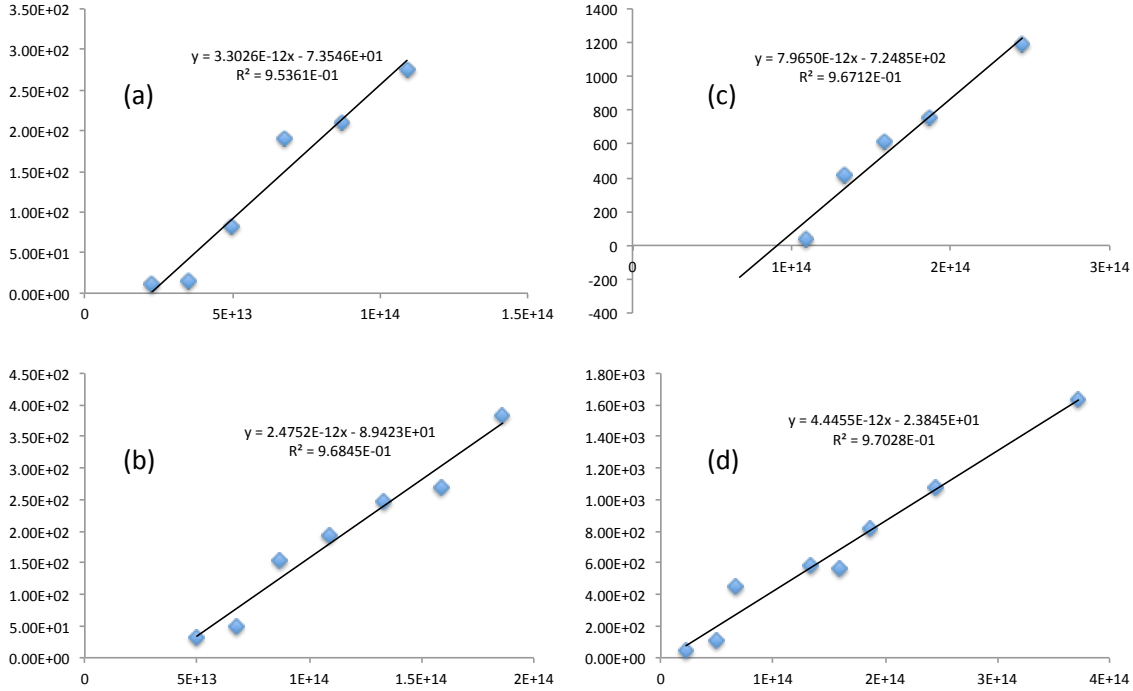

Figure 80: Plots of q^2 versus 1/tau. Slope is equal to diffusion coefficient. (a) 15°C, (b) 25°C, (c) 35°C (d) 45°C.

Polymer 5 15.1%wt. Water

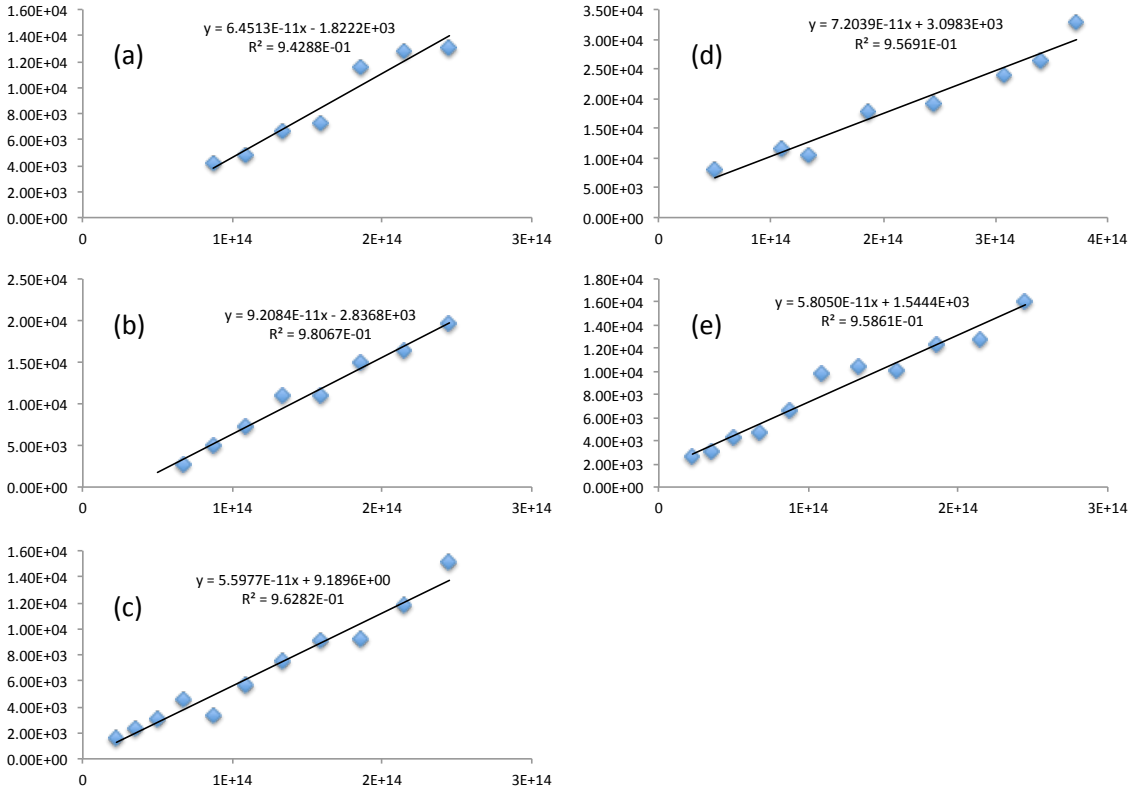

Figure 81: Plots of q^2 versus 1/tau. Slope is equal to diffusion coefficient. (a) 25°C, (b) 35°C, (c) 40°C (d) 45°C (e) 50°C.

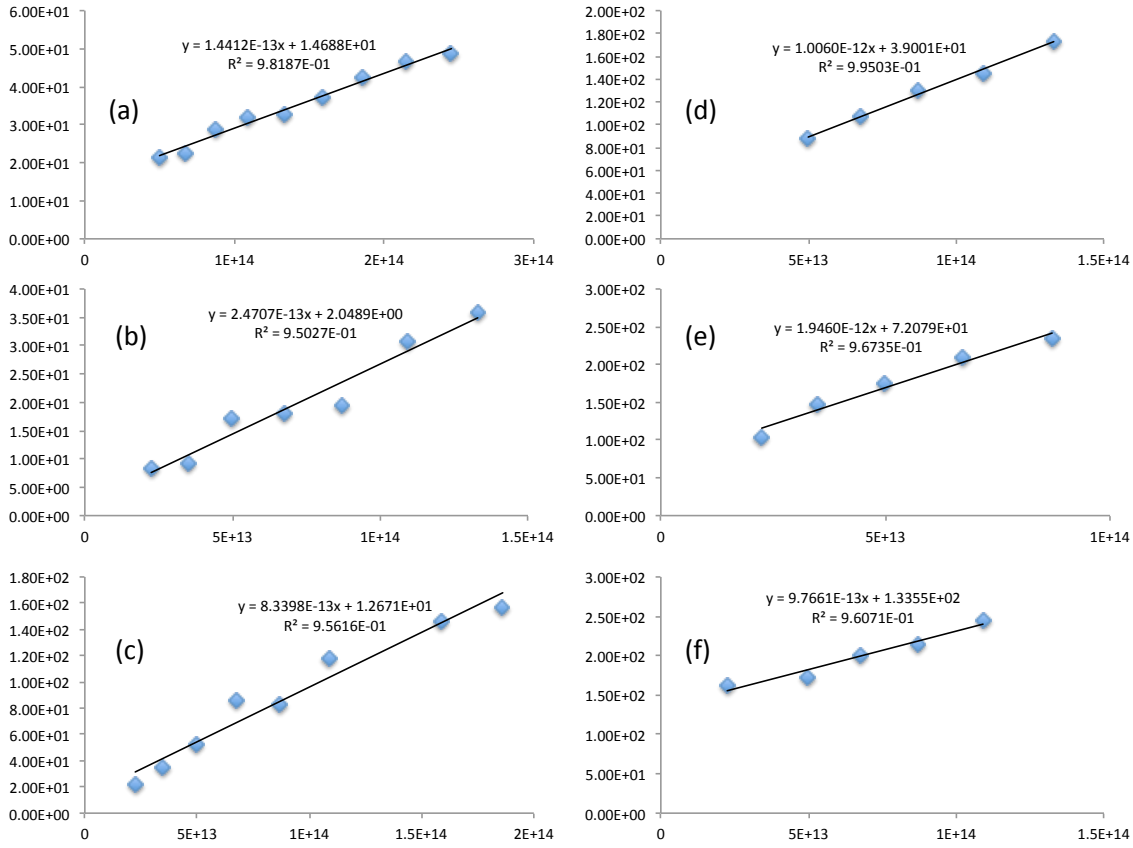

Figure 82: Plots of q^2 versus 1/tau. Slope is equal to diffusion coefficient. (a) 15°C, (b-c) 25°C, (d) 35°C (e) 40°C (f) 50°C.

Polymer 5 20%wt. Water

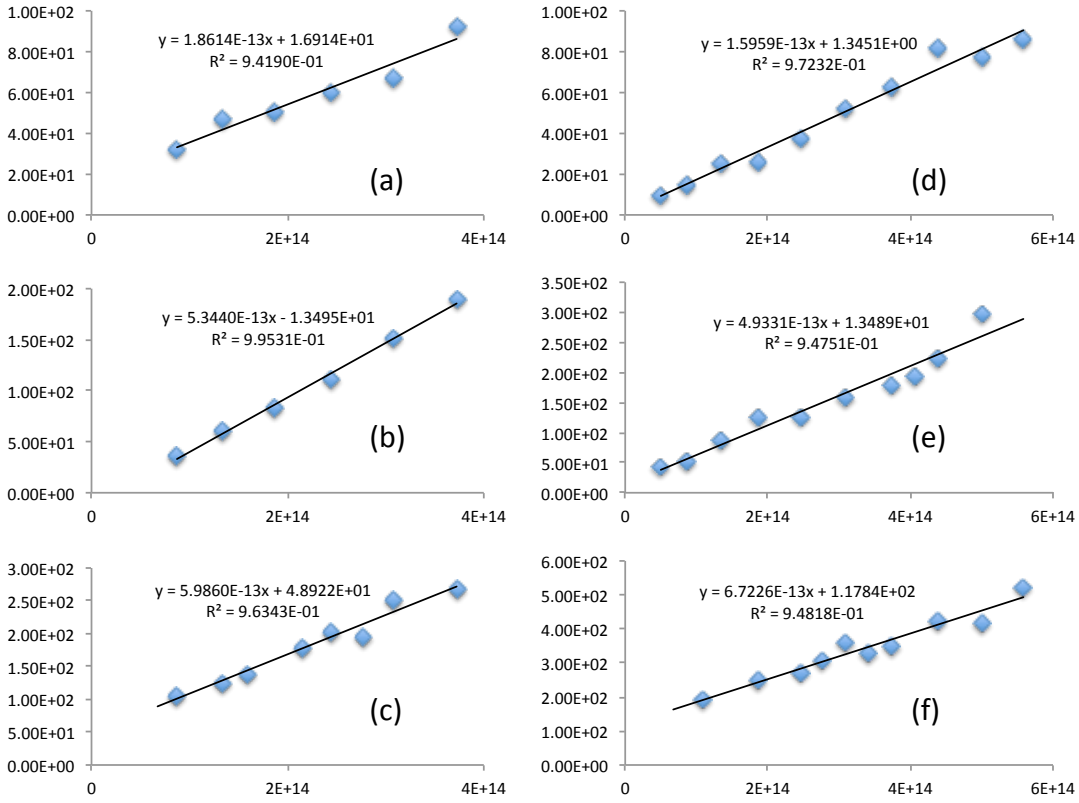

Figure 83: Plots of q^2 versus 1/tau. Slope is equal to diffusion coefficient. (a) 45°C, (b) 60°C, (c) 70°C, (d) 25°C after sitting overnight, (e) 45°C after sitting overnight, (f) 60°C after sitting overnight.

Polymer 3 0%wt. Water

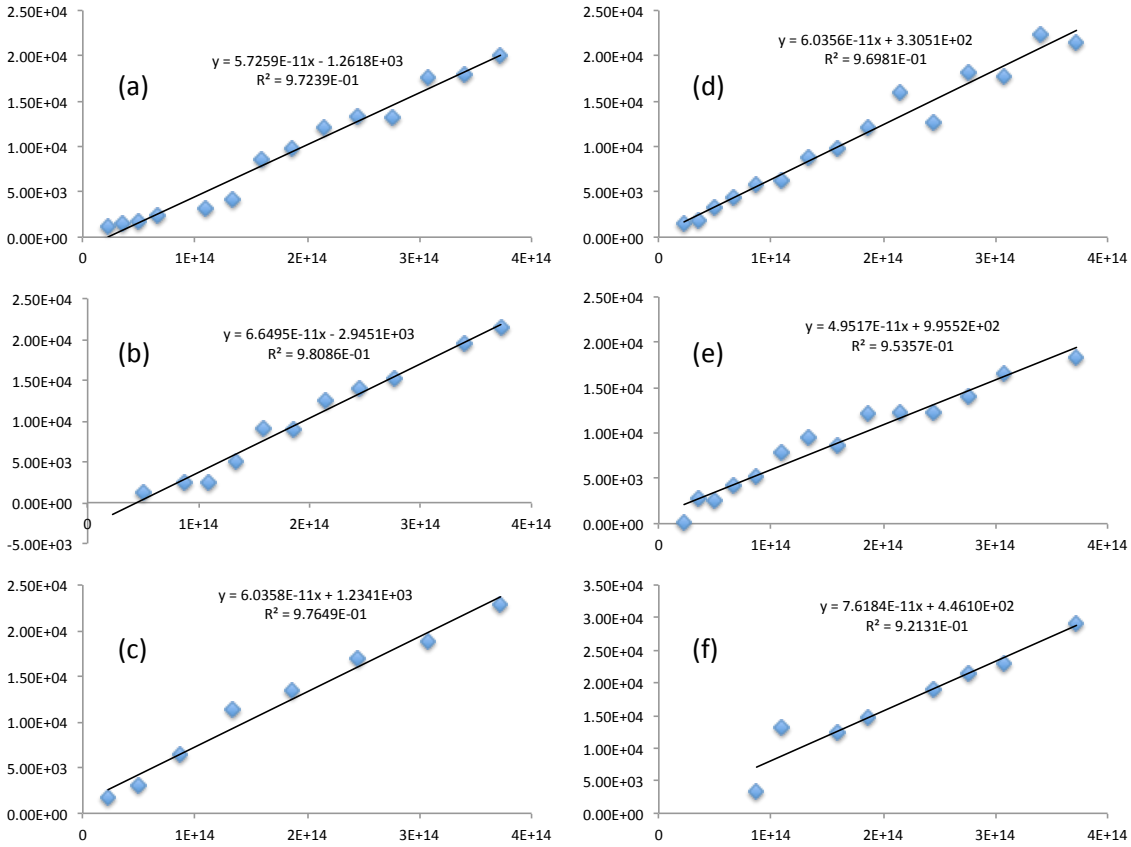

Figure 84: Plots of q^2 versus 1/tau. Slope is equal to diffusion coefficient. (a) 15°C, (b) 20°C, (c) 25°C (d) 30°C (e) 35°C, (f) 45°C.

Polymer 3 15.4%wt. Water

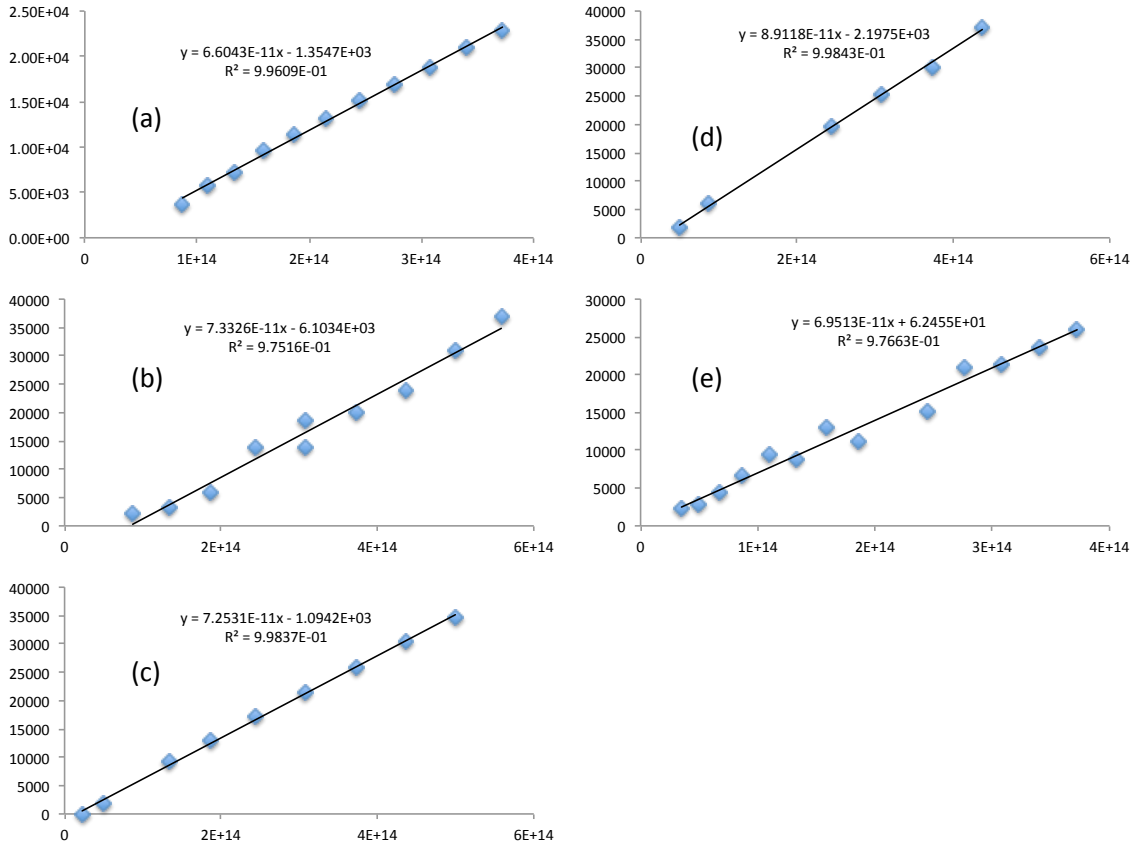

Figure 85: Plots of q^2 versus 1/tau. Slope is equal to diffusion coefficient. (a) 25°C, (b) 30°C, (c) 35°C (d) 40°C (e) 45°C.

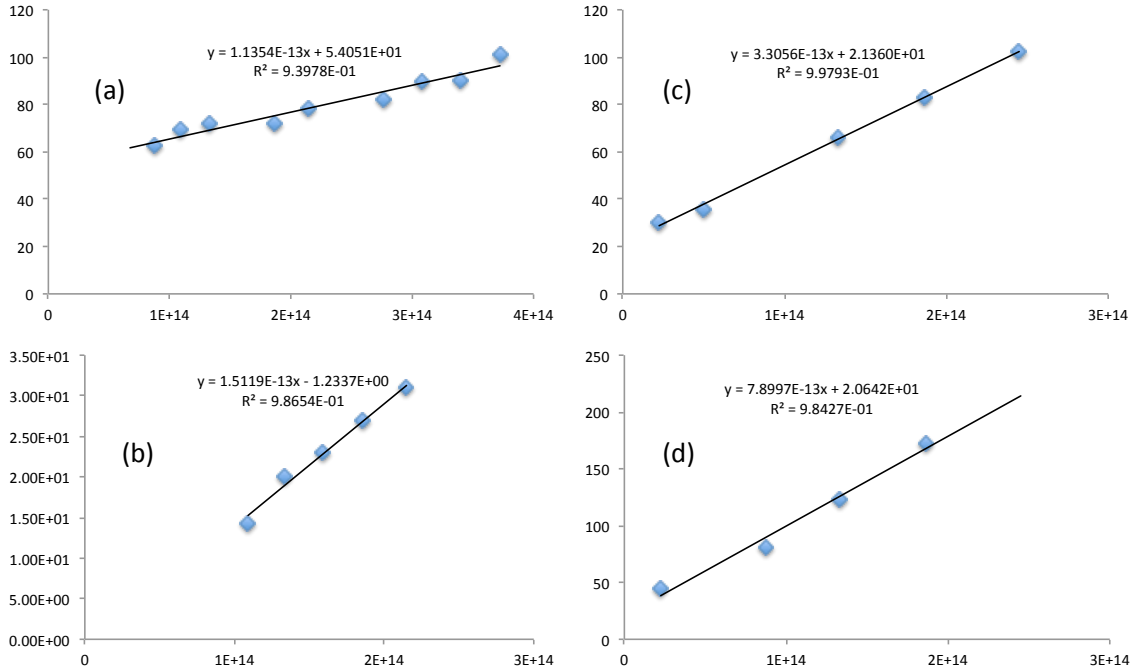

Figure 86: Plots of q^2 versus 1/tau. Slope is equal to diffusion coefficient. (a) 15°C, (b) 25°C, (c) 30°C (d) 35°C.

Polymer 3 17.4%wt. Water

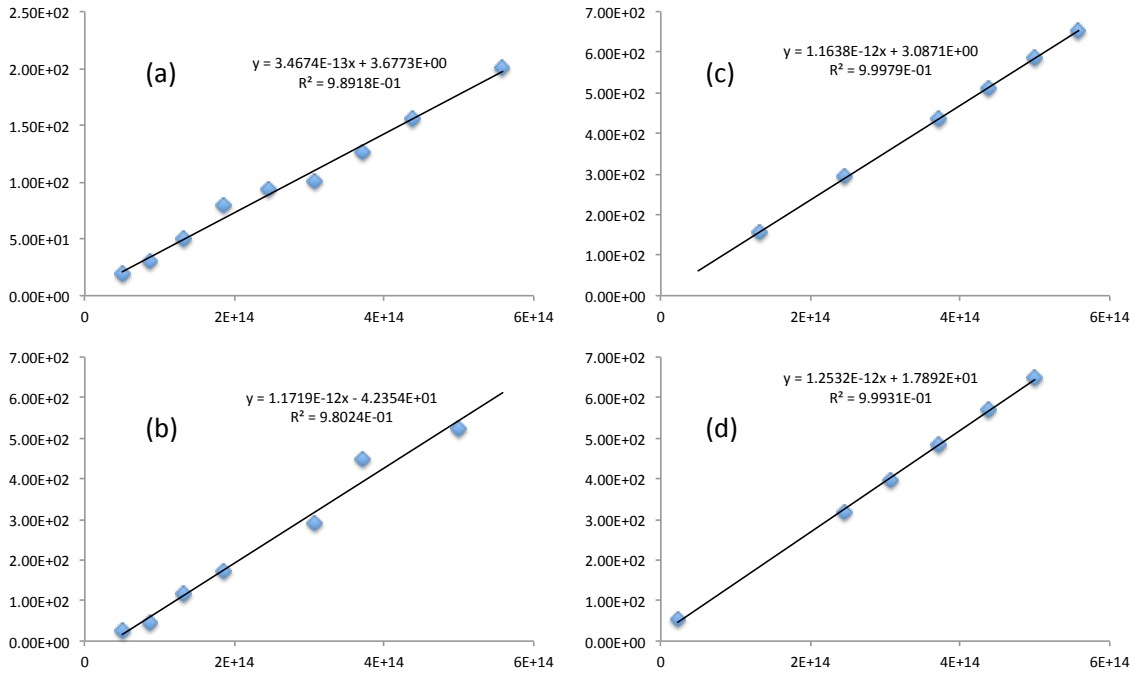

Figure 87: Plots of q^2 versus 1/tau. Slope is equal to diffusion coefficient. (a) 35°C, (b) 45°C, (c) 55°C (d) 65°C.

Appendix 7: CWC and THF CMC plots.

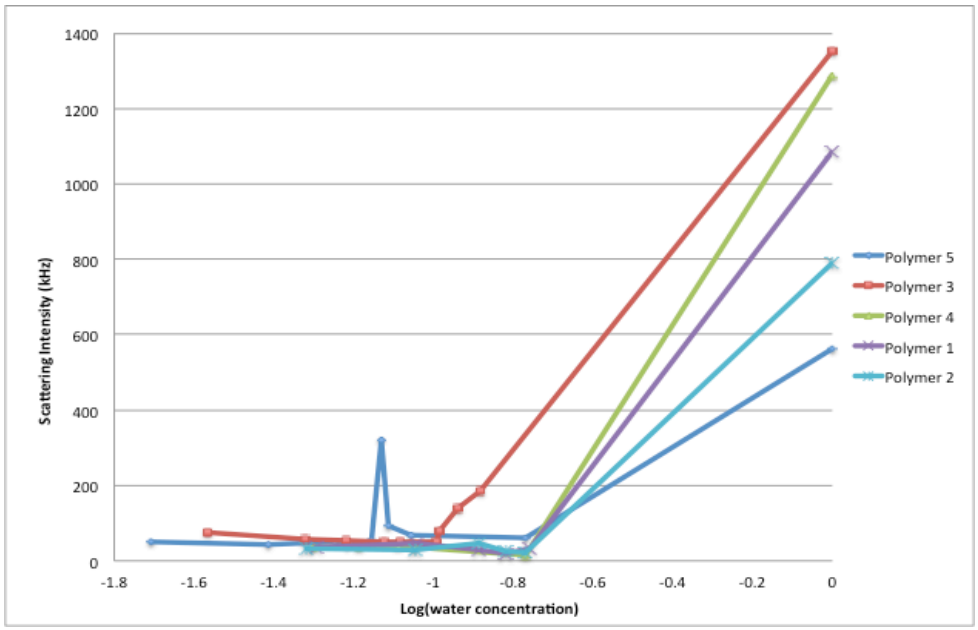

Figure 88: Water concentration versus scattering intensity of bottlebrush solutions in THF.

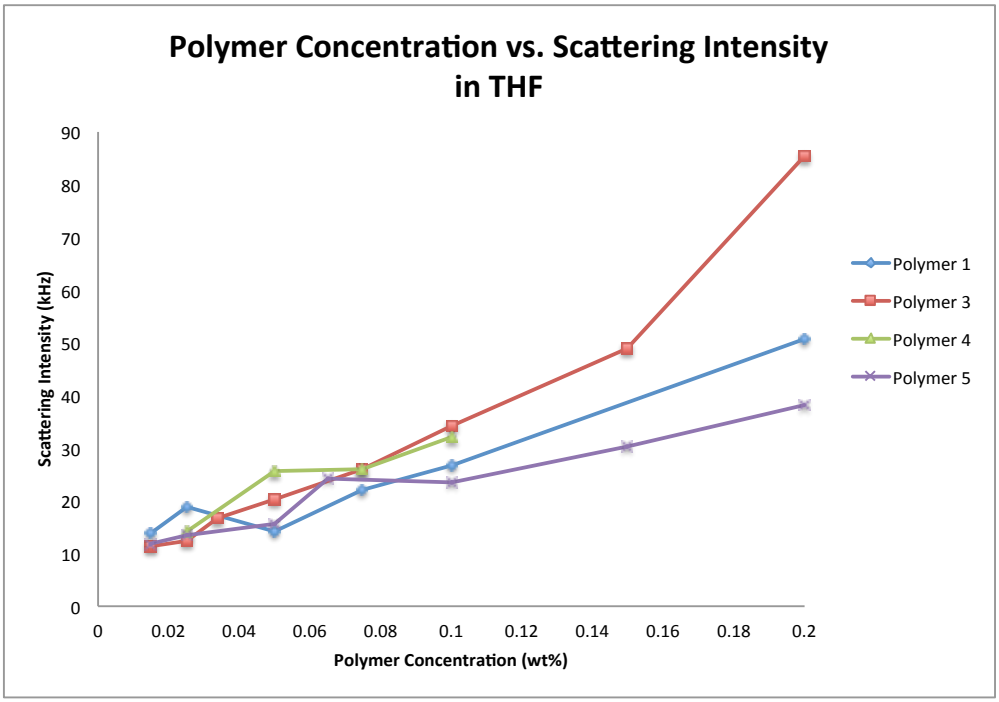

Figure 89: Bottlebrush polymer concentration versus scattering intensity in pure THF. Samples were made by dilution of 0.20wt% polymer in THF.

Appendix 8: SLS and *d*n/*d*c: We performed SLS on Polymer 1 to determine the aggregation number of the micelles formed. Polymer 1 was used because it exhibited the smallest micelles in water. The concentrations needed to determine *d*n/*d*c and for use in SLS are greater than what we had used for SLS and TEM. Concentrations from 0.25-1.00mg/ml were used. We were concerned that filtering of these samples by 0.2μm filter would measurably reduce concentration so we performed SLS with and without filtering. Interestingly, results were similar for both the filtered and unfiltered samples although we saw a decrease in concentration with filtering. To determine actual concentrations of polymer after filtering we dried a given volume of our samples and redissolved samples in deuterated chloroform with a known concentration of dichloromethane. Integrating dichloromethane and PEO peaks we could back calculate the concentrations of polymer in our *d*n/*d*c and SLS samples. Concentrations were intended to be 0.25, 0.50, 0.75, 1.0mg/ml but were determined to be 0.098, 0.17, 0.24, 0.26mg/ml respectively. These calculated values were used in SLS and determination of *d*n/*d*c for our filtered samples.

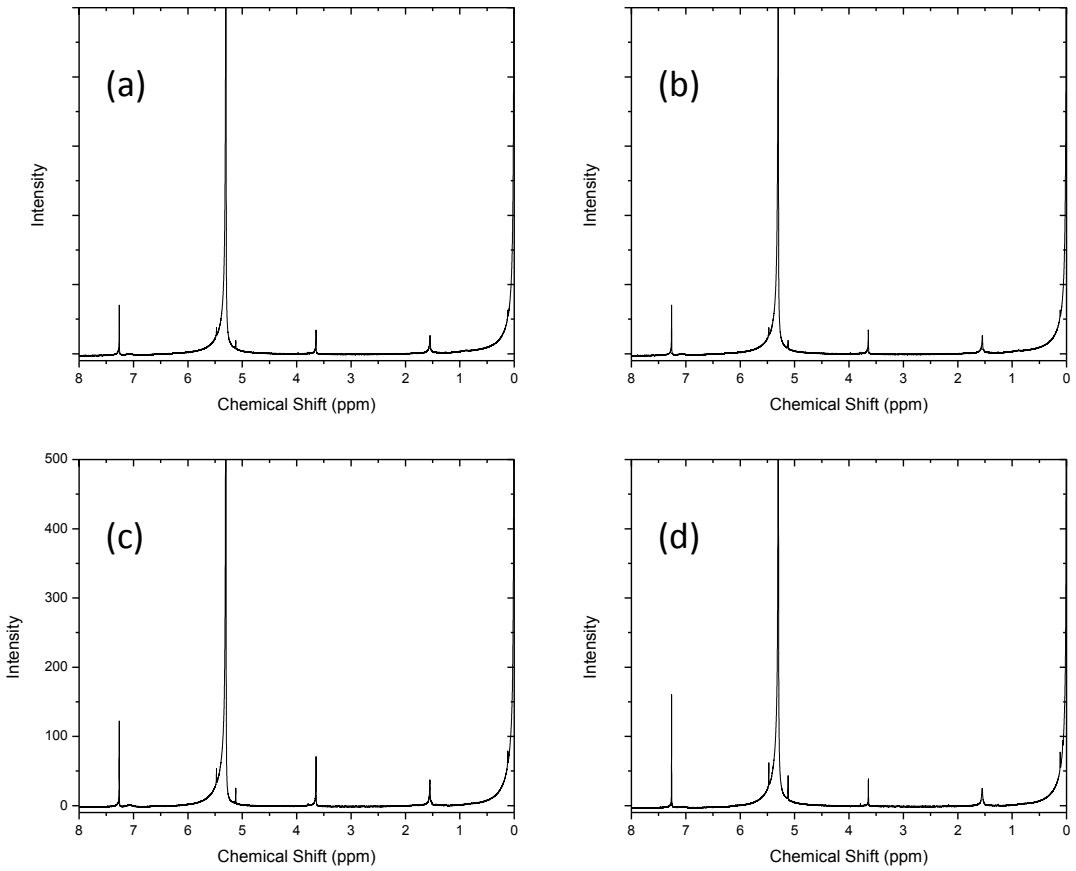

Figure 90: NMR of Polymer 1 from *d*n/*d*c and SLS samples redissolved in $CHCl_3$ with CH_2Cl_2. Concentrations were intended to be a-d) respectively, 0.25, 0.50, 0.75, 1.0mg/ml but were determined to be 0.098, 0.17, 0.24, 0.26mg/ml.

Our R_g/R_h values do not suggest that we have spherical micelles. Using SLS data from our unfiltered samples yields an $R_g/R_h = 1.18$ which indicates a vesicle bilayer structure. This may indicate that vesicles form for **Polymer 1** but we were unable to observe them using TEM. This we would assume these vesicles would have been observed by DLS. It may be possible that the R_h we have attributed to polymer micelles may actually correspond to vesicle morphology. SLS data from our filtered samples yields an $R_g/R_h = 2.16$ which indicates an extended cylindrical structure that would likely be in the range of 300nm length using **equation 7** and the radius of particles measured by TEM.

$$R_g^2 = L^2/12 + r^2/2$$

Equation 7: Relation of R_g to length (L) and radius (r) for cylindrical micelles.[98]

This length would be in line with TEM images of our other polymers however we did not observe these structures for Polymer 1.

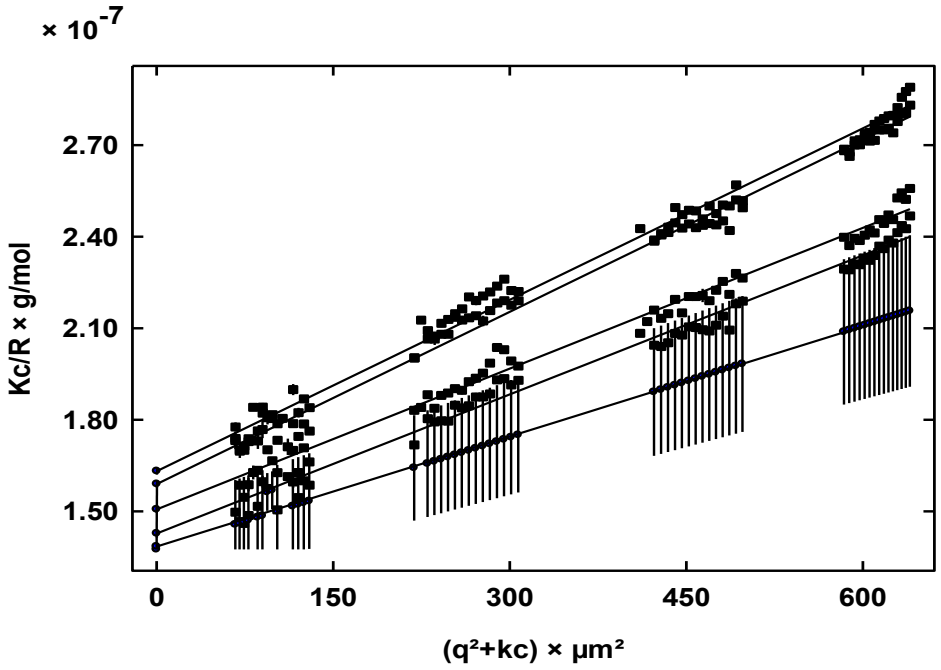

Figure 91: Zimm plot generated from SLS data of filtered samples of polymer 1.

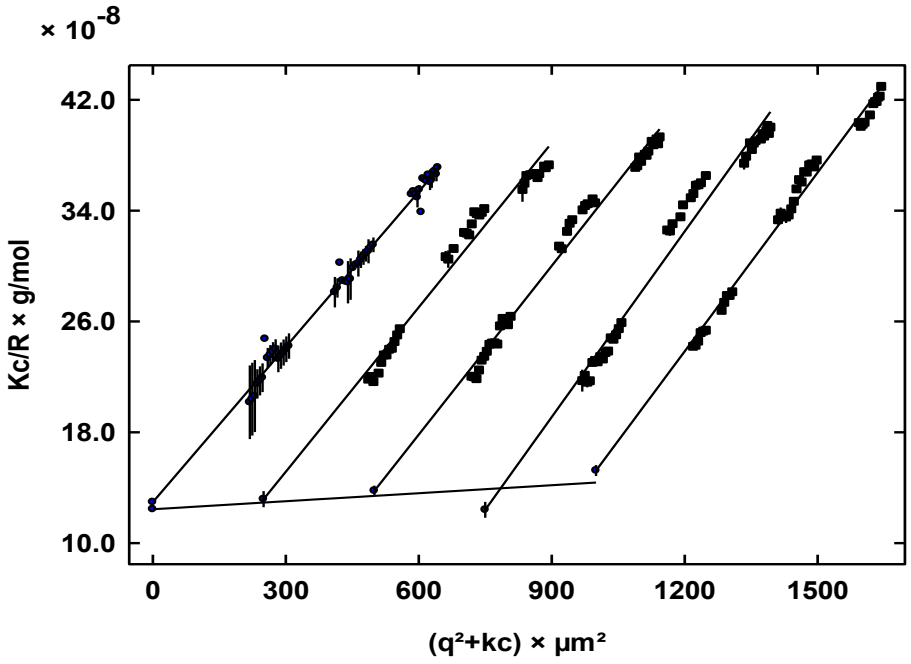

Figure 92: Zimm plot generated from SLS data of unfiltered samples of polymer 1.

Table 9: SLS results.

Sample	dn/dc (ml/g)	$M_w(c)$ (g/mol)	$M_w(q^2)$ (g/mol)	R_g (nm)	A_2 (mol*dm^3/g^2)	N_{agg} from $M_w(q^2)$
Polymer 1 Filtered	0.5397	8.036e+06 ±12.4%	7.717e+06 ±2.22%	92.99 ±1.38%	9.644e-09 ±116%	95
Polymer 1 Unfiltered	0.5784	7.271e+06 ±9.73%	7.222e+06 ±0.27%	51.04 ±0.4%	4.314e-08 ±77.9%	89

Appendix 9: Calculation of R_{max} and R_F:

Contour length (R_{max}) equation: The number of bonds (n), bond length (l = 1.54Å), and tetrahedral angle (θ = 68°) were used to calculate contour length of various blocks of the polymer.

$$R_{max} = nl\cos(\theta/2)$$

Equation 8: Contour length.[67]

Optimum chain size in a good solvent by Flory theory (R_F): Kuhn lengths (b) used were 8.4Å for PI and 11Å for PEO. Excluded volume (v) was taken as less than that in an athermal solvent ($<b^3$). Number of Kuhn monomers (N) was measured as N=R_{max}/b.

$$R_F = v^{1/5}b^{2/5}N^{3/5} \leq bN^{3/5}$$

Equation 9: Optimum chain size in a good solvent by Flory theory.[67]